Investigation of Mitochondrial Ribosome Regulators at the Inner Membrane

Dissertation

for the award of the degree

"Doctor rerum naturalium"

of the Georg-August-Universität Göttingen

within the doctoral program

"Molecular Biology of Cells"

of the Georg-August University School of Science (GAUSS)

submitted by

Sabine Poerschke

born in Wernigerode, Germany

Göttingen, July 2021

Members of the Thesis Committee and Examination Board:

Prof. Dr. Peter Rehling (Supervisor and first referee)	Department of Cellular Biochemistry University Medical Center Göttingen Göttingen, Germany
Prof. Dr. Ralph Kehlenbach (Second referee)	Department of Molecular Biology University Medical Center Göttingen Göttingen, Germany
Prof. Dr. Wolfgang Wintermeyer	Department of Physical Biochemistry Max-Planck-Institute for Biophysical Chemistry Göttingen, Germany

Further members of the Examination Board:

Dr. Sarah Adio	Institute for Microbiology and Genetics Department of Molecular Structural Biology Georg-August-Universität Göttingen Göttingen, Germany
Prof. Dr. Alexander Stein	Membrane Protein Biochemistry Max-Planck Institute for Biophysical Chemistry Göttingen, Germany
Prof. Dr. Henning Urlaub	Bioanalytical Mass Spectrometry Max-Planck Institute for Biophysical Chemistry Göttingen, Germany

Date of oral examination:

16th of September 2021

Affidavit

I hereby declare that my dissertation **"Investigation of Mitochondrial Ribosome Regulators at the Inner Membrane"** has been written independently and with no other sources and aids than quoted.

……

Sabine Poerschke

Göttingen, July 2021

Parts of this thesis will be communicated in the following publication:

Dennerlein, S.*, **Poerschke S.***, Oeljeklaus S., Wang C., Richter-Dennerlein R., Sattmann J., Bauerschmidt D., Kolander E., Stoldt S., Langer T., Jakobs S., Warscheid B. and Rehling P. "Defining the interactome of the human mitochondrial ribosome identifies SMIM4 and TMEM223 as respiratory chain assembly factors.**"**
eLife (2021; *under revision*)

*denotes equal contribution

Poerschke S., Oeljeklaus S., Schenzielorz A., Sattmann J., Warscheid B., Dennerlein S. and Rehling P. "Expanding the Knowledge of the Mitochondrial Insertase: TMEM126A is a novel interacting partner of the human OXA1L-complex."
(2021; *Manuscript prepared for submission*)

Joint authors contribution to the first manuscript

(Defining the interactome of the human mitochondrial ribosome identifies SMIM4 and TMEM223 as respiratory chain assembly factors)

Name: Sabine Poerschke

Individual contribution: Generation of the stable C12ORF73-FLAG-expressing HEK293T cell line. All experiments in regard to the analysis of C12ORF73. Fig. 1D; Replicates for Fig.2D; Fig. 3A; Replicates for Fig. 4F; Fig. 5; Supplement 5B, 5C; Fig. 6 Preparation of Figures. Involved in writing the introduction and material and methods. Proofreading the manuscript.

Contribution to the second manuscript

(Expanding the Knowledge of the Mitochondrial Insertase: TMEM126A is a novel interacting partner of the human OXA1L-complex)

Name: Sabine Poerschke

Individual contribution: All experiments, except for mass spectrometry analysis; Figure preparation and writing the whole manuscript

Table of Contents

List of Figures

List of Tables

List of Abbreviations

AAA	ATPases Associated with various cellular Activities
ADP	Adenosine diphosphate
APS	Ammonium persulfate
ATP	Adenosine triphosphate
BN	Blue native
bp	Base pairs
BSA	Bovine serum albumin
°C	Degree Celsius
CI	Complex I
CII	Complex II
CIII	Complex III
CIV	Complex IV
Cas9	CRISPR associated protein 9
CoQ	Ubiquinone
COX	Cytochrome *c* oxidase
CRISPR	Clustered regularly interspaced short palindromic repeats
ddH_2O	Double-deionized water
DMSO	Dimethyl sulfoxide
DNA	Deoxyribonucleic acid
ECL	Enhanced chemiluminescence
EDTA	Ethylenediaminetetraacetic acid
EGTA	Ethyleneglycoltetraacetic acid
FCS	Fetal calf serum
g	gram
GFP	Green fluorescent protein
h	hour(s)
HCL	Hydrochloric acid
HEK	Human embryonic kidney
HEPES	4-(2-hydroxyethyl)-1-piperazineethanesulfonic acid

HRP	Horseradish peroxidase
HSP	Heat shock protein
IBM	Inner boundary membrane
IgG	Immunoglobulin G
IMM	Inner mitochondrial membrane
IMS	Intermembrane space
kDa	Kilodalton
KD	Knockdown
KO	Knockout
l	Liter
M	Moles per liter
mA	Milliampere
mg	Milligram
MIA	Mitochondrial intermembrane space assembly machinery
MICOS	Mitochondrial contact site and cristae organizing system
min	Minute(s)
MITRAC	Mitochondrial translation regulation assembly intermediate of cytochrome *c* oxidase
mM	Millimoles per liter
MOPS	3-(N-morpholino) propane sulfonic acid
MPP	Mitochondrial processing peptidase
mRNA	Messenger RNA
MTS	Mitochondrial targeting sequence
MT-CYB	Mitochondrial-encoded cytochrome *b*
NADH	Nicotinamide adenine dinucleotide
nDNA	Nuclear DNA
nm	Nanometer
NT	Non-targeting
OMM	Outer mitochondrial membrane
ORF	Open reading frame
OXA	Oxidase assembly translocase

OXPHOS	Oxidative phosphorylation
PAGE	Polyacrylamide gel electrophoresis
PAM	Presequence translocase-associated motor
PBS	Phosphate buffered saline
PCR	Polymerase chain reaction
PK	Proteinase K
PMSF	Phenylmethylsulphonyl fluoride
PVDF	Polyvinylidene fluoride
RNA	Ribonucleic acid
rpm	Revolutions per minute
SAM	Sorting and assembly machinery
SEM	Standard error of the mean
SDS	Sodium dodecyl sulfate
SILAC	Stable isotope labeling of amino acids in cell culture
siRNA	Small interfering RNA
TBS	Tris buffered saline
TEMED	N,N,N',N'-Tetramethylethane-1,2-diamine
TIM22	Carrier translocase of the inner membrane
TIM23	Presequence translocase of the inner membrane
TMD	Transmembrane domain
TOM	Translocase of the outer membrane
Tris	Tris(hydroxymethyl)aminomethane
tRNA	Transfer RNA
V	Volt
WT	Wildtype
µl	Microliter
µg	Microgram
%	Percent
$\Delta\psi$	Membrane potential across the mitochondrial inner membrane

Abstract

Mitochondrial biogenesis relies on the proper assembly of proteins from dual genetic origin. Nuclear-encoded proteins are imported into the organelle and incorporated into multiprotein complexes together with proteins synthesized on mitochondrial ribosomes. The OXPHOS machinery is composed of such multiprotein complexes (I-V) which are embedded into the inner mitochondrial membrane. To guarantee the functionality of the OXPHOS system, the assembly of these protein complexes is a highly coordinated process and dependent on the attendance of so-called respiratory chain assembly factors. Over the years, an enormous amount of research has been devoted to investigating the detailed mechanisms of individual assembly steps of each OXPHOS complex and by this, many assembly factors were identified. Because most of the research has been gleaned from studies using the model organisms *S. cerevisiae*, it became fascinating to look into higher eukaryotes as well.

In this study, the interactome analysis of the human mitochondrial large ribosomal subunit mL62 identified TMEM223 as a novel potential assembly factor for complex IV and SMIM4, a protein of small molecular weight, involved in complex III biogenesis. By defining the interactors of SMIM4^{FLAG} we further explored C12ORF73, which was previously described as essential complex III assembly factor in vertebrates (Zhang *et al.*, 2020). Our main interest laid in the characterization of the biochemical and mechanistic role of these proteins regarding the respective complex assembly. For this purpose, transient siRNA approaches and a TMEM223 knockout cell line (TMEM223$^{-/-}$) were used to analyze apparent changes in mitochondrial biogenesis. Furthermore, the potential timeframes when these assembly factors are acting were defined by analyzing the interactome of SMIM4^{FLAG} and C12ORF73^{FLAG}.

One of the crucial steps in complex biogenesis is the insertion of mitochondrial-encoded proteins into the inner mitochondrial membrane. From studies in *S. cerevisiae* it is assumed that the human homolog OXA1L plays a leading role in this process.

Mass spectrometry analyses provided insights into the interactome of the OXA1L- complex and identified TMEM126A as a potential interaction partner. This study explores the versatile function of TMEM126A concerning the OXA1L interaction linked to the biogenesis of the OXPHOS machinery and mitochondrial translation.

1. Introduction

1.1. Mitochondria: a unique organelle

Due to their endosymbiotic origin, mitochondria are surrounded by two membranes like their bacterial ancestor (Saccone *et al.*, 2000). The resulting compartments of this spatial separation are unique and assign the morphology of mitochondria (Figure 1.1) The outer mitochondrial membrane (OMM) contains phospholipids, similar to the cell membrane, and harbors protein-based pores which allow the interchange of metabolites and other small molecules up to 2-6kDa (Vogel *et al.*, 2006). In addition, the OMM with its integrated protein-complexes represents the entry gate for mitochondrial proteins which are synthesized on cytosolic ribosomes. The inner mitochondrial membrane (IMM) separates the matrix from the intermembrane space (IMS) and forms so-called cristae structures with their tubular invagination. The IMM is especially protein-rich and organized into two distinct subdomains: the inner boundary membrane (IBM) and the cristae membrane (Herrmann and Neupert, 2000; Vogel *et al.*, 2006). The IBM is in close contact to the OMM for the purpose of protein import across the mitochondrial membranes and primarily harbors complexes of the import machinery. The majority of the IMM is organized in cristae structures within the complexes of the OXPHOS system are located. Both subdomains are connected by cristae junctions which are characterized by the presence of the mitochondrial contact site and cristae organizing system (MICOS) (Anand *et al.*, 2021; Pfanner *et al.*, 2019).

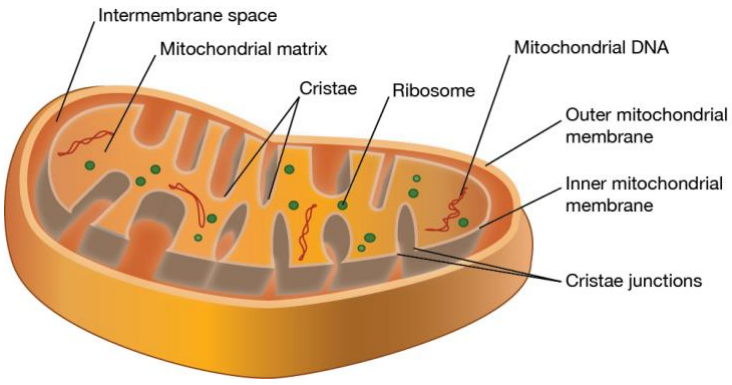

Figure 1.1 The structure of mitochondria. Mitochondria are double membrane bounded organelles and consist of an outer mitochondrial membrane and inner mitochondrial membrane. The mitochondrial inner membrane is shaped by so-called cristae structures which form cristae junctions close-by the outer membrane. Besides, the intermembrane space and the mitochondrial matrix form additional reaction compartments. Mitochondrial ribosomes and the mitochondrial DNA is located inside of the mitochondrial matrix.

The IMS represents a tiny compartment since the two membranes are only a few nanometers apart (~8nm) (Hansen and Herrmann, 2019; Herrmann and Neupert, 2000). Nevertheless, it contains different chaperones crucial for the protein import and is significantly involved in apoptotic signaling by segregating apoptotic components (Chacinska *et al.*, 2009; Wang and Youle, 2009). The mitochondrial matrix is the habitation of the mitochondrial DNA (mtDNA) and the mitochondrial gene expression machinery which also includes mitochondrial ribosomes (Yan *et al.*, 2019).

1.1.1. Structure of mitochondrial DNA

The mtDNA differs from the nuclear DNA (nDNA) but is quite similar to the bacterial chromosome. It is packaged as a circled, double-stranded DNA whereas the sense and the antisense strand are termed as heavy and light strand. In human, the mtDNA encodes for 37 genes, including the 13 polypeptides for the respiratory chain machinery, two rRNAs and 22 tRNAs which are required for the mitochondrial translation. The light strand contains 8 tRNAs and the polypeptide ND6, whereas 14 tRNAs, the two rRNAs and the other 12 polypeptides are located on the heavy strand. All 13 polypeptides represent core subunits of the OXPHOS complexes I, III, IV and V, and are crucial for the oxidative phosphorylation system (OXPHOS) (Richter-Dennerlein *et al.*, 2016; Stewart and Chinnery, 2021; Taanman, 1999). In contrast to nDNA, the mtDNA encloses only three promotor regions: LSP for the light strand and HSP1/HSP2 for the heavy strand which are localized within the D-loop (displacement loop) region. By this, mtDNA produces polycistronic transcripts. Additionally, the transcription and replication is conducted by the mitochondrial RNA polymerase (POLRMT), the mitochondrial transcription factor (TFAM), the transcription specificity factor: TFB1M and TFB2M, and the transcription termination factor (mTERF) (Stoccoro and Coppedè, 2021).

Due to the lack of histones in the structure, the mtDNA is vulnerable to stress-induced mutations and damage, which cause many human diseases (Gusic and Prokisch, 2021).

1.1.2. Mutation of mtDNA

Mutations of mtDNA are often associated with the dysfunction of the OXPHOS system and can end up in human diseases. The characteristic traits of these mitochondrial disorders are the presence of various neurological features associated with not only diabetes, Alzheimer´s disease and Parkinson's disease, but also with cardiovascular defects. It is assumed that mutations of the mtDNA can accumulate over time resulting in neurodegeneration and aging-related diseases (reviewed in Jang *et al.*, 2021; Yan *et al.*, 2019). Since the first mutation in mtDNA was observed in 1988 (Holt *et al.*, 1988), several mtDNA mutations were identified, for example a point mutation in complex V subunit ATP6 that leads to Leigh syndrome. Mutated mtDNA suggested to be involved also in cancer. 11% of prostate cancer patients harbor a mutation in the mitochondrial- encoded *COX1* which is the core subunit of complex IV (Barrientos *et al.*, 2009; Jang *et al.*, 2021; Mick *et al.*, 2007; Zhunina *et al.*, 2021).

1.2. The respiratory chain and oxidative phosphorylation

Mitochondria are ubiquitous organelles, their main purpose being the supply of cellular energy in the form of adenosine triphosphate (ATP), which is produced by the OXPHOS system. The OXPHOS machinery is composed of different multiprotein complexes and embedded into the IMM. In human, these multiprotein complexes are nominated as complex I-IV and the ATP synthase complex (complex V; Figure 1.2) (Winge, 2012). Apart from their individual functionality, the OXPHOS complexes can interact with each other by forming so-called supercomplexes (Brzezinski *et al.*, 2021; Schägger, 2002). To date, the function of supercomplexes is not known, but one possible explanation could be the efficacy of electron transport during oxidative phosphorylation (Hällberg and Larsson, 2014; Signes and Fernandez-Vizarra, 2018; Tang *et al.*, 2020).

During OXPHOS, electrons are supplied by the different metabolisms of nutrients, like sugar and fats, and by this an electrochemical proton gradient across the IMM is achieved. Except for complex II or succinate-ubiquinone oxidoreductase, all complexes of the respiratory chain have a proton-pumping activity (Figure 1.2). Complex I (NADH:ubiqionone oxidoreductase) shuttles two electrons from NADH to coenzyme Q, thereby four protons are translocated into the IMS. Complex II converts succinate to fumarate and transfers two electrons. Complex III or ubiquinol cytochrome *c*

oxidoreductase passes two protons per electron across the membrane using the Q-cycle mechanism. Finally, complex IV or cytochrome *c* oxidase catalyzes the oxidation of cytochrome *c* and reduction of oxygen to water by four electrons. Thus, four protons are translocated from the matrix into the IMS. Subsequently, the ATP synthase uses the provided proton gradient to generate ATP from ADP and inorganic phosphate (Fernandez-Vizarra and Zeviani, 2021; Letts and Sazanov, 2017; Signes and Fernandez-Vizarra, 2018).

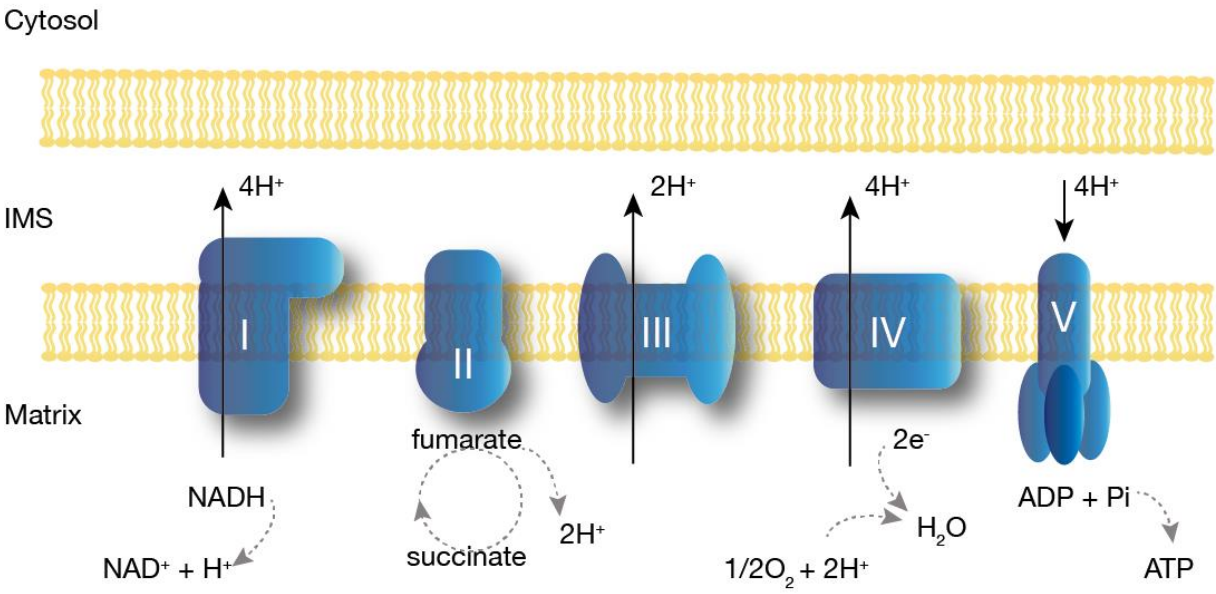

Figure 1.2 Schema of the respiratory chain from higher eukaryotes. The respiratory chain is composed of different multiprotein complexes and embedded into the inner mitochondrial membrane. Complex V generates ATP from ADP and inorganic phosphate by using the proton motive force generated via the proton-pumping activity of complex I, III and IV.

In human, many disorders are caused by the dysfunction of the OXPHOS machinery. Therefore, it is important to understand the intricate assembly mechanisms of the various complexes. Complex I, III, IV and V are composed of subunits from dual genetic origin, therefore, the assembly of mitochondrial- and nuclear-encoded subunits is a highly regulated process (Richter-Dennerlein *et al.*, 2016) This process includes the membrane insertion of mitochondrial-encoded proteins into the IMM which is underpinned by a multitude of assembly factors and ribosomal regulators within mitochondria. Because this study examines the relationship between the mitochondrial insertase OXA1L and novel assembly and interacting factors for

complex I and complex III, the next sections will focus on the early assembly steps of these special complexes.

1.2.1. Assembly of NADH:ubiquinone oxidoreductase

The largest complex of the OXPHOS machinery is complex I which provides 30-40% of the proton motive force required for the ATP synthesis (Giachin *et al.*, 2016). In mammalian cells, it is composed of 45 subunits arranged in different modules (N-, Q-, ND1- , ND2-, ND4-, and ND5-module; Table 1.1). These modules are organized in a L- shaped structure with a peripheral hydrophilic arm located in the matrix and a hydrophobic part forming the proton channel in the IMM (Figure 1.3). The seven subunits encoded by the mtDNA are embedded into the IMM and belong to the hydrophobic part (Giachin *et al.*, 2016; Mimaki *et al.*, 2012; Signes and Fernandez-Vizarra, 2018).

Table 1.1 Modules of the mammalian complex I and the corresponding subunits in order of their assembly.

	N-module	**Q-module**	**ND1-module**	**ND2-module**	**ND4-module**	**ND5-module**
Early subunits	NDUFV1	NDUFA5	MT-ND1	MT-ND2	NDUFB1	MT-ND5
	NDUFV2	NDUFS2	NDUFA3	NDUFC1	NDUFB4	NDUFB2
	NDUFS1	NDUFS3	NDUFA8	NDUFC2	NDUFB5	NDUFB3
	NDUFA2	NDUFS7	NDUFA13	NDUFAF1	NDUFB6	NDUFB7
		NDUFS8		MT-ND3	NDUFB10	NDUFB8
		NDUFAF3		MT-ND6	NDUFB11	NDUFB9
		NDUFAF4		MT-ND4L	MT-ND4	NDUFAB1
		NDUFAF6				
Late subunits	NDUFA6			NDUFA1		
	NDUFA12			NDUFA10		
	NDUFS4			NDUFS5		
	NDUFS6					
	NDUFV3					

Because of its different modules, the assembly of complex I is a complicated and highly monitored process. Previous studies provide the idea that nuclear-encoded complex I subunits can be assembled in sub-complexes even if mitochondrial-encoded subunits are absent (Dang *et al.*, 2020; Potluri *et al.*, 2004). This shows that the peripheral arm and the hydrophobic proton channel are independent from each other in the assembly state and are reliant on the commitment of various assembly factors which must be unique for each module.

So far, the most known complex I assembly factors are involved in the early assembly of complex I. Thereby, assembly factors are necessary to insert hydrophobic subunits to the IMM and to stabilize complex I intermediates (Giachin *et al.*, 2016; Heide *et al.*, 2012). In human, the most relevant assembly factors are NDUFAF1, ACAD9, ECSIT, TMEM126B and TIMMDC1 (Brandt, 2006; Giachin *et al.*, 2016; Mimaki *et al.*, 2012).

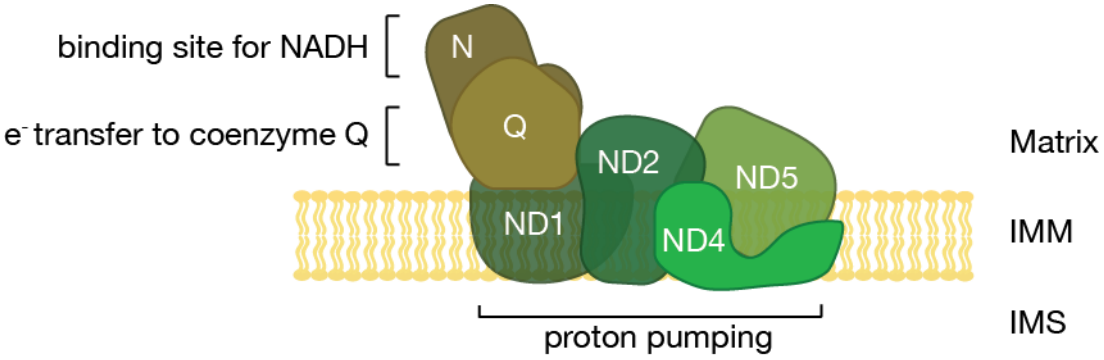

Figure 1.3 Model of complex I assembly. The Q-module binds to the ND1-module. Then, the ND2- and ND4-modules assemble in the inner mitochondrial membrane (IMM). The pre-assembled ND4- and ND5-modules join the complex. As last step, the tip of the whole complex formed by the N-module is incorporated. The proton translocase activity is conducted by the hydrophobic part in the IMM. Protons are translocated into the intermembrane space (IMS).

1.2.2. Assembly of ubiquinol-cytochrome *c* oxidoreductase

The entire knowledge about the assembly of complex III are based on studies from *S. cerevisiae* (Protasoni *et al.*, 2020). Due to structural similarities and the conservation of the first steps of complex III assembly, it is assumed that the intermediate steps are more comparable between yeast and mammalians with the comprehension of orthologous proteins (Figure 1.4). The biogenesis of complex III relies on the expression and coordinated assembly of ten nuclear-encoded subunits and the mitochondrial-encoded cytochrome *b* (MT-CYB). Together with cytochrome c_1 (CYC1)

and UQCRFS1, MT-CYB forms the catalytic core, which is organized in a tightly bound symmetrical dimer ($cIII_2$). Complex III assembly starts with the translation of MT-CYB on mitochondrial ribosomes. During the synthesis two translation factors are bound to the nascent polypeptide at the ribosomal exit tunnel – UQCC1 (yeast Cbp3) and UQCC2 (Cbp6). This starting point of assembly is called intermediate 0. Both translation factors mediate the insertion of newly synthesized MT-CYB into the IMM and dissociate once synthesis is completed. After incorporation of the first *haem b* (b_L) a third factor – UQCC3 (Cbp4) – joins the pre-complex and the second *haem* b_H can be integrated into the complex (intermediate I). The detachment of UQCC1/UQCC2 from the fully haemylated MT-CYB is triggered by the insertion of the structural subunit UQCRB (Qcr7) and UQCRQ (Qcr8) whereby the translation factors move back to the mitochondrial ribosome to activate a novel round of MT-CYB translation (intermediate II). The addition of UQCRFS1 (Rip1) together with the smallest subunit UQCR11 (Qcr10) to an already dimeric pre-complex III (pre-$cIII_2$) is the crucial $cIII_2$ maturation step and leads to its catalytic activity (Ghezzi and Zeviani, 2018; Ndi *et al.*, 2018; Signes and Fernandez-Vizarra, 2018; Smith *et al.*, 2012).

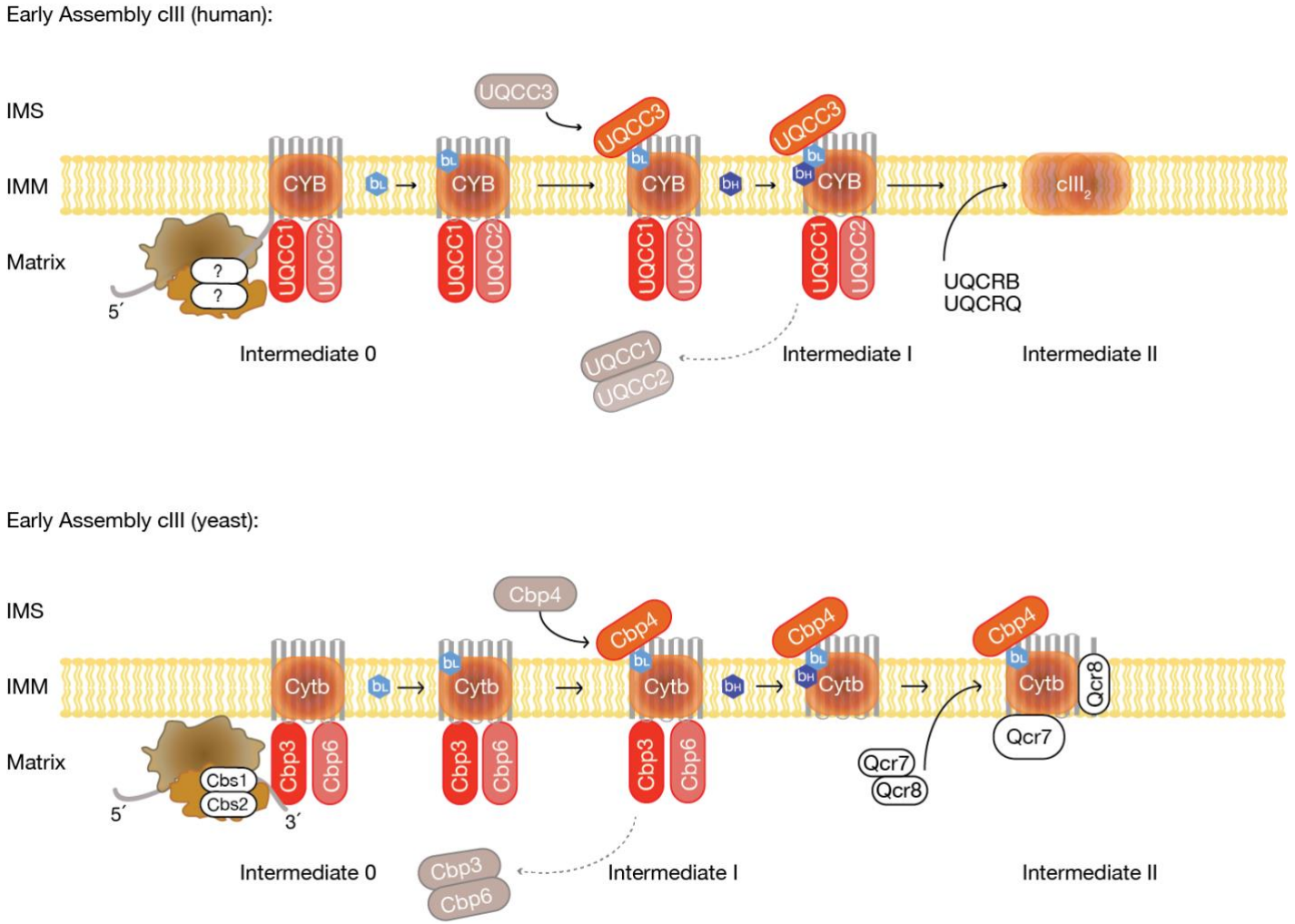

Figure 1.4 Schematic model of the assembly of the ubiquinol-cytochrome *c* oxidoreductase in yeast and human. Cytochrome *b*, the core subunit of complex III is inserted to the inner mitochondrial membrane co-translationally with the help of different assembly factors. The model of the assembly of the human complex III is based on the knowledge about orthologous proteins. Schema adapted from Ndi *et al.*. 2018.

1.3. Import of nuclear-encoded proteins into mitochondria

The mitochondrial proteome consists of 800 (yeast) to 1500(human) proteins but only 13 of these proteins are mitochondrial-encoded and subunits of the human oxidative phosphorylation system (OXPHOS) (Krämer *et al.*, 2021; Yasukawa and Kang, 2018). Since the majority of mitochondrial proteins are encoded by the nuclear genome, precursor proteins have to be imported from the cytosol through the mitochondrial membranes. This multistep process has to be coordinated in a stoichiometric and temporal manner and needs a mediated coordination of the mitochondrial translocation machinery and the precursor synthesis at cytosolic ribosomes (Nunnari and Suomalainen, 2012; Paschen and Neupert, 2001). The multicomponent translocation machineries are embedded in both the outer mitochondrial membrane (OMM) and the inner mitochondrial membrane (IMM) and consists of membrane-protein complexes and soluble proteins (Endo *et al.*, 2011; Maity and Chakrabarti, 2021). Even though it is well validated that the import of precursor proteins takes place post-transcriptionally, it cannot be obviated that it occurs as well in a co-translational manner (Dudek *et al.*, 2013). To guide precursor proteins to their destination inside mitochondria, most precursor proteins contain this information in the form of a mitochondrial targeting signal. In most cases, the targeting signal is a N-terminal leading sequence, also known as presequence or matrix-targeting sequence (MTS). This amphipathic α-helix is a 10 to 80 amino acid residue, positively charged and in most cases proteolytically removable after the import (Dudek *et al.*, 2013; Sokol *et al.*, 2014). Instead of the MTS, precursors can contain an internal targeting sequence as well. Whereas the properties of the MTS are widely conserved among different species, knowledge about internal targeting sequences remains largely elusive (Chacinska *et al.*, 2009; Neupert and Herrmann, 2007).

The carriage of proteins from the cytosol to the OMM is supported by the presence of cytosolic chaperones to maintain the solubility of precursor proteins and prevent folding and aggregation (Bhangoo *et al.*, 2007; Widmann and Christen, 1995). Once the precursor protein is escorted to the OMM, the import into mitochondria is initiated by the recognition of the targeting sequence via the translocase of the outer membrane – the TOM complex (Mori and Terada, 1998; W. Wang *et al.*, 2020).

Because the majority of our knowledge is based upon studies on *S. cerevisiae*, the following sections describe the general principles on the basis of this model organism given that most general mechanisms are conserved from yeast to human (reviewed in Dudek *et al.*, 2013; Figure 1.5).

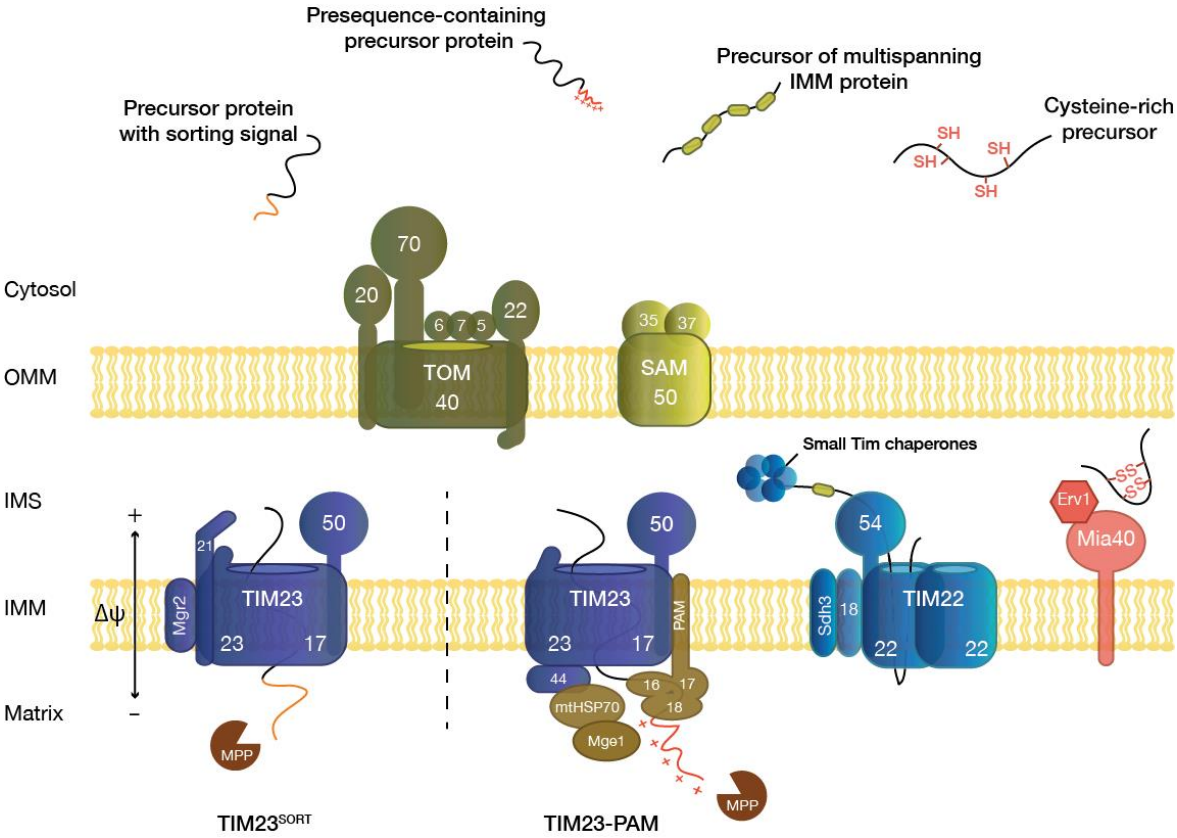

Figure 1.5 The major import pathways into mitochondria. Precursor proteins are imported from the cytosol into mitochondria using different translocases. The TOM complex is the general entry gate to cross the outer mitochondrial membrane (OMM). Proteins targeted to the inner mitochondrial membrane (IMM), or the matrix carry a presequence which is recognized by the TIM23 complex. Translocation for matrix proteins is warranted by the TIM23-PAM complex. Insertion into the IMM is conducted by the TIM22 complex and the small Tim chaperones. Cysteine-rich proteins belonging to the intermembrane space (IMS) are guided through the MIA pathway. β-barrel proteins are translocated to the OMM using the SAM complex. Schema adapted from Sokol *et al.*, (2014).

1.3.1. Translocation across the outer mitochondrial membrane

Independent from the mitochondrial targeting signal the translocase of the mitochondrial outer membrane (TOM complex) forms the entry gate for nearly all precursor proteins (Bausewein *et al.*, 2020; Chacinska *et al.*, 2009). On one hand, the TOM complex recognizes exclusively mitochondrial precursor proteins from the

cytosol and on the other hand it forms a channel which allows precursors to cross the hydrophobic outer membrane (Abe *et al.*, 2000; Harbauer *et al.*, 2014; Künkele *et al.*, 1998; Lithgow *et al.*, 1994). To recognize precursor proteins from the cytosol three subunits of the TOM complex act as receptors: Tom20, Tom22 and Tom70/Tom71. Whereas Tom20 and Tom22 mainly recognize precursors with presequences, Tom70 preferentially binds to precursors with internal targeting signals (Dudek *et al.*, 2013; Kiebler *et al.*, 1993; Wu and Sha, 2006). The core-subunit of the TOM complex is formed by the integral membrane protein Tom40 which is integrated into the OMM in a β-barrel structure and functions as a pore through which precursor proteins can pass (Dietmeier *et al.*, 1997; Endo and Yamano, 2010; Wasilewski *et al.*, 2017). Another component of the TOM complex are the so-called small Tom proteins – Tom5, Tom6, Tom7. Tom6 and Tom7 are acting in an antagonistic manner to stabilize the whole complex whereas Tom5 participates in the transfer of precursor proteins from Tom22 to Tom40 (Dietmeier *et al.*, 1997; Dudek *et al.*, 2013; Schmitt *et al.*, 2005).

1.3.1.1. The β-barrel assembly gate (SAM complex)

Because of the endosymbiotic origin, the mitochondrial outer membrane incorporates β-barrel proteins to allow the communication with the cytosol, e.g. transport of metabolites and organelle contact sites (Diederichs *et al.*, 2021; Schuler *et al.*, 2015; Walther and Rapaport, 2009). All known proteins from the outer membrane are nuclear-encoded and therefore imported as precursor proteins through the TOM complex into the intermembrane space (IMS). Then, the assembly and sorting of these precursor proteins into the outer membrane is mediated by the multi-subunit sorting and assembly machinery – SAM (Grevel *et al.*, 2020; Walther and Rapaport, 2009; Wiedemann and Pfanner, 2017).

The core component of the SAM complex is the β-barrel protein Sam50. It recognizes and binds to the β-signal of precursor proteins, guided through the SAM complex, together with its partner Sam35. Another subunit is the Sam37 protein which on the one hand promotes the release of precursor and on the other stabilizes the interaction of Sam50 with Sam35 (Diederichs *et al.*, 2021; Lionello *et al.*, 2020; Stojanovski *et al.*, 2007; Takeda *et al.*, 2021). Besides the channel protein VDAC, other β-barrel proteins are Tom40 as well as Sam50 (Höhr *et al.*, 2018).

1.3.2. Import into the intermembrane space

Mitochondrial proteins with characteristic cysteine residues, like the small Tim proteins or Cox17, are imported into the intermembrane space via the MIA pathway (mitochondrial intermembrane space assembly) (Chacinska *et al.*, 2008; Chatzi *et al.*, 2013; Mordas and Tokatlidis, 2015; Vögtle *et al.*, 2012). The import is redox-regulated and relies on the soluble protein and oxidoreductase Mia40, which uses its C-terminal tail to bind potential substrates. These substrates possess a specific cysteine region, arranged in two different motifs: CX_3C or CX_9C. Because Mia40 consists of a cysteine-proline-cysteine (CPC) motif, incoming precursor proteins form, together with Mia40, a transient intermolecular disulfide intermediate. After induction of disulfide bonds within the precursor itself, Mia40 rereleases the precursor into the intermembrane space (Chacinska *et al.*, 2009; Dudek *et al.*, 2013; Gabriel *et al.*, 2007; Sztolsztener *et al.*, 2013).

The second important component of this pathway, Erv1, is a sulfhydryl oxidase which acts as a recycler by accepting the electrons from the active CPC site from Mia40. Thereby, Mia40 is reoxidized and arising electrons are transmitted to cytochrome *c* (Ceh-Pavia *et al.*, 2013; Wrobel *et al.*, 2013).

1.3.3. The carrier translocase of the inner mitochondrial membrane

Hydrophobic, multi-spanning proteins of the inner mitochondrial membrane, containing internal targeting signals, are directed to the inner membrane via the unique TIM22 complex (Chacinska *et al.*, 2009; Rehling *et al.*, 2003). Most of these proteins belong to the family of mitochondrial metabolite carriers, like ADP/ATP carriers or to the phosphate carrier family (Söllner *et al.*, 1990; Zimmerman *et al.*, 1979). But additionally, three more proteins were investigated to be substrates of this translocase: Tim17, Tim22 and Tim23 (Káldi *et al.*, 1998). A long existing believe was that the substrates of the TIM22 complex must contain an even number of transmembrane domains. But recently, novel substrates were investigated which exhibit a putative topology of three and five transmembrane segments, e.g. pyruvate carrier proteins and members of the sideroflexin family (Gomkale *et al.*, 2020; Jackson *et al.*, 2021; Rampelt *et al.*, 2020).

After crossing the outer mitochondrial membrane (TOM complex), TIM22 substrates are escorted by a membrane-associated module composed of small Tim proteins (Tim9-Tim10-Tim12) throughout the intermembrane space until they reach the TIM22 complex. The TIM22 complex is embedded into the inner mitochondrial membrane and consists of the twin-pore Tim22, which forms the core subunit of the complex. The membrane potential (Δψ) - dependent insertion is then assisted by Tim54, Tim18 and Sdh3. Whereas Tim54 provides the binding site for proteins bound to the Tim9-Tim10-Tim12 intermediate, Tim18 is required for the assembly of Tim54 into the TIM22 complex (Callegari *et al.*, 2019; Dudek *et al.*, 2013; Jackson *et al.*, 2021; Truscott *et al.*, 2003a; Vasiljev *et al.*, 2004).

1.3.4. Translocation by the TIM23 complex

About two thirds of imported precursor proteins contain a N-terminal, cleavable presequence needed for the translocation via the major translocase of the inner mitochondrial membrane – the TIM23 complex (Callegari *et al.*, 2020). Both the translocation into the matrix including subsequent processing and the translocation into the IMM is mediated by this complex (Jensen and Dunn, 2002; Moulin *et al.*, 2019).

As mentioned before, the precursor proteins carry the targeting signal in form of a positively charged amphipathic α -helix. This helix varies in its length with 15-55 amino acid residues, even though precursors with less than ten or up to 100 residues have been described (Chacinska *et al.*, 2009; Mokranjac and Neupert, 2005; Straub *et al.*, 2016).

In addition, the presequence encloses three types of information to direct the precursor to its destination. First, the α -helix with its hydrophobic surface is recognized by Tom20, secondly the positively charged surface is necessary for the binding of Tom22 and thirdly, the overall positive net charge is crucial for the translocation using the membrane potential (Haucke *et al.*, 1995; Moulin *et al.*, 2019; Pfanner *et al.*, 2019; van der Laan *et al.*, 2006). Besides, the presequence contains a cleavable site which is recognized by the dimeric mitochondrial processing peptidase (MPP) when precursor proteins enter the matrix (Gakh *et al.*, 2002). A number of precursor proteins contain a hydrophobic sorting signal as well which is located directly after the matrix-targeting signal. This sorting signal is necessary in case precursor proteins should arrest in the inner mitochondrial membrane and are

released laterally into the lipid phase via the TIM23^{SORT} complex (Chacinska *et al.*, 2009; Moulin *et al.*, 2019).

The translocation via the TIM23 complex is a highly dynamic and versatile process but seems to be conserved from yeast to higher eukaryotes. The essential subunits forming the core (TIM23^{CORE}) are Tim50, Tim23 and Tim17. The non-essential part of the complex includes the proteins Tim21 and Mgr2 which then form the TIM23^{SORT} complex (Figure 1.5) (Chacinska *et al.*, 2009; Habib *et al.*, 2007; Lee *et al.*, 2020; Mokranjac and Neupert, 2005; Moulin *et al.*, 2019; van der Laan *et al.*, 2006). The pore across the inner mitochondrial membrane is formed by Tim23. Its N-terminal region located in the IMS is used as a receptor for incoming precursor proteins together with the intermembrane space domain of Tim50. Additionally, Tim50 is bound to the complex in its closed state to prevent ion leakage and dissipation of the membrane potential when precursor proteins are absent (Callegari *et al.*, 2020; Dudek *et al.*, 2013; Jensen and Dunn, 2002). The intermembrane space domain of Tim50 is not only bound to Tim23. It allows the interaction with Tom22 as well, together with precursor proteins in transit (Meinecke *et al.*, 2006). Tim17 is responsible for the stabilization of the whole complex, whereas Tim21 facilitates the transfer of precursor proteins to the pore (Chaudhuri *et al.*, 2020; Mick *et al.*, 2012). Once the precursor has been successfully transported, Tim21 dissociate from the complex and the precursor is laterally released to the inner mitochondrial membrane or further translocated into the matrix (Callegari *et al.*, 2020; Denkert *et al.*, 2017; Glick *et al.*, 1992; Meinecke *et al.*, 2006). For the translocation into the matrix another driving force is needed. This is warranted by the ATP-powered presequence translocase-associated motor – PAM (Marom *et al.*, 2011).

1.3.4.1. Matrix translocation using the import motor PAM

The translocation of precursor proteins into the mitochondrial matrix is aided by the import motor PAM (Marom *et al.*, 2011; Schulz *et al.*, 2015). This motor is based upon the heat-shock protein 70 (Hsp70) which constitutes the motor core and provides the ATPase activity (Dudek *et al.*, 2013; van der Laan *et al.*, 2010). In addition, the following co-chaperons are part of the motor complex: the J-protein Pam18, the J-like protein Pam16, Mge1, Tim44 and Pam17. Tim44, the scaffold protein, recognizes the precursor

proteins coming through the Tim23 channel and forms the membrane anchor for Hsp70. Pam16 and Pam18 acting in a module to stimulate the ATPase activity of Hsp70, whereas Pam17 is responsible for the integrity of the Pam16/Pam18 module by binding to Tim23 (Chacinska *et al.*, 2009; Frazier *et al.*, 2004; Schulz *et al.*, 2015; Truscott *et al.*, 2003). Finally, Mge1, the soluble nucleotide exchange factor, provokes the release of ADP from Hsp70. Consequently, the bound precursor is released into the matrix and a new reaction cycle of Hsp70 is initiated (Straub *et al.*, 2016; Westermann *et al.*, 1995).

1.4. The insertase for mitochondrial-encoded proteins

Although the majority of proteins of the inner mitochondrial membrane are imported from the cytosol, a proper membrane biogenesis of the OXPHOS complexes depends on the insertion of nuclear-and mitochondrial encoded membrane proteins. Hence, in eukaryotes, the mitochondrial translation machinery is responsible for the synthesis of a small number of polypeptides (Bohnert *et al.*, 2007; Szyrach *et al.*, 2003). All these polypeptides are core subunits of the OXPHOS complexes and therefore essential for the functionality of mitochondria. Mitochondrial-encoded proteins are exported to the inner membrane via its N-terminal domain, facilitated by the inner membrane protein Oxa1 (oxidase assembly factor 1), which is a member of the conserved Oxa1/YidC/Alb3 protein family (Hell *et al.*, 1998; Krüger *et al.*, 2012; Preuss *et al.*, 2005; Reif *et al.*, 2005). The relevance of Oxa1 in the biogenesis of the respiratory chain complexes is well established, but a detailed molecular picture on how Oxa1 operates while membrane insertion of polypeptides into the lipid bilayer is missing (Hell *et al.*, 2001; Krüger *et al.*, 2012). Even though the most studies are done in *S. cerevisiae*, the role of the human OXA1L protein is not well investigated yet. Therefore, the following sections address the knowledge of Oxa1 and its conserved homologs among prokaryotes and eukaryotes.

1.4.1. The conserved Oxa1/YidC/Alb3 protein family

Because membrane proteins make up 25-30% of the cellular proteome, its insertion and assembly into the right complexes are elementary for the cell's viability. Proteins that act as insertases for these membrane proteins are well-conserved among bacteria and certain eukaryotic organelles (Hell *et al.*, 2001). In bacteria, the insertion is mediated by YidC, a conserved protein of the IMM, which number of paralogs can vary. In gram-positive bacteria, like *Bacillus*, *Lactobacillus*, *Actinobacteria* and *Clostridi*a, two paralogs are present: YidC1 and YidC2. Both proteins comprise a core-domain which spans the membrane five times. In contrast to YidC1, a long C-terminal region of YidC2 is responsible for binding the ribosome which increases the folding rate of membrane proteins. Gram-negative bacteria contain only one version of YidC, which possess an extra transmembrane segment at the N -terminal domain (Funes *et al.*, 2011; Luirink *et al.*, 2001; Scotti *et al.*, 2000).

In the thylakoid membrane of chloroplasts, two proteins are involved in insertion into and across the membrane: Alb3 and Alb4 (Funes *et al.,* 2011; Itoh *et al.,* 2021). As YidC2 from bacteria, Alb3 contains a long C-terminal domain too which is lacking in the Alb4 protein.

The mitochondrial insertase Oxa1 shares a conserved domain with YidC consisting of five transmembrane spans. Like YidC2, Oxa1 contains a positively charged C-terminal tail which is responsible for binding the mitochondrial ribosome. Another distant homolog of YidC is Cox18/Oxa2 in *S. cerevisiae* and *Neurospora crassa*. Cox18 is responsible specifically for the biogenesis of Cox2 (cytochrome *c* oxidase subunit 2) and helps with the insertion post-transcriptionally by binding the C-terminal domain (Funes *et al.*, 2011; Zhang *et al.*, 2009).

Over the years, scientist corroborated the belief that Oxa1 and Alb3 hypothetically derived from the YidC protein of the endosymbiont (Zhang *et al.*, 2009). But recent studies have explored that the eukaryotic Oxa1 and Alb3 have two prokaryotic origins and did not arise directly from the YidC of proteobacteria, and therefore have diverse evolutionary histories (Scotti *et al.*, 2000; Zhang *et al.*, 2009). Nevertheless, a number of recent studies have reported that a mitochondria-targeted version of YidC can functionally replace Oxa1 in *S. cerevisiae*, whereas the YidC from *Escherichia coli* can be substituted by Alb3 and Alb4 of *Arabidopsis thaliana* (Bohnert *et al.*, 2010; Herrmann *et al.*, 1997; Reif *et al.*, 2005).

For this reason, it is of particular importance to understand the molecular functionality of the human insertase as well and draw comparisons between Oxa1 of *S. cerevisiae* and OXA1L in mammals.

1.4.1.1. The Oxa1 protein

The Oxa1 protein of *S. cerevisiae* is a nuclear-encoded mitochondrial protein of 36kDa, located in the IMM. Because it contains a N-terminal presequence, it is imported into mitochondria as a precursor and inserted into the IMM by Oxa1 itself. The import of Oxa1 is membrane potential dependent and requires the processing of the N - terminal tail (~90 amino acid residues) by MPP in the matrix (Altamura *et al.*, 1996; Bohnert *et al.*, 2010).

Oxa1 and its human homolog OXA1L consist of five transmembrane domains which span the IMM, whereas the N-terminal domain reside in the IMS, and the C-terminal tail is exposed to the matrix (Figure 1.6). Interestingly, the C-terminal region of Oxa1 in plants, fungi and animals show no obvious conservation at a primary sequence level (Krüger *et al.*, 2012; Szyrach *et al.*, 2003). The role of the C-terminal tail has been extensively studied *in vitro* as well as *in organello* and it was documented that both in *S. cerevisiae* and human, the C-terminal tail forms a α-helical domain which is necessary to bind to the mitochondrial ribosome (Haque *et al.*, 2010; Stiller *et al.*, 2016). Previous studies have examined, that the mitochondrial ribosome is anchored to the IMM by the large mitochondrial subunit L45 protein (mL45) which is associated with OXA1L (Itoh *et al.*, 2021). In addition, Oxa1 acts as a protein-conducting channel by forming a pore for its translocase activity. Electrophysiological single channel analysis investigated the size of this pore (0.6-2nm Ø) and defined that one active unit is built by four discrete channels, that are regulated in a substrate and membrane potential dependent manner. Thereby, each pore of one native Oxa1 unit is large enough to guide through polypeptides in an unfolded or secondary structure (Kohler *et al.*, 2009; Krüger *et al.*, 2012; Nargang *et al.*, 2002).

Primarily, Oxa1 was identified in two independent studies to investigate unknown yeast proteins involved in the biogenesis of the OXPHOS machinery (Bauer *et al.*, 1994; Bonnefoy *et al.*, 1994). Mutations in the *OXA1* nuclear gene in *S. cerevisiae* led to a complete respiratory deficiency and a lack of cytochrome oxidase activity as well as a defect in the assembly of the ATP synthase (Altamura *et al.*, 1996; Stuart, 2002). This pleiotropic phenotype conditioned by *oxa1* mutants indicated a more comprehensive function of Oxa1 in the overall biogenesis of the respiratory chain.

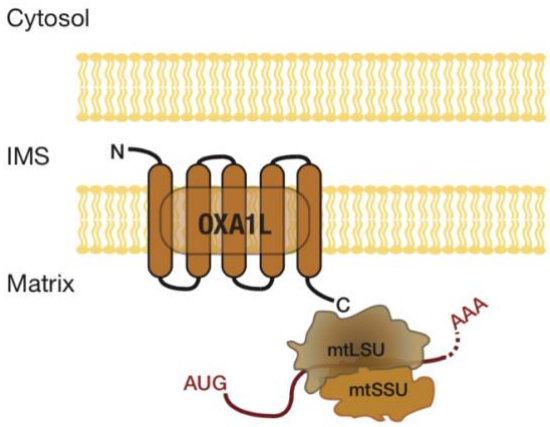

Figure 1.6 The human insertase OXA1L. OXA1L spans the inner mitochondrial membrane (IMM) five times and binds with its C-terminal tail to the mitochondrial ribosome**.** By this, nascent chains are inserted to the IMM co-translationally. Adapted from Haque *et al.*, 2010.

1.4.2. The OXA-related assembly of respiratory chain complexes

The insertion of proteins from the mitochondrial matrix to the IMM is warranted by the OXA (oxidase assembly) pathway and used by mitochondrial-encoded proteins as well as a subset of nuclear-encoded proteins (Oxa1, Cox18 and Mdl1) (Bohnert *et al.*, 2010; Stiller *et al.*, 2016). As mentioned before, all mitochondrial-encoded proteins, 7 (*S. cerevisiae*) or 13 (human), represent subunits of the OXPHOS complexes and require the OXA pathway for its insertion (Table 1.2).

Table 1.2 Mitochondrial-encoded subunits of the respiratory chain at its corresponding complexes in yeast and human.

OXPHOS complex	***S. cerevisiae***	**Mammalian**
NADH dehydrogenase		ND1, ND2, ND3, ND4/4L, ND5, ND6
Succinate dehydrogenase	-	-
Cytochrome bc_1 complex	Cytochrome *b*	Cytochrome *b*
Cytochrome oxidase complex	Cox1, Cox2, Cox3	COX1, COX2, COX3
ATP synthase	Atp6, Atp8, Atp9	ATP6, ATP8

Oxa1 interacts with mitochondrial proteins prior to their synthesis being completed by binding to the nascent polypeptide chains associated with the mitochondrial ribosome. From cross-linking studies in yeast, it is well known that Oxa1 interacts in an early stage with Cox1, Cox2, Cox3 and cytochrome *b,* while it needs the mitochondrial ribosome to stabilize these interactions (He and Fox, 1997; Hell *et al.*, 2001). Besides, Oxa1 is required for the co-translational insertion of Atp6, Atp8 and Atp9 (Jia *et al.*, 2003a). In yeast as well as in human it is established that Oxa1/OXA1L interacts with its C -terminal tail with the mitochondrial ribosome (Haque *et al.*, 2010; Jia *et al.*, 2003). Previous studies in *S. cerevisiae* have shown that deletion of the entire C-terminus blocks the insertion of mitochondrial translation products and therefore affects the biogenesis of the whole OXPHOS machinery. Interestingly, a truncation of the C- terminal domain does not influence the insertion of the nuclear-encoded membrane proteins Cox18 and Oxa1 itself, which are inserted to the IMM by the OXA pathway, too (Szyrach *et al.*, 2003). This study suggested the importance of Oxa1 and its role, not only as an insertase for membrane proteins into the IMM, but also as a checkpoint for the biogenesis of the OXPHOS machinery.

Most of our knowledge is based on studies done in *S. cerevisiae*. Even if Oxa1 is conserved, the similarities between Oxa1 and the human homolog OXA1L are only 33% (Thompson *et al.*, 2018). It is assumed that OXA1L functions in the same way as the yeast Oxa1 protein. However, obtained data regarding the deletions of OXA1L *in vitro* outlined the effect on complex I and complex V but, surprisingly, not on complex IV (Stiburek *et al.*, 2007). Additionally, a first male patient was identified harboring a biallelic *OXA1L* variant associated with a complex IV deficiency in skeletal muscle, which stands in opposition to the *in vitro* studies (Thompson *et al.*, 2018).

To this day, it is controversially debated how Oxa1/OXA1L mediates the insertion of proteins and it is tempting to speculate that other interacting partners are part of this insertion machinery (Krüger *et al.*, 2012). Especially since all other translocases within mitochondria are composed as multiprotein complexes, it is hard to believe that the OXA pathway includes solely the Oxa1/OXA1L protein.

1.5. Aims of this work

The mitochondrial inner membrane harbors multiprotein complexes, such as translocases and the complexes of the OXPHOS machinery. In the biogenesis of these complexes a multitude of so-called assembly factors are involved besides the structural subunits. Therefore, the assembly process must be coordinated in a highly temporal and stoichiometric manner above all, the subunits are from dual genetic origin. Even though the minority of mitochondrial proteins are encoded by a mitochondrial transcription and translation machinery, the co-translational insertion of these proteins seems to be a vital step for mitochondrial reliability.

From previous studies it is known that proteins involved in the assembly are bound to assembly intermediates at different stages (Richter-Dennerlein *et al.*, 2016; Soto *et al.*, 2012). To investigate regulators already bound to the human mitochondrial ribosome, the interactome of the subunit mL62 was analyzed by mass spectrometry. By this, SMIM4 and TMEM223 were identified, mitochondrial proteins of unknown function. In this study, the functionality of these proteins was analyzed biochemically in regard to the respective OXPHOS complexes. The protein-network of SMIM4 was further analyzed in HEK293T cells and explored the protein C12ORF73 as potential interacting partner.

In the second part of this study, the interactome of the OXA1L protein from HEK293T cells was determined using mass spectrometry analyses. Because the insertion of mitochondrial- encoded proteins into the inner membrane is guided by the insertase OXA1L, it was of particular interest to identify novel constituents of the human OXA1L-complex, which eventually support this task. We identified TMEM126A, a membrane protein described in parallel to this study as complex I assembly factor (D'Angelo *et al.*, 2021; Formosa *et al.*, 2021) and examined its role in the mitochondrial biogenesis. This study aimed to investigate the function of TMEM126A trough use of siRNA and CRISPR/Cas9-generated knockout cell lines. Since OXA1L is connected to the mitochondrial ribosome in a translational-independent manner (Richter-Dennerlein *et al.*, 2016), the interaction between TMEM126A and the mitochondrial ribosome was investigated under different conditions.

2. Results

2.1. Manuscript 1

Defining the interactome of the human mitochondrial ribosome identifies SMIM4 and TMEM223 as respiratory chain assembly factors

Sven Dennerlein[1,*], Sabine Poerschke[1,*], Silke Oeljeklaus[2,3], Cong Wang[1], Ricarda Richter-Dennerlein[1,4], Johannes Sattmann[1], Diana Bauermeister[1], Elisa Hanitsch[1], Stefan Stoldt[4,5,7], Thomas Langer[6], Stefan Jakobs[4,5,7], Bettina Warscheid[2,3] and Peter Rehling[1,4,8#]

[1]Department of Cellular Biochemistry, University Medical Center Göttingen, 37073, Göttingen, Germany

[2]Biochemistry and Functional Proteomics, Institute of Biology II, Faculty of Biology, University of Freiburg, 79104, Freiburg, Germany

[3]Signalling Research Centres BIOSS and CIBSS, University of Freiburg, 79104, Freiburg, Germany

[4]Cluster of Excellence "Multiscale Bioimaging: from Molecular Machines to Networks of Excitable Cells" (MBExC), University of Göttingen, Germany

[5]Department of NanoBiophotonics, Mitochondrial Structure and Dynamics Group, Max Planck Institute for Biophysical Chemistry, D-37077 Göttingen, Germany

[6]Department of Mitochondrial Proteostasis, Max Planck Institute for Biology of Ageing, D-50931 Cologne, Germany

[7]Department of Neurology, University Medical Center Göttingen, Germany.

[8]Max Planck Institute for Biophysical Chemistry, Göttingen, Germany.

*Authors contributed equally

Correspondence: Peter Rehling, Department of Cellular Biochemistry, University Medical Center Göttingen, Humboldtallee 23, 37073 Göttingen, Germany. Fax: +49 551 395979; Tel: +49 551 395947; Email: peter.rehling@medizin.uni-goettingen.de

Abstract

Human mitochondria express a genome that encodes thirteen core subunits of the oxidative phosphorylation system (OXPHOS). These proteins insert into the inner membrane co-translationally. Therefore, mitochondrial ribosomes engage with the OXA1L-insertase and membrane-associated proteins, which support membrane insertion of translation products and early assembly steps into OXPHOS complexes. To identify ribosome-associated biogenesis factors for the OXPHOS system, we purified ribosomes and associated proteins from mitochondria. We identified TMEM223 as a ribosome-associated protein involved in complex IV biogenesis. TMEM223 stimulates translation of COX1 mRNA and is a constituent of early COX1 assembly intermediates. Moreover, we show that SMIM4 together with C12ORF73 interacts with newly synthesized cytochrome *b* to support initial steps of complex III biogenesis in complex with UQCC1 and UQCC2. Our analyses define the interactome of the human mitochondrial ribosome and reveal novel assembly factors for complex III and IV biogenesis that link early assembly stages to the translation machinery.

Keywords: Mitochondria, Ribosome, Oxidative Phosphorylation, Assembly, Translation

Introduction

Mitochondria play key roles in a plethora of cellular processes such as signaling processes, metabolism, and energy production (Pfanner et al. 2019). Among this multitude of functions, cellular energy conversation by oxidative phosphorylation (OXPHOS) is a hallmark. ATP is produced by the mitochondrial OXPHOS system, which is comprised of the respiratory chain complexes I – IV and the F_1F_o-ATP-synthase (complex V). Except for complex II, these multi-subunit complexes in the inner mitochondrial membrane (IMM) are composed of nuclear- and mitochondrial-encoded proteins.

The human mitochondrial genome (mtDNA) encodes 2 rRNAs, 22 tRNAs and 13 proteins. These proteins are synthesized by membrane-associated mitochondrial ribosomes (mt-ribosome) to insert their translation products into the membrane co-translationally (Pfeffer et al. 2015; Englmeier et al. 2017). Subsequently, these subunits have to engage with nuclear-encoded, imported subunits to form functional enzyme machineries. This process requires a large number of chaperone-like assembly factors, which promote the maturation of the complexes through a number of assembly intermediates.

Since the accumulation of non-assembled OXPHOS proteins or subcomplexes can lead to the production of cellular damaging radicals (e.g. ROS), their assembly processes are highly regulated in a stoichiometrically and temporally manner, which is facilitated by a plethora of assembly factors. These biogenesis factors act at different maturation stages and stabilize assembly intermediates, insert cofactors or ensure the correct protein membrane integrity.

The assembly pathway of the cytochrome *c* oxidase is one of the best characterized processes (Dennerlein et al. 2017; Timón-Gómez et al. 2017). The three core proteins COX1, COX2 and COX3 are encoded by the mtDNA. COX1 represents the step-stone of the assembly pathway, while COX2 and COX3 get added in a sequential manner. In the yeast *Saccharomyces cerevisiae* (*S. cerevisiae*), COX1 translation is regulated by translational activators that bind to the 5' untranslated region (UTR) of COX1 mRNA. However, due to the lack of a significant 5'UTR of human COX1 mRNA, such a mechanism probably does not exist in human mitochondria. It has been recently shown that COX1 translation is regulated by early and late assembly stages. MITRAC (mitochondrial translation regulation assembly intermediate of the

cytochrome *c* oxidase) represents the COX1 specific assembly intermediate, which comprises at least two sub-complexes (MITRAC^{early} and MITRAC^{late}) (Mick et al. 2012; Richter-Dennerlein et al. 2016). MITRAC^{early}, which interacts directly with the mt-ribosome during COX1 synthesis, is considered as the COX1 translation regulation complex, containing C12ORF62 and MITRAC12 (Richter-Dennerlein et al. 2016). In MITRAC^{late} the first nuclear-encoded subunit, COX4I1, joins the assembly intermediate impairing the accomplishment of COX1 synthesis. Thus, the transition from MITRAC^{early} to MITRAC^{late} represents a key regulatory step for COX1 synthesis and downstream events during cytochrome *c* oxidase biogenesis. However, how the MITRAC complexes regulate COX1 translation on a molecular level remains unclear.

Other mitochondrial OXPHOS assembly pathways, such as for the cytochrome *c* reductase (complex III) have been predominantly investigated in *S. cerevisiae*. The biogenesis of the cytochrome *c* reductase relies on the expression and coordinated assembly of ten nDNA-encoded subunits and one mtDNA-encoded subunit, cytochrome *b* (CytB). The assembly process starts with the translation of CytB. During synthesis two translation factors are bound to the nascent polypeptide emerging at the exit tunnel – Cbp3 (UQCC1) and Cbp6 (UQCC2), forming intermediate 0 (Fernández-Vizarra and Zeviani 2018; Ndi et al. 2018). Both translation factors mediate the insertion of newly-synthesized CytB into the IMM and dissociate once synthesis is complete. After incorporation of the first haem-b (bL), a third factor – Cbp4 (UQCC3) joins the pre-complex and the second heam bH gets integrated (intermediate I) (Fernández-Vizarra and Zeviani 2018; Ndi et al. 2018). The release of Cbp3/Cbp6 (UQCC1/UQCC2) from the fully hemylated CytB is triggered by the insertion of the structural subunits Qcr7 (UQCRB) and Qcr8 (UQCRQ). In yeast, the translation activators Cbp3/Cbp6 are now available to initiate a new translation cycle of CytB (intermediate II) (Fernández-Vizarra and Zeviani 2018; Ndi et al. 2018). The addition of Rip1 (UQCRFS1) together with the smallest subunit Qcr10 (UQCR11) to a dimeric subcomplex (pre-cIII2) is a crucial maturation step and ensures its catalytic activity. The composition of the cytochrome c reductase from yeast to human is highly similar, where cytochrome c1 (CYC1), Rip1 (UQCRFS1) and CytB (CYTB) form the core, which is organized in a tightly bound symmetrical dimer.

To define the interplay of translation and assembly of mitochondrial OXPHOS complexes we defined the interactome of the human mt-ribosome under mild solubilization conditions. Among the identified proteins, we detected the

uncharacterized protein TMEM223 and show that it is involved in cytochrome *c* oxidase assembly. Furthermore, we identified SMIM4, which interacts with the recently described cytochrome *c* reductase assembly factor C12ORF73 (Zhang et al. 2020). We demonstrate that both proteins are involved in cytochrome c reductase biogenesis and that their interplay links mitochondrial translation to cytochrome c reductase assembly.

Results

Identification of TMEM223 and SMIM4 as mt-ribosome-associated proteins

At the IMM, the mt-ribosome synthesizes thirteen essential OXPHOS subunits in human. During translation it associates with the OXA1L insertase and early assembly factors of the OXPHOS system (Itoh et al. 2021). To identify factors that are associated with the mt-ribosome and thereby cater to OXPHOS biogenesis, we generated a human HEK293T cell line that enables inducible expression of a FLAG-tagged version of the ribosomal subunit mL62^{FLAG} (Richter-Dennerlein et al. 2016). mL62 is a component of the 39S large ribosomal subunit (39S mtLSU) (Richter et al. 2010; Brown et al. 2014; Greber et al. 2014; Busch et al. 2019). To capture interactions of proteins with the mitochondrial translation machinery, we performed co-immunoisolation experiments under mild solubilization conditions. Proteins that co-purified with mL62^{FLAG} were subjected to sucrose gradient centrifugation and gradient fractions analyzed by western blotting. As expected, the gradient distribution of mL62^{FLAG} revealed a free pool of mL62^{FLAG} in fractions 1 to 3 (Figure 1A), a fraction of mL62^{FLAG} that co-sedimented with the 39S mtLSU (fractions 7 and 8) and with the 55S mt-ribosome (fraction 10) as previously reported (Richter et al. 2010).

To identify mt-ribosome-associated proteins in human mitochondria, we defined the interactome of mL62^{FLAG} by quantitative mass spectrometry using stable isotope labelling with amino acids in cell culture (SILAC) (Figure 1B, Supplement Table 1). As expected, we recovered all components of the mt-ribosome with high enrichment factors (Figures 1B and C). In addition, we found proteins of mtDNA and mtRNA maintenance, mt-ribosome biogenesis factors, and known OXPHOS assembly factors in the mL62^{FLAG} interactome (Figure 1C). Additionally, we identified the uncharacterized protein TMEM223 and the putative mt-ribosome interacting protein SMIM4 (Busch et al. 2019). To confirm the interaction of TMEM223 and SMIM4 with the mt-ribosome, we performed immunoisolations of mL62^{FLAG} from solubilized mitochondria and subjected the eluates to western blot analysis (Figure 1D). TMEM223 (Figure 1D, left panel) and SMIM4 (Figure 1D, right panel) were readily detectable in the eluate together with the ribosomal proteins uL1m and uS14m. Accordingly, TMEM223 and SMIM4 represent so far uncharacterized interactors of the mt-ribosome.

TMEM223 is an inner mitochondrial membrane protein

The identification of the uncharacterized TMEM223 as a new mt-ribosome interacting protein led us to investigate the function of this protein. TMEM223 displays two putative transmembrane spans but lacks a defined N-terminal targeting sequence (Figure 2A). To address the submitochondrial localization of TMEM223, we subjected mitochondria to hypo-osmotic swelling and carbonate extraction experiments (Figures 2B and C). To detect TMEM223, we used an antibody directed against the C-terminus of the protein. Upon Proteinase K treatment of mitoplasts, a faster migrating C-terminal fragment of TMEM223 was detected (Figure 2B). This finding indicates that the C-terminus was exposed to the mitochondrial matrix and that the fragment represents the second transmembrane domain and the C-terminus. As TMEM223 was resistant to carbonate extraction (Figure 2C), we concluded that TMEM223 is an integral protein of the IMM with its N- and C-termini facing the mitochondrial matrix.

To investigate the function of TMEM223, we generated a TMEM223 knockout cell line (TMEM223$^{-/-}$) utilizing a CRISPR/Cas9 approach. For this, we targeted the TMEM223 gene and confirmed the genomic modification by sequencing. The TMEM223$^{-/-}$ cell line displayed nucleotide exchanges that resulted in a premature stop codons. Loss of TMEM223 was further confirmed by western blot analysis of purified mitochondria (Figure 2D). In TMEM223$^{-/-}$ mitochondria, we observed a reduction of complex IV constituents (COX4I1, COX6A) and early COX1 assembly factors (C12ORF62, MITRAC12). In contrast, proteins of other OXPHOS complexes, such as NDUFA9 (complex I), SDHA (complex II), RIESKE (complex III), and ATP5B (complex V) remained unaffected. Accordingly, loss of TMEM223 impaired specifically the abundance of complex IV subunits.

TMEM223 is involved in cytochrome *c* oxidase biogenesis

The reduction of complex IV subunits prompted us to investigate mitochondrial OXPHOS complexes. We observed a selective reduction of the cytochrome *c* oxidase by Blue Native-PAGE (BN-PAGE) analyses, while other OXPHOS complexes remained unaffected (Figure 3A). For a quantitative assessment, we measured cytochrome *c* oxidase activity using a colorimetric assay. In agreement with the BN-PAGE analyses, the activity of the cytochrome *c* oxidase in TMEM223$^{-/-}$ cells was reduced to 62.5% of wild type (Figure 3B).

Since we identified TMEM223 as a mt-ribosome-associated protein and observed a reduction of the cytochrome *c* oxidase, we asked whether TMEM223 was required for translation of mitochondrial-encoded complex IV subunits. Therefore, we performed [^{35}S]methionine labelling of mitochondrial translation products. These analyses revealed a significant decrease in the levels of newly synthesized COX1 while other mitochondrial-encoded proteins, including COX2 and COX3, displayed no significant differences in TMEM223$^{-/-}$ compared to wild type (Figure 3C). These data suggest an involvement of TMEM223 in the early stages of cytochrome *c* oxidase biogenesis. To address this, we performed FLAG-immunoisolations using tagged constituents of the early COX1 assembly intermediates (MITRAC complexes), namely C12ORF62/COX14 (Weraarpachai et al. 2012; Richter-Dennerlein et al. 2016) (Figure 3D) and MITRAC12/COA3 (Mick et al. 2012) (Figure 3E). As a control, we used MITRAC7, a later stage assembly factor of COX1 (Dennerlein et al. 2015) (Figure 3F). TMEM223 was recovered in the eluate of C12ORF62^{FLAG} and MITRAC12^{FLAG}, but was not present in MITRAC7^{FLAG} purifications (Figures 3D-F). These findings support a role of TMEM223 in the first steps of cytochrome *c* oxidase biogenesis and show that it interacts with early MITRAC complexes.

Protein interaction network of SMIM4

Our mass spectrometric analysis identified the uncharacterized protein SMIM4 as a new mt-ribosome-associated protein (Figures 1B and D). SMIM4 displays one predicted transmembrane domain (amino acid 20 to 41) (Figure 4A). To investigate localization and function of SMIM4, we generated a stable HEK293T cell line, allowing for inducible expression of a C-terminally FLAG-tagged variant of SMIM4 (SMIM4^{FLAG}). We investigated the sub-cellular localization of SMIM4^{FLAG} by STED super-resolution light microscopy using a FLAG-specific antibody. Comparison with a TOM22 specific antibody labeling showed that SMIM4^{FLAG} localizes to mitochondria (Figure 4B). To investigate the submitochondrial localization of SMIM4, we performed hypo-osmotic swelling and carbonate extraction experiments. The C-terminal FLAG epitope of SMIM4 became accessible to Proteinase K digestion upon disruption of the outer mitochondrial membrane (Figure 4C). Furthermore, SMIM4 was resistant to carbonate extraction (Figure 4D) indicating that SMIM4 is an integral IMM protein facing its C-terminus to the intermembrane space (IMS).

To assess the function of SMIM4, we first defined its interactome. For this, we analyzed SMIM4^{FLAG}-containing protein complexes purified from mitochondria following a SILAC-based quantitative mass spectrometry approach (Figure 4E, Supplement Table 2). SMIM4^{FLAG} efficiently isolated components of the 28S mtSSU and 39S mtLSU supporting its interaction with the mt-ribosome (Figures 1C and D). Additionally, we identified in SMIM4^{FLAG} complexes the cytochrome *c* reductase (complex III) assembly factors UQCC1, UQCC2 and C12ORF73 (Tucker et al. 2013; Fernández-Vizarra and Zeviani 2018; Ndi et al. 2018; Zhang et al. 2020) as well as components of the mitochondrial quality control system, such as the *m*AAA-protease (AFG3L2 and SPG7), the *i*AAA-protease (YME1L), the membrane scaffolds SLP2 and prohibitins (PHB1, PHB2). In agreement with the mass-spectrometric analysis, we detected YME1L, SLP2, AFG3L2 and PHB1, C12ORF73, and UQCC1 in the SMIM4^{FLAG} eluate by immunoblotting (Figure 4F). Interestingly, proteins acting in later assembly steps of the cytochrome *c* reductase such as UQCC3 and RIESKE (Wanschers et al. 2014; Fernández-Vizarra and Zeviani 2018; Ndi et al. 2018) were not detected. In summary, SMIM4 is an integral protein of the IMM that interacts with the mitochondrial quality control machinery and early cytochrome *c* reductase biogenesis factors.

C12ORF73 and SMIM4 are involved in cytochrome *c* reductase maturation

C12ORF73 was recently found to contribute to cytochrome *c* reductase biogenesis. However, its function in the assembly process remains elusive. To define its role in cytochrome *c* reductase assembly, we generated an inducible C12ORF73^{FLAG}-expressing HEK293T cell line. We confirmed mitochondrial localization of C12ORF73^{FLAG} by STED super-resolution light microscopy, applying a specific FLAG antibody and as mitochondrial marker an antibody directed against TOM22 (Figure 5 - figure supplement 1A) (Stoldt et al. 2019). The C12ORF73^{FLAG} signal was superimposable with the mitochondrial marker TOM22 supporting mitochondrial localization of the protein in human cells. Biochemical analyses to determine the submitochondrial localization of C12ORF73^{FLAG} showed that the protein was resistant to carbonate extraction and that its C-terminus was accessible to protease treatment when the outer membrane was disrupted by hypo-osmotic swelling (Figure 5 – figure supplement 1B and C). These results confirmed that C12ORF73 represents a protein

of the IMM that exposes its C-terminus into the intermembrane space, which agrees with previous studies (Zhang et al. 2020).

Since we found C12ORF73 together with early cytochrome *c* reductase assembly factors in the interactome of SMIM4^{FLAG} (Figures 4E and F), we dissected the interaction of C12ORF73 with the cytochrome *c* reductase assembly machinery. To this end, we subjected mitochondrial extracts of C12ORF73^{FLAG}-containing mitochondria to immunoisolations and analyzed the eluates by western blotting (Figure 5A). Similar to SMIM4 co-immunoisolations (Figure 4F), we recovered UQCC1 and UQCC2, but not UQCC3 or RIESKE, co-isolating with C12ORF73^{FLAG} (Figure 5A). As SMIM4 (Figures 4 E and F) and C12ORF73 (Figure 5A) isolated early cytochrome *c* reductase assembly factors, we determined the function of these proteins utilizing siRNA-mediated depletion. Hence, we investigated protein levels in whole cell extracts after siRNA-mediated depletion. SMIM4 was reduced in C12ORF73-depleted cells and *vice versa* SMIM4 ablation led to decreased C12ORF73 levels indicating an interdependency of these factors (Figure 5B). While we observed a subtle increase of UQCC3 in SMIM4-depleted cells, UQCC1 and UQCC2 were slightly reduced upon C12ORF73 knockdown (Figure 5B). To investigate cell viability upon SMIM4 or C12ORF73 depletion, we quantified cell numbers after 72h siRNA-mediated knock-down in glucose- or galactose-containing media (Figure 5C). In both cases we observed a drastic reduction in cell growth to approximately 50% compared to the wild type.

Considering the interaction of SMIM4 (Figures 4E and F) and C12ORF73 (Figure 5E) with cytochrome *c* reductase assembly factors and the growth phenotype upon 72h protein depletion (Figure 5C), we assessed mitochondrial OXPHOS complexes upon SMIM4 or C12ORF73 depletion by BN-PAGE analyses (Figures 5D and E). siRNA-mediated knockdown of SMIM4 led to a strong reduction of cytochrome *c* reductase and to a minor extend of the cytochrome *c* oxidase, while other OXPHOS complexes remained unaffected (Figure 5D). Knockdown of C12ORF73 impaired the level of the NADH:ubiquinone oxidoreductase, cytochrome *c* reductase, and also slightly the cytochrome *c* oxidase (Figure 5E).

SMIM4 and C12ORF73 participate in early steps of cytochrome *c* reductase assembly

To define SMIM4- and C12ORF73-contaning complexes in cytochrome *c* reductase biogenesis, we solubilized mitochondria under mild conditions and separated protein complexes by first dimension BN-PAGE followed by a second dimension SDS-PAGE (Figure 6A). UQCC1 and UQCC2 were detected in two complexes between 132 – 250 kDa and in a smaller complex of approximately 70 kDa. UQCC3 appeared in a complex that migrated slightly slower than the biggest complex of UQCC1 and UQCC2 as well as in a complex below 66 kDa. SMIM4- and C12ORF73-containing complexes mainly co-migrated with the largest UQCC1- and UQCC2-containing complex, but moderately faster than the biggest UQCC3 complex. These data supported the idea that SMIM4 and C12ORF73 are part of an early cytochrome *c* reductase assembly intermediate with UQCC1 and UQCC2. When we isolated C12ORF73^{FLAG}-containing complexes from mitochondria and subjected these purified complexes to BN-PAGE followed by SDS-PAGE, C12ORF73^{FLAG} isolated UQCC1, UQCC2, and SMIM4, all of which migrated in a single complex (Figure 6B). These results demonstrate that C12ORF73^{FLAG} forms a complex with UQCC1, UQCC2, and SMIM4 but not with UQCC3. In agreement with this, SMIM4 and C12ORF73 were efficiently isolated with UQCC1^{FLAG} and UQCC2^{FLAG} but only in minor amounts with UQCC3^{FLAG}. RIESKE was only present in the UQCC3^{FLAG} eluate (Figure 6C).

The interaction between SMIM4, C12ORF73, UQCC1, and UQCC2 as early cytochrome *c* reductase assembly factors implies that SMIM4 and C12ORF73 interact with newly synthesized cytochrome *b* (CYTB). Therefore, we performed [^{35}S]methionine labelling of newly translated mitochondrial-encoded proteins and subjected cellular extracts to immunoisolation using antibodies against SMIM4 or C12ORF73 (Figure 6D). As expected, both immunoisolations clearly enriched newly synthesized CYTB.

As SMIM4 and C12ORF73 were present in early assembly intermediates and their loss led to a reduction of the cytochrome *c* reductase, we addressed at which stage a loss of C12ORF73 affects cytochrome *c* reductase assembly. For this we determined assembly intermediates upon loss of C12ORF73. To this end, we depleted C12ORF73 in UQCC1^{FLAG}-expressing cells and subjected mitochondrial extracts to immunoisolations. Purified complexes were analyzed by BN-PAGE followed by SDS-PAGE (Figure 6E). In comparison to the control, we observed an accumulation of a

cytochrome *c* reductase subcomplex containing CYTB, UQCC1^{FLAG} and UQCC2 in C12ORF73-ablated cells (Figure 6E, red arrow). In summary, our work defined SMIM4 and C12ORF73 as two new factors that act early in the biogenesis of the cytochrome *c* reductase.

Discussion

Recent analyses shed light on the mitochondrial translation machinery and provide an understanding of the biogenesis and the structural organization of the mt-ribosome (Brown et al. 2014; Hällberg and Larsson 2014; Amunts et al. 2015; Ferrari et al. 2020; Kummer and Ban 2021; Maiti et al. 2021). Additionally, factors that regulate the translation of mitochondrial-encoded proteins have been identified (Kummer and Ban 2021). However, the mechanisms underlying coordination of mitochondrial translation with OXPHOS assembly and the involved factors remain poorly understood (Hällberg and Larsson 2014; Richter-Dennerlein et al. 2015; Dennerlein et al. 2017; Kummer and Ban 2021).

In this study we aimed to define the interactome of the mt-ribosome in human cells with a special focus on its membrane-bound interaction partners. Using mild solubilization and purification conditions, we identified previously described auxiliary factors (Busch et al. 2019; Kummer and Ban 2021) and the IMM proteins TMEM223 and SMIM4 as mt-ribosome interactors. In agreement, a recent complementary proteomic study in mouse, which identified new mt-ribosome biogenesis factors, also listed SMIM4 in the group of uncharacterized mt-ribosome interacting proteins (Busch et al. 2019). We show that TMEM223 is involved in assembly of the cytochrome *c* oxidase, while SMIM4 and the interacting C12ORF73 contribute to the biogenesis of the cytochrome *c* reductase.

We show that TMEM223 is an IMM protein. Thus, our data represent experimental evidence for a prediction by Sanchez-Caballero et al. (2020) (Sánchez-Caballero et al. 2020). TMEM223 acts early in the assembly process of the mitochondrial-encoded COX1 and is required for cytochrome *c* oxidase assembly. Interestingly, depletion of TMEM223 affects COX1 synthesis. This is in line with the observation that TMEM223 is found in the early assembly MITRAC intermediate together with C12ORF62. C12ORF62 was previously shown to bind mt-ribosomes and is required for efficient COX1 translation (Weraarpachai et al. 2012; Richter-Dennerlein et al. 2015; 2016; Dennerlein et al. 2017). However, TMEM223 is released from COX1 during assembly of other subunits, as it is not associated in association with later MITRAC complexes, which are characterized by the presence of MITRAC7. These findings support the idea of TMEM223 representing a new early COX1 assembly factor that links biogenesis processes with translation.

In addition to TMEM223, we identified SMIM4 as a mt-ribosome-associated factor. Our work link SMIM4 to known early assembly factors for complex III (UQCC1 and UQCC2) and identified C12ORF73 as SMIM4-associated protein. Both, SMIM4 and C12ORF73; are functional interdependent, since loss of C12ORF73 leads to a reduction of SMIM4 and *vice versa* loss of SMIM4 leads to a reduction of C12ORF73. We show that SMIM4 and C12ORF73 regulate cytochrome *c* reductase assembly. The interactions with newly synthesized CYTB and UQCC1 and UQCC2 position both proteins in the very early steps of the assembly process. Assembly of the cytochrome *c* reductase has been poorly investigated in mammals but is considered to recapitulate the process in the yeast system based on the high similarity in structure and composition of the yeast and human complexes (Zara et al. 2009; Smith et al. 2012; Fernández-Vizarra and Zeviani 2018; Ndi et al. 2018). The assembly process initiates with the synthesis of CytB and the association of the translational regulators Cbp3 (human UQCC1) and Cbp6 (UQCC2). Subsequently, Cbp3 (UQCC3) joins CytB. SMIM4 and C12ORF73 interact predominantly with UQCC1 and UQCC2 but not with UQCC3. Accordingly, both proteins are involved in the early steps of cytochrome *c* reductase assembly. Interestingly, SMIM4 and C12ORF73 are not conserved in yeast, indicating differences in complex *c* reductase assembly between yeast and human. In a recent analysis, the zebrafish homolog of C12ORF73, BRAWNIN (BR), was suggested to contribute to cytochrome *c* reductase assembly (Zhang et al. 2020). However, depletion experiments did not reveal any assembly intermediates. Accordingly, BR was suggested to act prior to complex dimerization. On the other hand, BN- and SDS-PAGE analyses indicated that BR partially comigrated with the dimerized form of the cytochrome *c* reductase (Zhang et al. 2020). In our study, siRNA-mediated depletion of C12ORF73 or SMIM4 caused a reduction of the cytochrome *c* reductase. In contrast to the reports on BR (Zhang et al. 2020), C12ORF73 does not interact with late complex constituents but rather shows exclusively an association with the early assembly factors UQCC1 and UQCC2. This observation positions SMIM4 and C12ORF73 to early assembly steps rather than to the late complex formation stages. This is further underlined by the fact that both proteins are only present in the UQCC1 and UQCC2 assembly intermediates.

In conclusion, we defined the interactome of the human mt-ribosome and identified three previously uncharacterized membrane proteins as mt-ribosome-associated factors. Importantly, we unravel their functions as cytochrome *c* reductase

401 and cytochrome *c* oxidase assembly factors that support the immediate assembly of
402 newly synthetized proteins into further assembly intermediates. Functional
403 characterisation defined TMEM223 as essential for cytochrome *c* oxidase maturation,
404 while SMIM4 / C12ORF73 acting as cytochrome *c* reductase biogenesis factors.
405
406

Acknowledgments

We thank B. Knapp, C. Ronsör and F. Holtkotte for technical assistance. Supported by the European Research Council Advanced grants (ERCAdG No. 835102, SL) and (ERCAdG No. 339580, PR), Deutsche Forschungsgemeinschaft (DFG) under Germany's Excellence Strategy - EXC 2067/1-390729940 to PR, SJ, RRD, the DFG-funded FOR2848 (project P01, TL; P04, SJ & PR), SFB1190 (P13, PR), the DFG-funded Emmy-Noether grant (RI 2715/1-1, RRD). BS is supported by the European Research Council Consolidator Grant 648235 and the Deutsche Forschungsgemeinschaft (DFG) Project 403222702/SFB 1381 and Germany's Excellence Strategy (CIBSS –EXC-2189 – Project ID 390939984).

Materials and Methods

Cell culture of HEK293T cells

Human embryonic kidney cell lines (HEK293-Flp-In T-Rex; HEK293T; Thermo Fisher) were cultured either in high glucose (4,5mg/ml) or galactose (0,9mg/ml) containing DMEM media; supplemented with 10% (v/v) FBS (Capricorn Scientific), 1mM sodium pyruvate, 2mM L-glutamine, and 50µg/ml uridine at 37°C under a 5% CO_2 humidified atmosphere. Cell counts were performed by using the Neubauer counting chamber. For inhibition of cytosolic translation, DMEM was supplemented with 100µg/ml emetine dihydrochloride hydrate (Sigma-Aldrich). Cells for SILAC analysis were cultured as previously described (Mick et al. 2012).

Cell lines were regularly tested for mycoplasma contaminations (Eurofins Genomics) and passage.

HEK293T cell lines expressing, SMIM4^{FLAG} (NM_001124767) and C12ORF73^{FLAG} (NM_001135570.3) under the control of a tetracycline-inducible CMV promotor or UQCC1^{FLAG} (NM_001184977.2), UQCC2^{FLAG} (NM_032340.4) and UQCC3^{FLAG} (NM_001085372.3) (non-inducible) were generated as descripted previously (Mick et al. 2012).

The Knockout cell line of TMEM223 was generated as described previously (Aich et al. 2018). Briefly, the TMEM223 specific oligonucleotides GCAAGGCACGACGCTGCAAC and its revers complement were cloned into the pX330 vector and co-transfected with the pEGFP-N1 plasmid into HEK293T WT cells. Three days after transfection, single cells were sorted by flowcytometry. Single colonies were screened by immunoblotting and sequencing of the corresponding gene region.

Cultivation and STED super-resolution light microscopy of HEK293T cells

HEK293T cells were cultivated in DMEM, containing 4,5g/L Glucose and GlutaMAX^{TM} additive (Thermo Fisher Scientific, Waltham, MA, USA) supplemented with 1mM sodium pyruvate (Sigma Aldrich, St. Louis, MO, USA /Merck Millipore, Burlington, MA, USA) and 10% (v/v) fetal bovine serum (Merck Millipore, Burlington, MA, USA).

Prior microscopy, cells were cultivated on glass cover slides for 1–3 days at 37°C and 5% CO_2. Expression of SMIM4^{FLAG} and C12ORF73^{FLAG} was induced by incubation with 1µg/ml Doxycycline-hyclate (Sigma Aldrich, St. Louis, MO, USA/ Merck Millipore,

Burlington, MA, USA) for 24 hours. Fixation and labeling was done as described previously (Wurm et al. 2010). Essentially, cells were fixed using an 8% (w/v) formaldehyde solution, permeabilized by incubation with a 0.25% (v/v) Triton X-100 solution and blocked with a 5% (w/v) bovine serum albumin (BSA) solution.
The investigated proteins were labeled by antisera specific for TOM22 (Anti-Tom22, Rabbit, Merck Millipore/Sigma-Aldrich, HPA003037, Lot: B119406), TOM22 (Anti-TOM22-FITC, Mouse, Miltenyi Biotec, clone 1C9-2, 130-124-227, Lot: 5201105895), and FLAG-antibody (Anti-FLAG, Mouse, Merck Millipore/Sigma-Aldrich, clone M2, F3165, Lot: SLBQ7119V), respectively. Detection was accomplished via secondary antibodies custom labeled with the dyes ALEXA Fluor594 (Thermo Fisher Scientific, Waltham, MA, USA) or Abberior STAR RED (Abberior, Göttingen, Germany), respectively. DNA was labeled via Quant-iT PicoGreen dsDNA reagent (Thermo Fisher Scientific, Waltham, MA, USA). The samples were mounted using Mowiol containing 1,4-Diazabicyclo[2.2.2]octan (DABCO). STED images were acquired using a quad scanning STED microscope (Abberior Instruments, Göttingen, Germany) equipped with a UPlanSApo 100x/1,40 Oil objective (Olympus, Tokyo, Japan). For excitation of the respective dyes, laser beams featuring wave lengths of 485nm, 561nm and 640nm were used. STED was performed applying a laser beam with a wavelength of 775nm. For all images a pixel size of 15nm was utilized. With the exception of contrast stretching, no further image processing was applied.

siRNA constructs and application

To generate knockdown cells, HEK293T wild type cells were transiently transfected with siRNA oligonucleotides against SMIM4 (5'-GCA-GUC-AAU-AAA-GUC-AAU-A-3'), C12orf73 (5'-ACA-CAA-ACC-UCA-AGU-UUC-U-3'), UQCC1 (5'-GAU-GCC-UGA-UAC-AUU-CAA-U-3'), UQCC2 (5'-CUC-CAU-UCA-AAC-UAC-UAC-A-3') and UQCC3 (5'-GGA-AGC-AGG-AAA-UGC-UAA-A-3') to a final concentration of 33nM and non-targeting siRNA used as control (Eurogentec). Lipofectamine RNAi-MAX (Invitrogen) was used as transfection reagent, following the manufacturer´s protocol. Afterwards, cells were incubated at 37°C under 5% CO_2 atmosphere for 72h.

[^{35}S]methionine labeling of newly synthesized mitochondrial-encoded proteins

HEK293T cells were starved with FCS/methionine-free media. After inhibition of cytosolic translation by adding 100µg/ml emetine dihydrochloride hydrate (Sigma-Aldrich) cells were incubated for 1 hour with [^{35}S]methionine in a concentration of 0.2mCi/ml in fully supplemented DMEM without methionine. In case of puromycin treatment, samples were pulsed-labeled with [^{35}S]methionine for 10min before addition of 2µg/ml puromycin for another 20min incubation step.
Subsequently, cells were harvested and washed with PBS, and used for further analysis on SDS-PAGE and autoradiography. Radioactive signals could be detected on Storage Phosphor Screens via a Typhoon FLA 7000 scanner (GE Healthcare) after several days of incubation.

Cytochrome *c* oxidase activity assay

The activity of the cytochrome *c* oxidase was measured as described previously (Dennerlein et al. 2015). A cytochrome c oxidase specific activity microplate assay kit (Mitosciences,Abcam) was used, following the manufacturer's protocol. The specific activity of the cytochrome *c* oxidase was measured according to the manufacturer's instructions. In general, 15mg of cell lysate was used per well. The oxidization of cytochrome *c* was measured at 550nm, representing cytochrome *c* oxidase activity.

Isolation of mitochondria

Mitochondria were isolated according to a modified protocol (Panov and Orynbayeva 2013). Cells were harvested using PBS and resuspended in cold TH-buffer (300mM Trehalose, 10mM KCl, 10mM HEPES; pH7.4) with 2mM PMSF and 0.1mg BSA/ml. Subsequently, cells were gently homogenized twice using a Potter S dounce homogenizer (Sartorius) and pelleted at 400xg for 10min at 4°C after each homogenization step. The supernatant was collected and remaining cell debris were removed by additional centrifugation (800xg, 8min, 4°C). Afterwards, mitochondria were pelleted at 11.000xg for 10min at 4°C and pooled mitochondria pellets were washed with BSA-free TH-buffer and collected by centrifugation as described before. Finally, mitochondria were resuspended in BSA-free TH buffer and stored at -80°C or used right away.

Protein localization and Protease Protection Assays

Carbonate extraction and mitochondrial swelling experiments were performed as previously described (Mick et al. 2012). For carbonate extraction, mitochondria were isolated as described and resuspended in buffer containing 10mM 3-(N-morpholino) propanesulfonic acid (MOPS) (pH7.2), 50mM NaCl and either 1% Triton X-100 or 0.1M carbonate at pH10.5 or 11.8. Insoluble membranes were pelleted by 55,000rpm at 4°C, 45min in a TLA-55 rotor (Beckman Coulter). For submitochondrial localization, mitochondria were either suspended in SEM buffer (250mM sucrose, 1mMEDTA, and 10mM MOPS [pH7.2]), to osmotically stabilize mitochondria, or in EM buffer (1mM EDTA, and 10mM MOPS [pH7.2]), to rupture the outer mitochondrial membrane. In the following Proteinase K (PK) was added as indicated. Furthermore, mitochondria were lysed with 1%Triton X-100 in the presence of PK for positive control. All reactions were stopped after 10min by addition of PMSF (2mM final concentration), followed by trichloroacetic acid (TCA) precipitation.

Affinity purification of protein complexes

Isolated mitochondria or cells were lysed in solubilization buffer (150mM NaCl, 10% glycerol (v/v), 20mM MgCl2, 2mM PMSF, 50mM Tris-HCl, pH7.4, 1% digitonin (v/w) protease inhibitor) in a ratio of 1-2µg/µl for 30min at 4°C and 850 rpm. Lysates were cleared by centrifugation, (15min, 16.000x g, 4°C) and transferred onto anti-FLAG M2 agarose beads (Sigma-Aldrich) for FLAG immunoprecipitation. After 1-hour binding at 4°C, beads were washed several times (10x) with washing buffer (50mM Tris-HCl, pH7.4, 150mM NaCl, 10% glycerol (v/v), 20mM $MgCl_2$, 1mM PMSF, 0.3% digitonin (v/w)) to remove unbound proteins. Bound proteins were eluted with FLAG peptide (Sigma) by a 30 min incubation step at 850rpm at 4°C. Samples were analyzed via SDS-PAGE and immunoblotting or quantitative mass spectrometry.

For antibody immunoprecipitation same protocol was used as descripted above. Lysed mitochondria or cells were transferred onto protein A-Sepharose (PAS) containing crosslinked SMIM4 or C12orf73 antibody in a Mobicol spin column (MoBiTec). Bound proteins at PAS-anti SMIM4/C12orf73 columns were eluted by adding 0.1M glycine, pH2.8 for 6min at 650rpm at room temperature.

552 **Immunoblotting via Western Blot**

553 Proteins were separated using an SDS-PAGE and afterwards transferred onto PVDF
554 membrane (Millipore) by semidry blotting (Blotting buffer). Primary antibodies were
555 incubated overnight at 4°C or 1 hour at room temperature. Secondary antibodies
556 (rabbit or mouse) were incubated at RT for additional 1-2 hours. Signals were
557 visualized on X-ray films using the enhanced chemiluminescence detection kit (GE
558 Healthcare), and quantifications were performed using ImageQuant TL 7.0 soft-ware
559 (GE Healthcare) with a rolling ball background subtraction.

560

561 **Blue native and second dimension analysis**

562 BN-PAGE was performed as descripted previously (Mick et al. 2012). Isolated
563 mitochondria or cells were solubilized in a concentration of 1µg/µl in BN-PAGE lysis
564 buffer containing 1% digitonin or 1% DDM (20mM Tris-HCl, pH7.4, 0.1mM EDTA,
565 50mM NaCl, 10% glycerol (v/v), 1mM PMSF). After a 20min incubation step on ice
566 debris were removed by centrifugation for 15min, 16.000xg at 4°C. The remaining
567 supernatant was resuspended in BN-PAGE Loading dye (5% Coomassie Brilliant Blue
568 G250 (v/w), 500mM 6-aminocaproic acid, 100mM Bis-Tris–HCl, pH7.0) and applied to
569 electrophoresis on a 4-13% or 2.5-10% gradient gel (Quelle). Afterwards, proteins
570 were either transferred to a PVDF membrane by Western Blot method or subjected to
571 2D-PAGE analysis. In case of 2D-PAGE analysis, signal BN-PAGE stripes were cut
572 out from gel and further used in SDS-PAGE separation.

573

574 **Quantitative mass spectrometry and data analysis**

575 Affinity-purified SILAC-labelled mL62^{FLAG} and SMIM4^{FLAG} complexes were processed
576 for quantitative LC-MS analysis following a gel-based approach. Reduction and
577 alkylation of cysteine residues and subsequent tryptic in-gel digestion of proteins were
578 performed as described before (Peikert et al. 2017). Peptides were desalted using
579 StageTips, dried *in vacuo*, and reconstituted in 0.1% trifluoroacetic acid. LC-MS
580 analyses were carried out using an UltiMate 3000 RSLCnano HPLC system (Thermo
581 Fisher Scientific) coupled to an Orbitrap Elite mass spectrometer (Thermo Fisher
582 Scientific). Peptides were separated on a C18 reversed-phase nano LC column (for
583 mL62^{FLAG} samples: Acclaim PepMap^{TM}, 500mm x 75µm, 2µm particle size, 100Å
584 packing density [Thermo Fisher Scientific], flow rate of 0.25µl/min; for SMIM4^{FLAG}
585 samples: nanoEase^{TM} M/Z HSS C18 T3, 250mm x 75µm, 1.8µm particle size, 100Å

packing density [Waters], flow rate of 0.3µl/min) using a binary solvent system consisting of 4% dimethyl sulfoxide/0.1% formic acid (solvent A) and 48% methanol/30% acetonitrile/4% dimethyl sulfoxide/0.1% formic acid (solvent B). The gradients employed for peptide elution were as follows: 1% solvent B for 5min, 1%-65% B in 50min, 65%-95% B in 5min, 5min at 95% B for mL62^{FLAG} samples and 7% solvent B for 5 min, 7%-65% B in 65min, 65%-80% B in 5min, 5min at 80% B for SMIM4^{FLAG} samples.

The Orbitrap Elite was operated in a data-dependent mode. MS survey scans were acquired at a mass range of *m/z* 370-1,700 and a resolution of 120,000 (at *m/z* 400). The target value was 10^6 ions and the maximum injection time 200ms. Up to 15 (mL62^{FLAG} complexes) or 25 (SMIM4^{FLAG} complexes) of the most intense multiply charged peptide ions were selected for fragmentation by collision-induced dissociation in the linear ion trap at a normalized collision energy of 35%, an activation q of 0.25 and an activation time of 10ms. The target value was set to 5,000 ions, the maximum injection time to 150ms, the isolation width to 2.0*m/z*, and the dynamic exclusion time to 45sec.

MS raw data were analyzed with MaxQuant/Andromeda (version 1.4.1.2 for mL62^{FLAG} and 1.5.5.1 for SMIM4^{FLAG} data; (Cox and Mann 2008; Cox et al. 2011)) and searched against the UniProt human proteome set including isoforms (release versions 08/2014 for mL62^{FLAG} and 08/2018 for SMIM4^{FLAG} data) using default settings except that the minimum requirements for protein identification and relative quantification were set to one unique peptide and one SILAC peptide pair, respectively. Arg10 and Lys8 were set as heavy labels. Carbamidomethylation of cysteine residues was considered as fixed, and N-terminal acetylation and oxidation of methionine as variable modifications. The options 'match between runs' and 'requantify' were enabled.

Experiments were performed in four biological replicates including label-switch. Lists of proteins identified in the analyses of mL62^{FLAG} and SMIM4^{FLAG} complexes are provided in Supplementary Table S1 and S2, respectively.

Figure legends:

Figure 1. TMEM223 and SMIM4 interact with the mitochondrial ribosome. (A) Mitochondria isolated from cells expressing mL62^{FLAG} were subjected to co-immunoprecipitation. Natively isolated complexes were separated by sucrose density gradient ultracentrifugation. Fractions (1-15) were analyzed by western blotting, using indicated antibodies against components of the 39S mtLSU (mL62, uL1m, uL3m, uL23m) and 28S mtSSU (uS14m, bS16m) subunits. (B) Mitochondria were isolated from wild type (WT) and mL62^{FLAG}-expressing cells, cultured in SILAC-medium, and subjected to co-immunoisolation. Eluates were analysed by quantitative mass spectrometry (LC-MS/MS) (n=4). Ribosomal proteins of the mtLSU and mtSSU are indicated in red and blue, respectively. Dashed lines indicate a p-value of 0.05 and mean mL62^{FLAG}/WT ratios. (C) Scheme of proteins identified in (B). (D) Complexes containing mL62^{FLAG} were purified as in (A) and (B) and analyzed by western blotting. Total, 0.75 %; Eluate, 100 %.

Figure 2. TMEM223 is a mitochondrial membrane protein. (A) Membrane topology of TMEM223. The predicted transmembrane spans (TM1 and TM2) with corresponding amino acids (aa) are indicated. IMS: intermembrane space; IMM: inner mitochondrial membrane. (B) and (C) Submitochondrial localization of TMEM223. Wild type mitochondria were treated with Proteinase K (PK) under iso-osmotic (Mito), hyper-osmotic conditions (swelling, MP), or solubilized with Triton X-100 (TX-100) (B). Mitochondrial proteins were extracted in sodium carbonate containing buffer at different pH. (total, T; pellet, P; soluble fraction, S) (C).
(D) Protein steady state levels in TMEM223$^{-/-}$ cells. Mitochondrial lysates from wild type (WT) and TMEM223$^{-/-}$ cells were analysed by western blotting using indicated antibodies.

Figure 3. TMEM223 is involved in cytochrome c oxidase biogenesis
(A) Isolated mitochondria from WT and TMEM223$^{-/-}$ cells were solubilized in DDM-containing buffer, separated on 2.5%-10% (Complex I) or 4-13% (Complex II-V) BN-PAGE and analyzed by western blotting. OXPHOS complexes were detected with indicated antibodies. (B) Cytochrome *c* oxidase activity was measured in cellular extracts from WT and TMEM223$^{-/-}$ photometrically (mean±SEM, n=4). (C)

Mitochondrial protein synthesis in TMEM223$^{-/-}$. Indicated cell lines were grown in the presence of [^{35}S] methionine for 1h to monitor synthesis of mitochondrial-encoded proteins. Cell lysates were subjected to SDS-PAGE and analyzed by digital autoradiography (upper panel) and western blotting (lower panel). Newly synthesized proteins were quantified using image quant software and calculated as a percentage of WT (mean±SEM; n=3). (E) TMEM223 interacts with early cytochrome *c* oxidase assembly factors. Mitochondria isolated from WT, C12ORF62^{FLAG}, MITRAC12^{FLAG} or MITRAC7^{FLAG} cells were subjected to co-immunoisolation and samples analyzed by western blotting. (Total, 0.75 %; Eluate, 100 %).

Figure 4: SMIM4 is a mitochondrial protein, interacting with cytochrome c reductase and mitochondrial quality control proteins. (A) Schematic presentation of SMIM4 membrane topology. The predicted transmembrane domain (aa 20-41) is indicated. Intermembrane space, IMS; inner mitochondrial membrane, IMM. (B) Immunofluorescence microscopy of HEK293T cells expressing SMIM4^{FLAG}. Cells were induced with doxycycline for 24 h (+Dox). SMIM4^{FLAG} was labelled using a FLAG-specific antiserum. Mitochondrial marker, TOM20. Detection via secondary antibodies custom labeled with the dyes ALEXA Fluor594 or Abberior STAR RED respectively. DNA was labeled via Quant-iT PicoGreen dsDNA reagent. Scale bars: 10 µm (overview), 500 nm (magnification). (C) Submitochondrial localization of SMIM4^{FLAG}. Mitochondria isolated from SMIM4^{FLAG}-expressing cells were treated with proteinase K (PK) either under iso-osmotic (Mito), hyperosmotic (swelling, mitoplasts (MP). (D) SMIM4 is an integral membrane protein. Mitochondrial proteins were extracted using sodium carbonate (at indicated pH), or Triton X-100 (TX-100). Samples (total, T; pellet, P; soluble fraction, S) were analyzed by western blotting using antibodies. (E) Mitochondrial extracts from wild type (WT) and SMIM4^{FLAG}-expressing cells cultured in SILAC medium were subjected to native-immunoprecipitation, and analyzed by quantitative mass spectrometry (LC-MS/MS) (n=4). Cytochrome *c* reductase assembly factors and components of the mitochondrial quality control system are indicated in black. The dashed horizontal line indicates a p-value of 0.05, the solid vertical line a mean SMIM4^{FLAG}/WT ratio of 10. (F) Samples obtained by co-immunuprecipitation of wild type (WT) or SMIM4^{FLAG}-containing mitochondrial lysates were analyzed by western blotting (Total, 1.5 %; Eluate, 100 %).

Figure 5: Loss of SMIM4 or C12ORF73 affects cytochrome *c* reductase biogenesis (A) FLAG-immunoisolation of C12ORF73^{FLAG}. Samples were analyzed by SDS-PAGE and western blotting. (Total, 1.5 %; Eluate, 100 %). (B) Western blot analyses of SMIM4 or C12ORF73 depleted cells. HEK293T cells were treated with indicated siRNAs and cultured either in glucose- or galactose-containing media for 72h. Cell extracts were subjected to SDS-PAGE separation and western blotting. (C) Loss of SMIM4 or C12ORF73 affects cell growth. HEK293T cells were transfected with siRNAs as in Figure 6B. Cells were cultured either in glucose- or galactose-containing media for 72h; cell counts are presented as percentage relative to non-targeting siRNA treated cells (siNT; indicated as dashed line). (mean±SEM, n=3). (D) and (E) BN-PAGE analyses of mitochondrial protein complexes upon SMIM4 (B) or C12ORF73 ablation (C). Mitochondria were solubilized with DDM (N-Dodecyl-beta-Maltoside) and subjected to BN-PAGE followed by western blot analyses.

Figure 6: SMIM4 and C12ORF73 promote cytochrome *c* reductase assembly. (A) SMIM4 and C12ORF73 co-migrate with cytochrome *c* reductase assembly intermediates. Wild type mitochondrial lysates were subjected to BN-PAGE (2.5%-10% for Complex I; 4%-13% Complex II-V) analyses followed by second dimension SDS-PAGE and western blotting. (B) C12ORF73^{FLAG} isolates cytochrome *c* reductase assembly intermediates. Mitochondria isolated from C12ORF73^{FLAG}-expressing cells were solubilized and subjected to co-immunoisolation. Natively eluted complexes were separated by BN-PAGE and subjected to second dimension SDS-PAGE followed by western blot analyses using indicated antibodies. (C) Immunoprecipitations of UQCC1^{FLAG}, UQCC2^{FLAG} and UQCC3^{FLAG}. Eluates were analyzed by SDS-PAGE followed by Western blotting with indicated antibodies. (D) Mitochondrial translation products were labelled with [^{35}S] methionine for 1h prior to co-immunoprecipitation using anti-SMIM4, -C12ORF73 or control antibodies (αIgG^{con}). Eluates were separated by SDS-PAGE followed by western blotting, and analyzed by digital autoradiography (upper panel) and immunodetection (lower panel) (Total, 2%; Eluate, 100%). (E) Mitochondria isolated from control or C12ORF73-depleted cells were lysed in digitonin-containing buffer and complexes separated by BN-PAGE followed by second dimension SDS-PAGE. Cytochrome *c* reductase sub-

assembly complexes were monitored with indicated antibodies. (red arrow mark cytochrome *c* reductase subcomplexes in C12ORF73-deficient samples).

Figure 5 - Supplement 1. C12ORF73 is an inner mitochondrial protein in human

(A) STED super-resolution light microcopy images of TOM22 and C12ORF73^{FLAG} in HEK293T cells. TOM22 and C12ORF73^{FLAG} were labeled by specific antisera. Detection via secondary antibodies custom labeled with the dyes ALEXA Fluor594 or Abberior STAR RED respectively. Scale bars: 10 µm (overview), 500 nm (magnification).

(B) and (C) Submitochondrial localization of C12ORF73. (B) Sodium carbonate buffers with different pH as indicated were used to extract mitochondrial membrane proteins. (total, T; pellet, P; soluble fraction, S). (C) Different amounts of Proteinase K (PK) were added under iso-osmotic (Mito), and hyper-osmotic (MP) conditions or during Triton X-100 (TX-100) treatment.

References

Aich A, Wang C, Chowdhury A, Ronsör C, Pacheu-Grau D, Richter-Dennerlein R, et al. COX16 promotes COX2 metallation and assembly during respiratory complex IV biogenesis. Elife. eLife Sciences Publications Limited; 2018 Jan 30;7.

Amunts A, Brown A, Toots J, Scheres SHW, Ramakrishnan V. Ribosome. The structure of the human mitochondrial ribosome. Science. 2015 Apr 3;348(6230):95–8.

Brown A, Amunts A, Bai X-C, Sugimoto Y, Edwards PC, Murshudov G, et al. Structure of the large ribosomal subunit from human mitochondria. Science. American Association for the Advancement of Science; 2014 Nov 7;346(6210):718–22.

Busch JD, Cipullo M, Atanassov I, Bratic A, Silva Ramos E, Schöndorf T, et al. MitoRibo-Tag Mice Provide a Tool for In Vivo Studies of Mitoribosome Composition. Cell Reports. 2019 Nov 5;29(6):1728–9.

Cox J, Mann M. MaxQuant enables high peptide identification rates, individualized p.p.b.-range mass accuracies and proteome-wide protein quantification. Nat Biotechnol. Nature Publishing Group; 2008 Dec;26(12):1367–72.

Cox J, Neuhauser N, Michalski A, Scheltema RA, Olsen JV, Mann M. Andromeda: a peptide search engine integrated into the MaxQuant environment. J Proteome Res. American Chemical Society; 2011 Apr 1;10(4):1794–805.

Dennerlein S, Oeljeklaus S, Jans D, Hellwig C, Bareth B, Jakobs S, et al. MITRAC7 Acts as a COX1-Specific Chaperone and Reveals a Checkpoint during Cytochrome c Oxidase Assembly. Cell Reports. 2015 Sep 8;12(10):1644–55.

Dennerlein S, Wang C, Rehling P. Plasticity of Mitochondrial Translation. Trends Cell Biol. 2017 Jun 9.

Englmeier R, Pfeffer S, Förster F. Structure of the Human Mitochondrial Ribosome Studied In Situ by Cryoelectron Tomography. Structure. 2017 Oct 3;25(10):1574–1581.e2.

760 Fernández-Vizarra E, Zeviani M. Mitochondrial complex III Rieske Fe-S protein
761 processing and assembly. Cell Cycle. Taylor & Francis; 2018;17(6):681–7.

762 Ferrari A, Del'Olio S, Barrientos A. The Diseased Mitoribosome. FEBS Lett. John
763 Wiley & Sons, Ltd; 2020 Dec 12.

764 Greber BJ, Boehringer D, Leibundgut M, Bieri P, Leitner A, Schmitz N, et al. The
765 complete structure of the large subunit of the mammalian mitochondrial ribosome.
766 Nature. Nature Publishing Group; 2014 Nov 13;515(7526):283–6.

767 Hällberg BM, Larsson N-G. Making Proteins in the Powerhouse. Cell Metab. 2014
768 Aug;20(2):226–40.

769 Itoh Y, Andréll J, Choi A, Richter U, Maiti P, Best RB, et al. Mechanism of membrane-
770 tethered mitochondrial protein synthesis. Science. American Association for the
771 Advancement of Science; 2021 Feb 19;371(6531):846–9.

772 Kummer E, Ban N. Mechanisms and regulation of protein synthesis in mitochondria.
773 Nat Rev Mol Cell Biol. Nature Publishing Group; 2021 Feb 16;:1–19.

774 Maiti P, Lavdovskaia E, Barrientos A, Richter-Dennerlein R. Role of GTPases in
775 Driving Mitoribosome Assembly. Trends Cell Biol. 2021 Jan 5.

776 Mick DU, Dennerlein S, Wiese H, Reinhold R, Pacheu-Grau D, Lorenzi I, et al.
777 MITRAC links mitochondrial protein translocation to respiratory-chain assembly
778 and translational regulation. Cell. 2012 Dec 21;151(7):1528–41.

779 Ndi M, Marin-Buera L, Salvatori R, Singh AP, Ott M. Biogenesis of the bc1 Complex
780 of the Mitochondrial Respiratory Chain. Journal of Molecular Biology. 2018 Oct
781 19;430(21):3892–905.

782 Panov A, Orynbayeva Z. Bioenergetic and antiapoptotic properties of mitochondria
783 from cultured human prostate cancer cell lines PC-3, DU145 and LNCaP. PLoS
784 ONE. Public Library of Science; 2013;8(8):e72078.

785 Peikert CD, Mani J, Morgenstern M, Käser S, Knapp B, Wenger C, et al. Charting
786 organellar importomes by quantitative mass spectrometry. Nat Commun. Nature
787 Publishing Group; 2017 May 9;8(1):15272–14.

788 Pfanner N, Warscheid B, Wiedemann N. Mitochondrial proteins: from biogenesis to
789 functional networks. Nat Rev Mol Cell Biol. Nature Publishing Group; 2019
790 May;20(5):267–84.

791 Pfeffer S, Woellhaf MW, Herrmann JM, Förster F. Organization of the mitochondrial
792 translation machinery studied in situ by cryoelectron tomography. Nat Commun.
793 Nature Publishing Group; 2015 Jan 22;6(1):6019–8.

794 Richter R, Rorbach J, Pajak A, Smith PM, Wessels HJ, Huynen MA, et al. A functional
795 peptidyl-tRNA hydrolase, ICT1, has been recruited into the human mitochondrial
796 ribosome. EMBO J. John Wiley & Sons, Ltd; 2010 Mar 17;29(6):1116–25.

797 Richter-Dennerlein R, Dennerlein S, Rehling P. Integrating mitochondrial translation
798 into the cellular context. Nat Rev Mol Cell Biol. 2015 Oct;16(10):586–92.

799 Richter-Dennerlein R, Oeljeklaus S, Lorenzi I, Ronsör C, Bareth B, Schendzielorz AB,
800 et al. Mitochondrial Protein Synthesis Adapts to Influx of Nuclear-Encoded Protein.
801 Cell. 2016 Oct 6;167(2):471–483.e10.

802 Sánchez-Caballero L, Elurbe DM, Baertling F, Guerrero-Castillo S, van den Brand M,
803 van Strien J, et al. TMEM70 functions in the assembly of complexes I and V.
804 Biochim Biophys Acta Bioenerg. 2020 Aug 1;1861(8):148202.

805 Smith PM, Fox JL, Winge DR. Reprint of: Biogenesis of the cytochrome bc(1) complex
806 and role of assembly factors. Biochim Biophys Acta. 2012 Jun;1817(6):872–82.

807 Stoldt S, Stephan T, Jans DC, Brüser C, Lange F, Keller-Findeisen J, et al. Mic60
808 exhibits a coordinated clustered distribution along and across yeast and
809 mammalian mitochondria. Proc Natl Acad Sci USA. National Academy of
810 Sciences; 2019 May 14;116(20):9853–8.

811 Timón-Gómez A, Nývltová E, Abriata LA, Vila AJ, Hosler J, Barrientos A. Mitochondrial
812 cytochrome c oxidase biogenesis: Recent developments. Seminars in Cell &
813 Developmental Biology. 2017 Sep.

814 Tucker EJ, Wanschers BFJ, Szklarczyk R, Mountford HS, Wijeyeratne XW, van den
815 Brand MAM, et al. Mutations in the UQCC1-interacting protein, UQCC2, cause

816 human complex III deficiency associated with perturbed cytochrome b protein
817 expression. Moraes CT, editor. PLoS Genet. Public Library of Science;
818 2013;9(12):e1004034.

819 Wanschers BFJ, Szklarczyk R, van den Brand MAM, Jonckheere A, Suijskens J,
820 Smeets R, et al. A mutation in the human CBP4 ortholog UQCC3 impairs complex
821 III assembly, activity and cytochrome b stability. Hum Mol Genet. 2014 Dec
822 1;23(23):6356–65.

823 Weraarpachai W, Sasarman F, Nishimura T, Antonicka H, Auré K, Rötig A, et al.
824 Mutations in C12orf62, a factor that couples COX I synthesis with cytochrome c
825 oxidase assembly, cause fatal neonatal lactic acidosis. Am J Hum Genet. 2012
826 Jan 13;90(1):142–51.

827 Wurm CA, Neumann D, Schmidt R, Egner A, Jakobs S. Sample preparation for STED
828 microscopy. Methods Mol Biol. Humana Press; 2010;591:185–99.

829 Zara V, Conte L, Trumpower BL. Evidence that the assembly of the yeast cytochrome
830 bc1 complex involves the formation of a large core structure in the inner
831 mitochondrial membrane. FEBS J. John Wiley & Sons, Ltd; 2009
832 Apr;276(7):1900–14.

833 Zhang S, Reljić B, Liang C, Kerouanton B, Francisco JC, Peh JH, et al. Mitochondrial
834 peptide BRAWNIN is essential for vertebrate respiratory complex III assembly. Nat
835 Commun. Nature Publishing Group; 2020 Mar 11;11(1):1312–6.

836

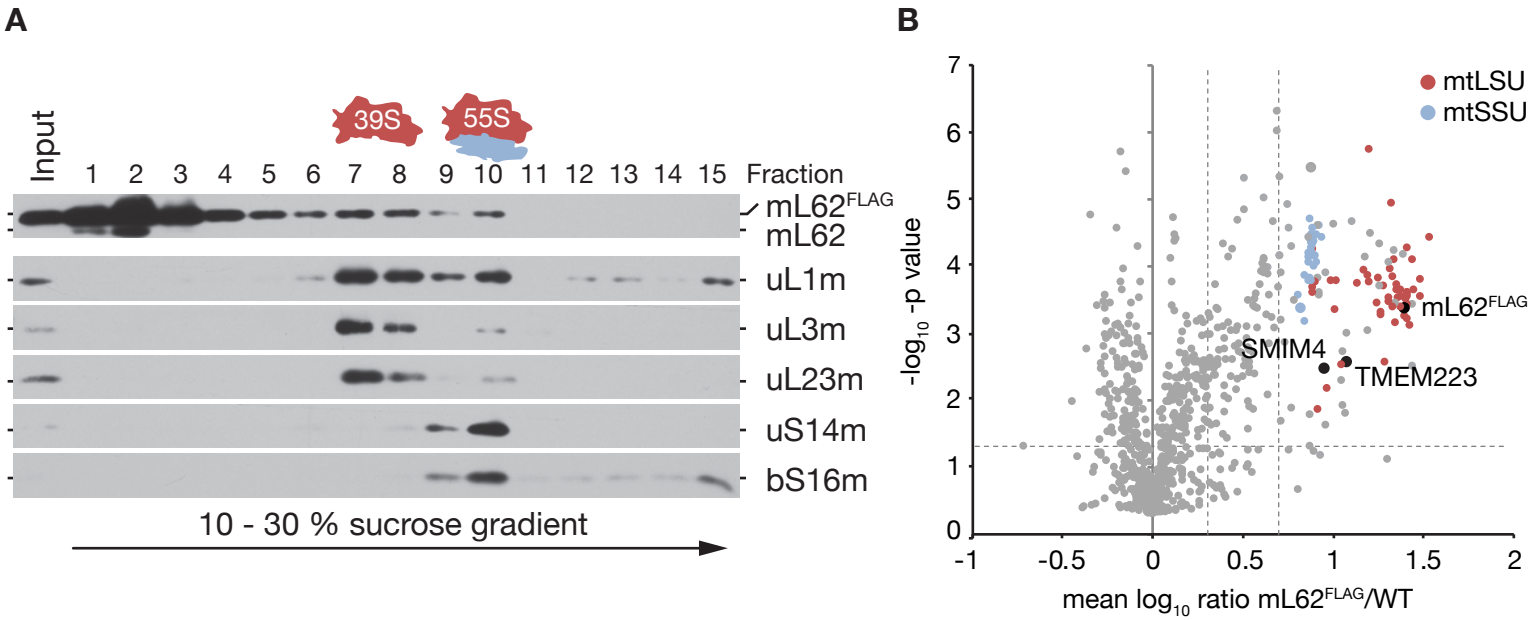

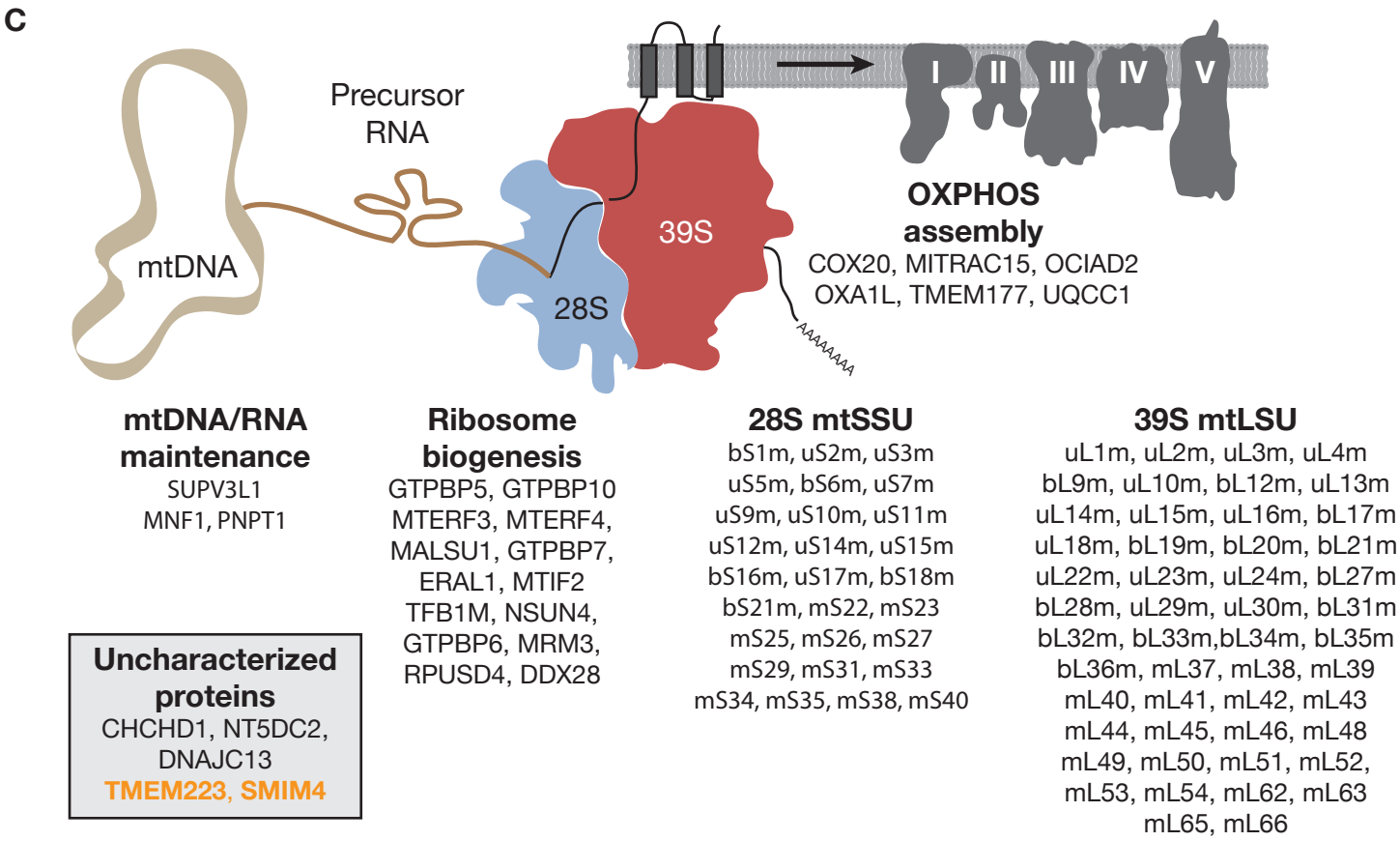

mtDNA/RNA maintenance
SUPV3L1
MNF1, PNPT1

Ribosome biogenesis
GTPBP5, GTPBP10
MTERF3, MTERF4,
MALSU1, GTPBP7,
ERAL1, MTIF2
TFB1M, NSUN4,
GTPBP6, MRM3,
RPUSD4, DDX28

28S mtSSU
bS1m, uS2m, uS3m
uS5m, bS6m, uS7m
uS9m, uS10m, uS11m
uS12m, uS14m, uS15m
bS16m, uS17m, bS18m
bS21m, mS22, mS23
mS25, mS26, mS27
mS29, mS31, mS33
mS34, mS35, mS38, mS40

39S mtLSU
uL1m, uL2m, uL3m, uL4m
bL9m, uL10m, bL12m, uL13m
uL14m, uL15m, uL16m, bL17m
uL18m, bL19m, bL20m, bL21m
uL22m, uL23m, uL24m, bL27m
bL28m, uL29m, uL30m, bL31m
bL32m, bL33m,bL34m, bL35m
bL36m, mL37, mL38, mL39
mL40, mL41, mL42, mL43
mL44, mL45, mL46, mL48
mL49, mL50, mL51, mL52,
mL53, mL54, mL62, mL63
mL65, mL66

Uncharacterized proteins
CHCHD1, NT5DC2,
DNAJC13
TMEM223, SMIM4

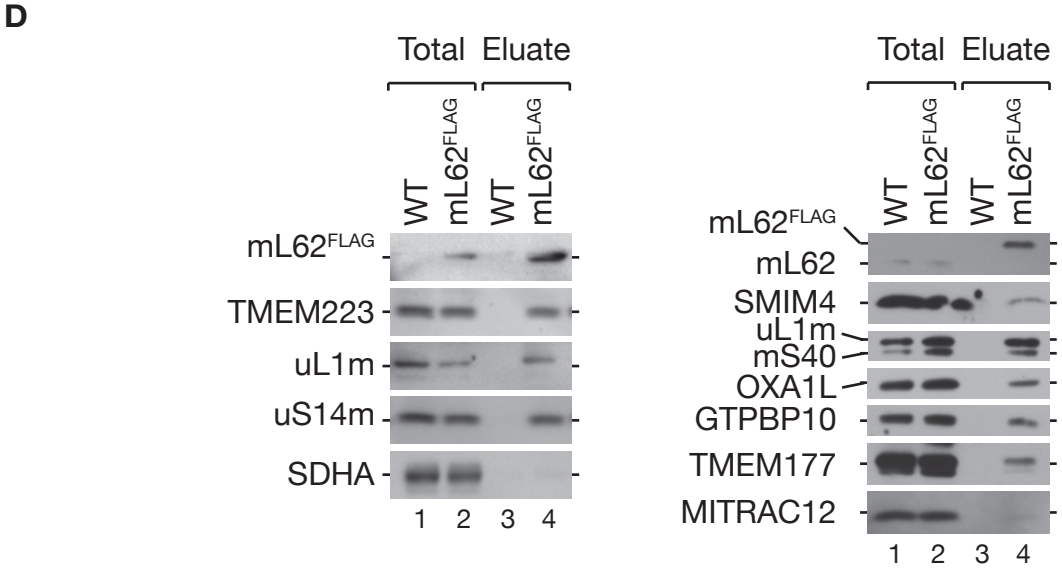

Figure 1 Dennerlein et al.

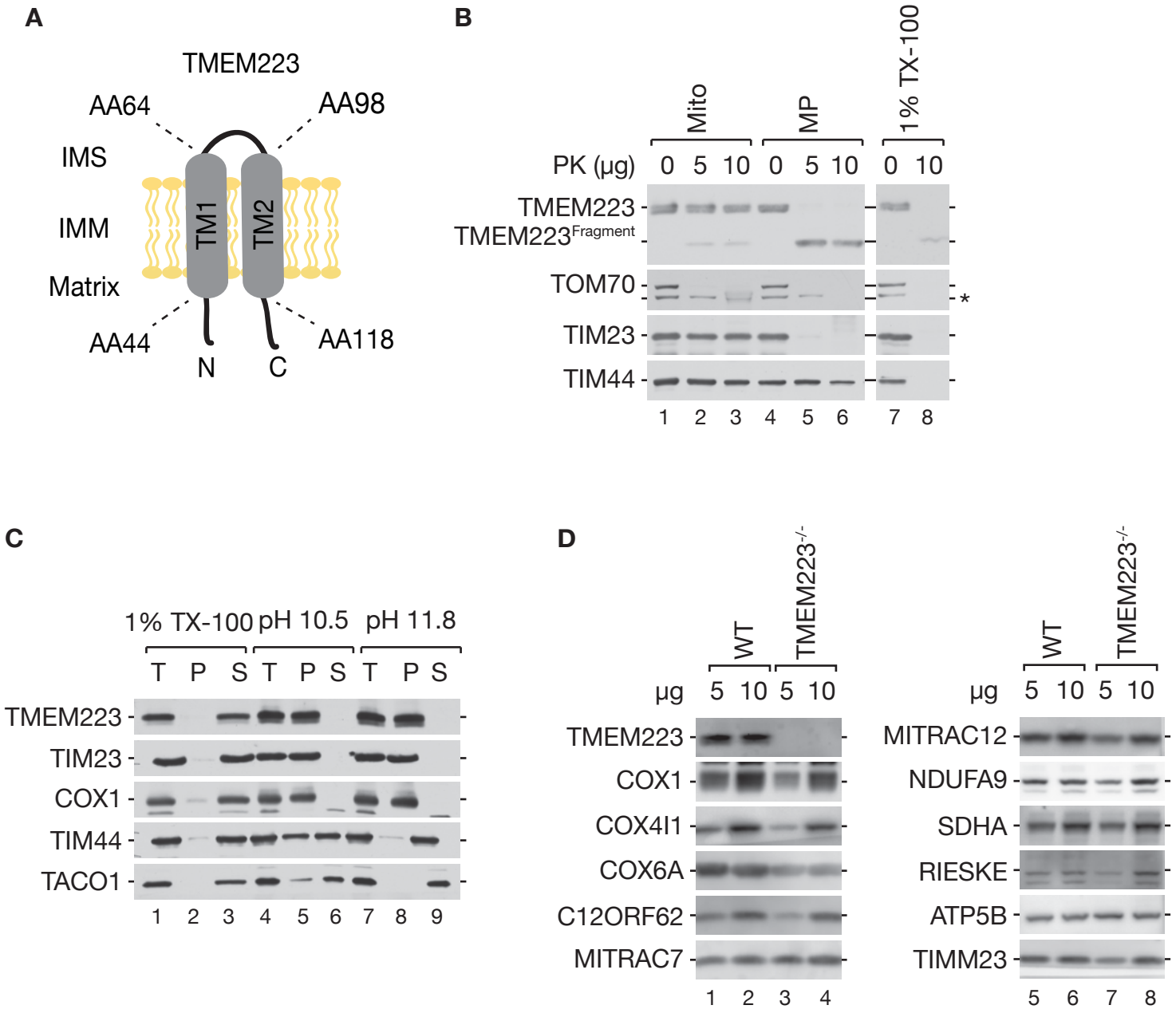

Figure 2 Dennerlein et al.

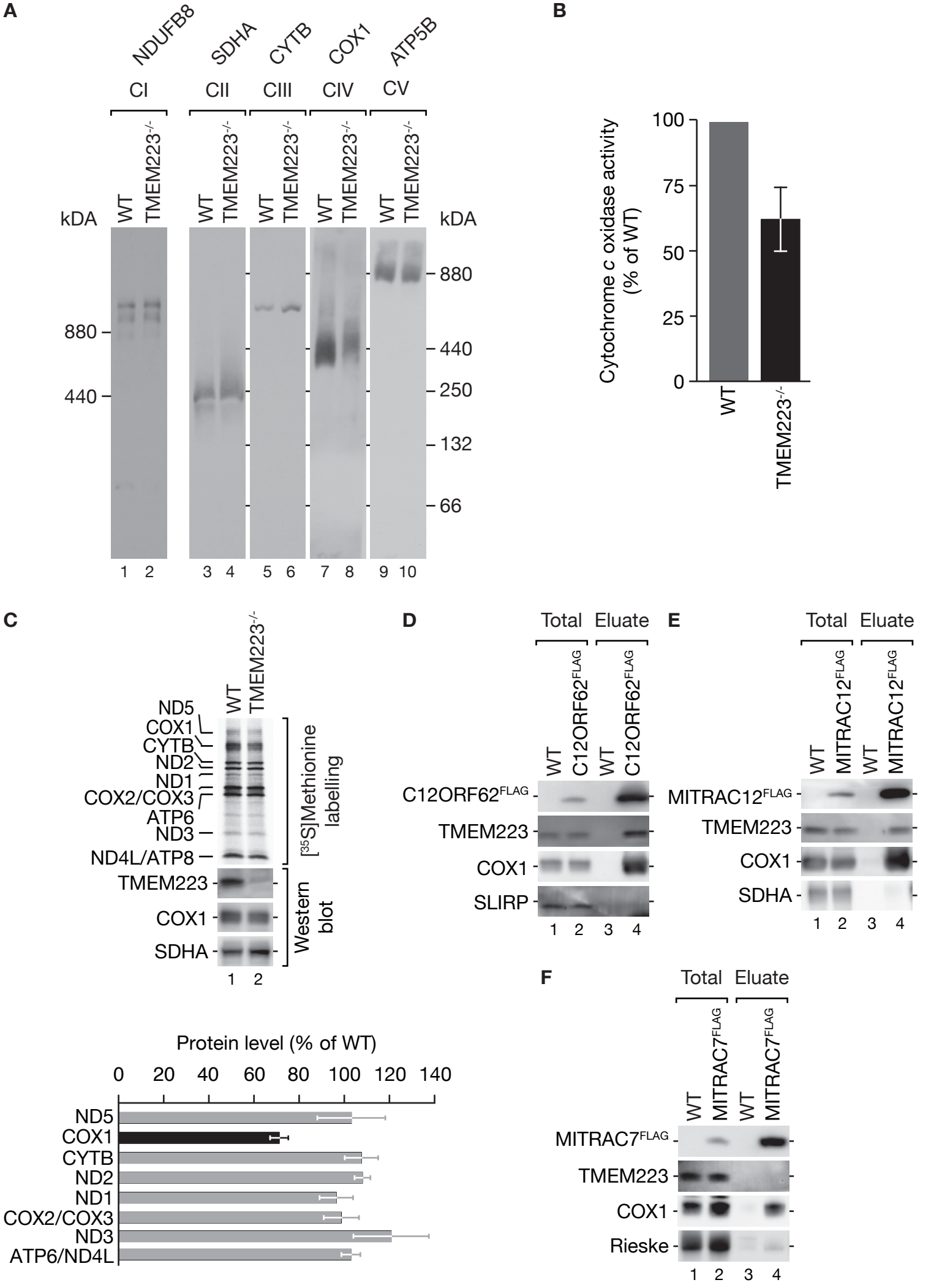

Figure 3 Dennerlein et al.

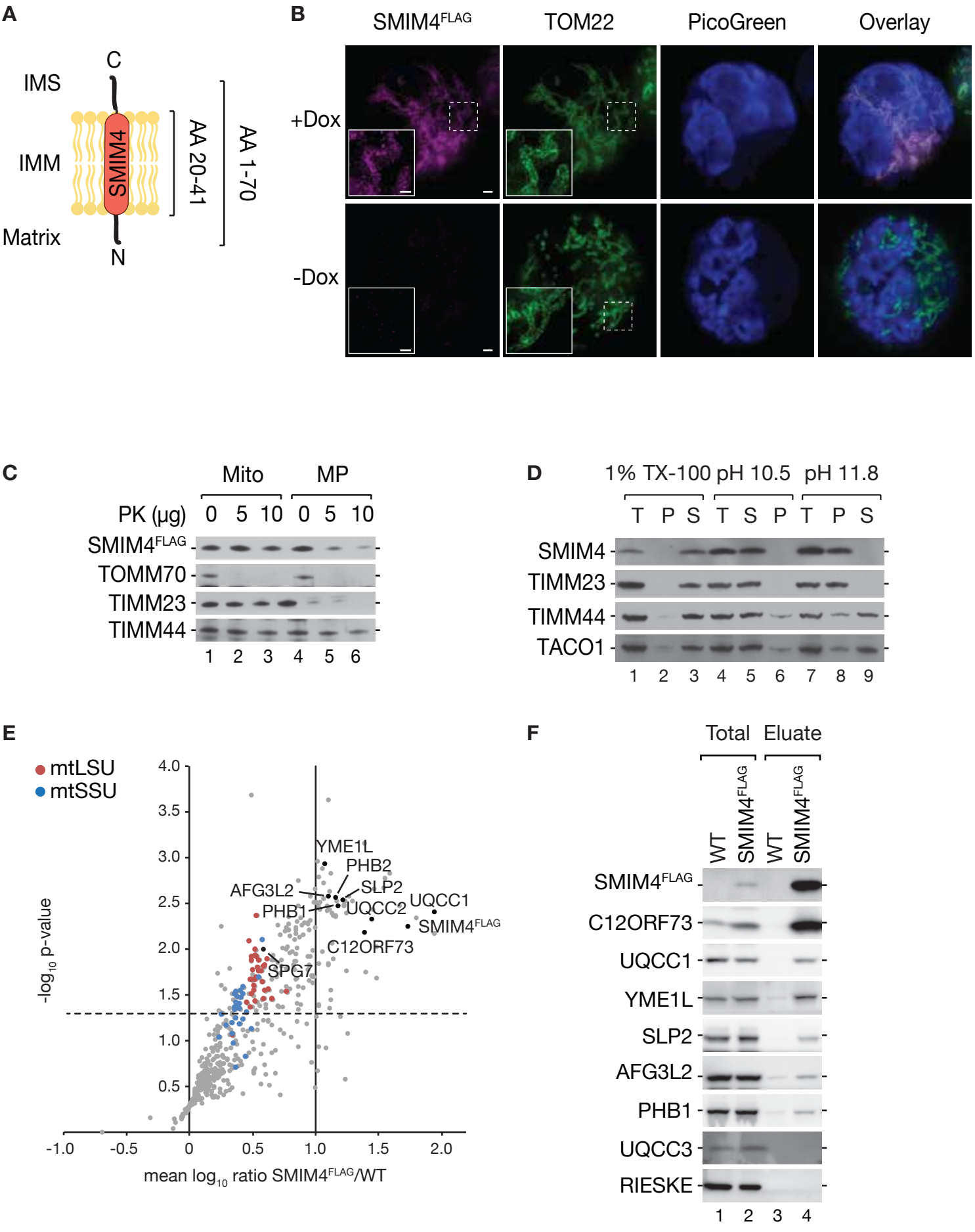

Figure 4 Dennerlein et al.

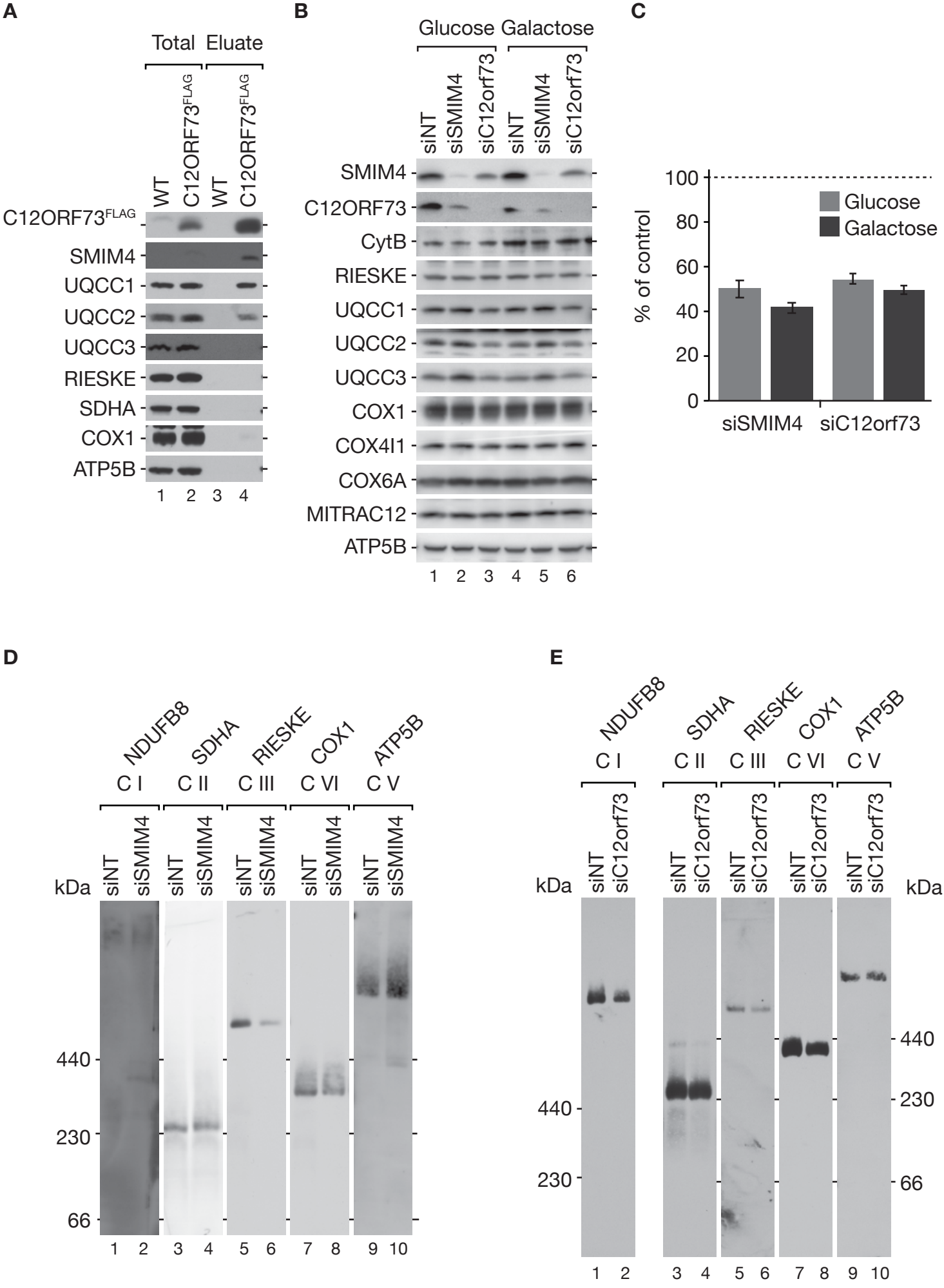

Figure 5 Dennerlein et al.

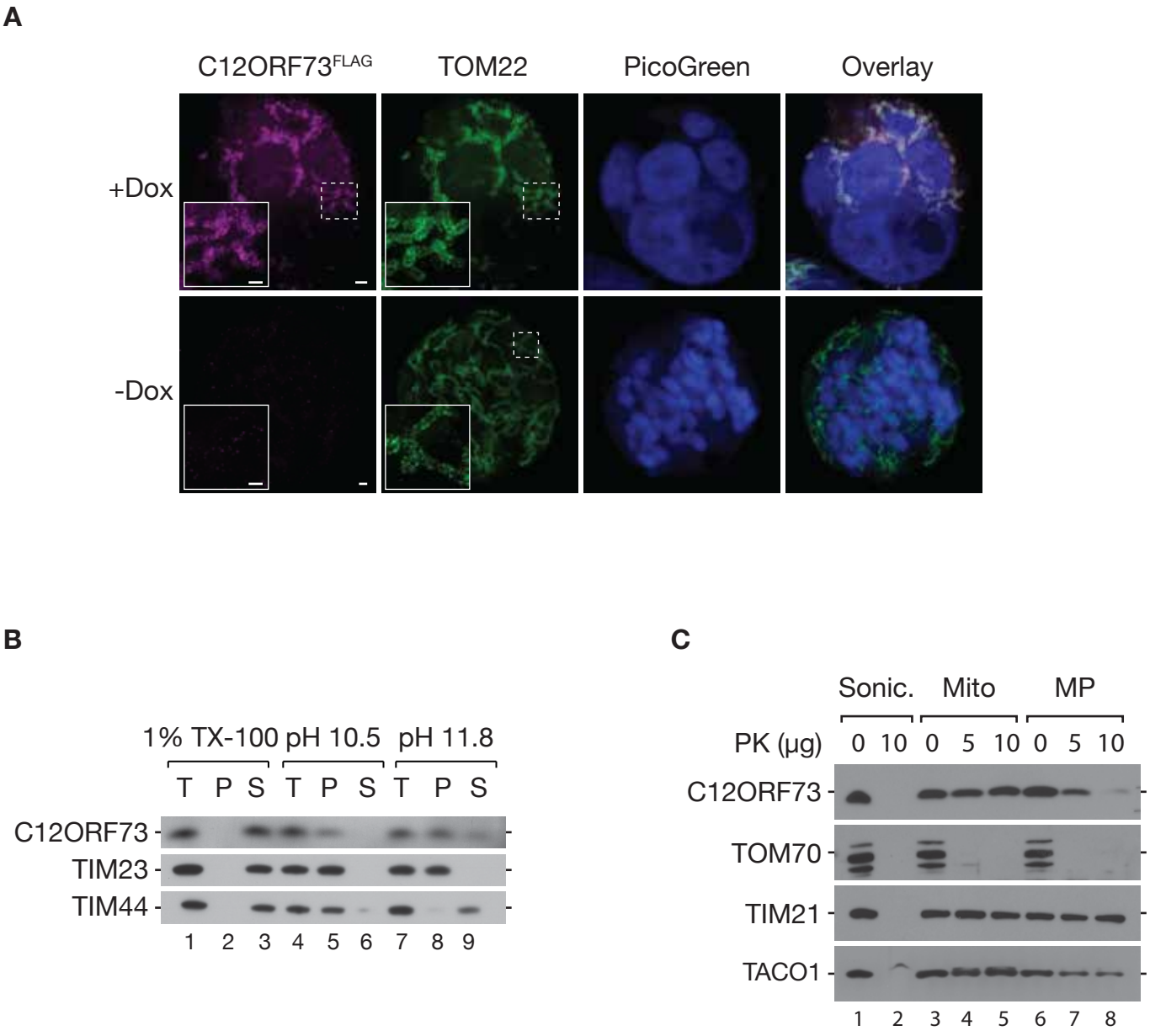

Figure 5 - figure supplement 1 Dennerlein et al.

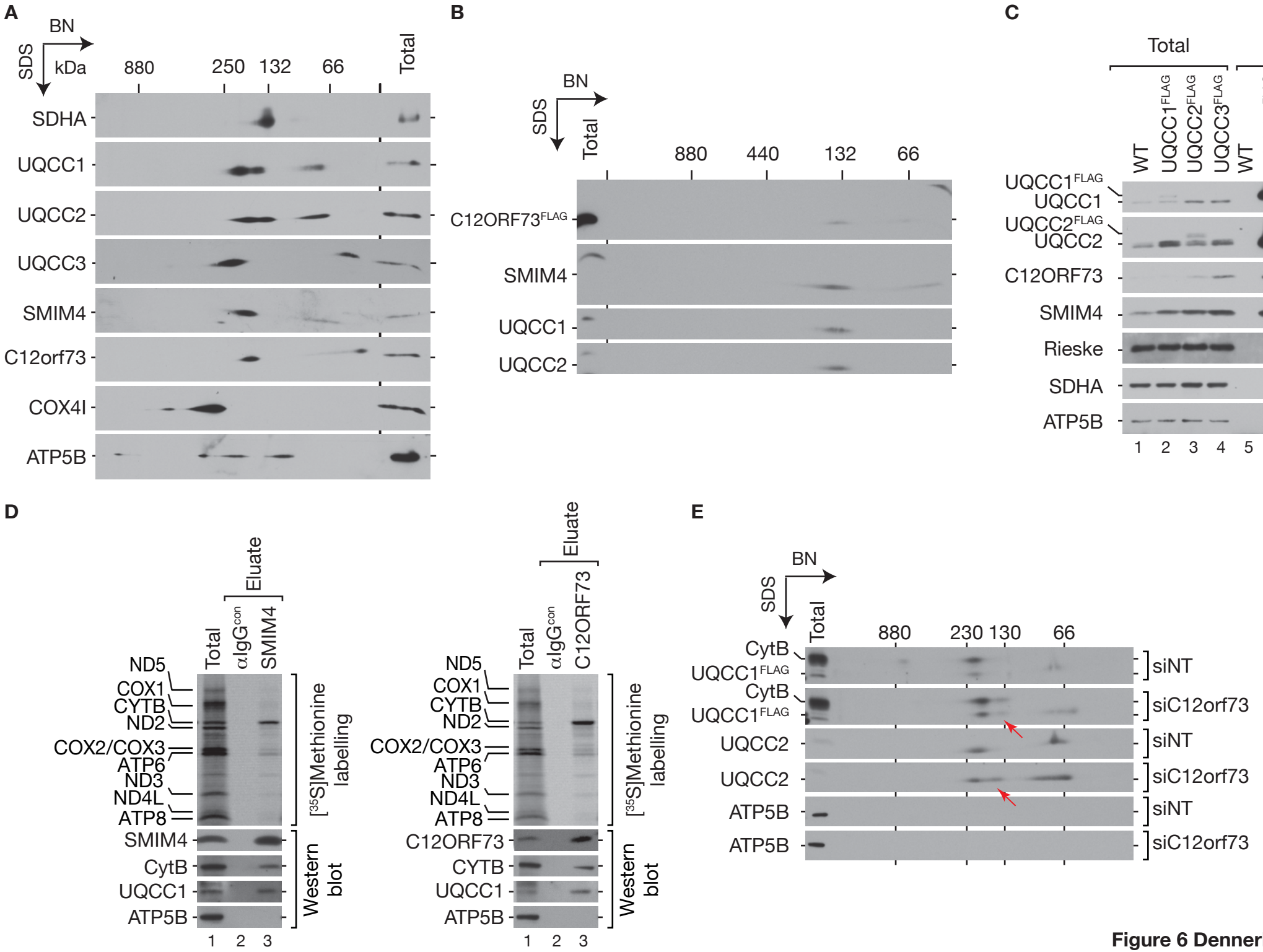

Figure 6 Dennerlein et al.

2.2. Manuscript 2

Expanding the Knowledge of the Mitochondrial Insertase: TMEM126A is a novel interacting partner of the human OXA1L- complex

Sabine Poerschke[1], Silke Oeljeklaus[2,3], Alexander Schenzielorz[2,3], Johannes Sattmann[1], Bettina Warscheid[2,3], Sven Dennerlein[1] and Peter Rehling[1,4]

[1]Institute for Cellular Biochemistry, University of Göttingen, D-37073 Göttingen, Germany

[2]Institute for Biology II, Faculty for Biology, Functional Proteomics, University Freiburg, D- 79104 Freiburg, Germany

[3]BIOSS Centre for Biological Signaling Studies

[4]Max Planck Institute for Biophysical Chemistry, D-37077 Göttingen, Germany

2.2.1. Introduction

Mitochondria are unique organelles with a very distinct morphology and a stunning variety of functions. The mitochondrial matrix harbors the mitochondrial DNA (mtDNA) which encodes for 13 polypeptides, all of them being essential components of the oxidative phosphorylation system (OXPHOS). In aerobic cells, mitochondria produce most of the cellular energy in form of ATP using the respiratory chain complex, formed by multi-subunit enzyme complexes (I-IV) and the ATP synthase (V) (Pfanner *et al.,* 2019). These complexes are composed of nuclear- as well as mitochondrial-encoded subunits. Only 1% of the mitochondrial proteome gets synthesized by mitochondrial ribosomes. Hence, the majority of proteins is nuclear-encoded and needs to be imported into the organelle. The import into mitochondria through the outer mitochondrial (OMM) and inner mitochondrial membrane (IMM) is guaranteed by various translocases, such as the TOM complex in the OMM or the TIM23 complex in the IMM which are embedded into the membranes. However, the proper assembly of these subunits from dual genetic origin is a highly regulated process which must be controlled in a temporal and stoichiometric manner (Meisinger *et al.*, 2008).

In yeast, mitochondrial-encoded polypeptides are exported into the IMM by the insertase Oxa1– a membrane protein of the Oxa1/YidC/Alb3 protein family (Funes *et al.*, 2011). Oxa1 and its human homolog OXA1L span the IMM five times whereas the C -terminal tail is exposed to the mitochondrial matrix (Jia *et al.*, 2003). By this, Oxa1/OXA1L interacts with nascent polypeptide chains prior their synthesis is completed on mitochondrial ribosomes (Haque *et al.*, 2010; Kohler *et al.*, 2009; Szyrach *et al.*, 2003). In yeast, Oxa1 was identified to be crucial for the assembly of complex IV (Bonnefoy *et al.*, 1994) and complex V (Altamura *et al.*, 1996) of the OXPHOS system. Furthermore, it has been proposed that Oxa1 is necessary for the co-translational insertion of all mitochondrial-encoded polypeptides: Cox1, Cox2, Cox3, Atp6, Atp8, Atp9 and cytochrome *b* (He and Fox, 1997; Hell *et al.*, 2001; Stuart, 2002). Moreover, a subset of nuclear-encoded substrates are dependent on the membrane insertion using the OXA-pathway, such as Cox18 and Mdl1, as well as Oxa1 itself (Bohnert *et al.*, 2010; Fiumera *et al.*, 2009).

Because the majority of previous studies is based on the yeast *Saccharomyces cerevisiae (S. cerevisiae)* as a model organism, our knowledge about the human OXA1L insertase machinery is still limited. Preceding analyses provide insights how OXA1L is bound to the mitochondrial ribosome and which ribosomal subunits are involved in this interaction (Itoh *et al.*, 2021). In addition, shRNA-mediated knockdowns of *OXA1L* in human cell lines lead to a disturbed complex I and complex IV assembly (Stiburek *et al.*, 2007). Considering these functions, it was not surprising, that an *OXA1L* patient was identified, who displayed a tissue-specific OXPHOS deficiency jointly responsible for hypotonia and a severe encephalopathy which end up in a lethal cardiorespiratory arrest of the 5-years old patient (Thompson *et al.*, 2018).

According to this, it is indisputable that OXA1L is one of the checkpoints for the biogenesis of OXPHOS machinery because of its insertase activity for primary mitochondrial-encoded subunits. Nonetheless, a molecular picture is missing how especially the human OXA1L protein fulfills its functions, and which other interacting partners are vital for the OXA1L-complex. Therefore, we defined the human OXA1L interactome and identified TMEM126A as a novel component of the human OXA1L-complex and determined biochemically its impact on the OXPHOS assembly and mitochondrial translation in association with OXA1L.

2.2.2. Results

2.2.2.1. Mapping the constituents of the human OXA1L complex

OXA1L is considered as the human mitochondrial insertase of the 13 mitochondrial encoded proteins, however, its interacting partners are not defined. To elucidate the constituents of the human OXA1L-complex in more detail, we created stable HEK293T cell lines, expressing OXA1L with a FLAG-tag at different positions (Figure 1A). Considering the interaction of the C-terminus with the mitochondrial ribosome (Haque *et al.*, 2010) the inducible FLAG-tags were either introduced near the C- terminus, after amino acid 326 or 397, or behind the predicted presequence in the N- terminal region (amino acid 74) (Figure 1A). To investigate the functionality of these proteins, isolated mitochondria were subjected to a FLAG-immunoisolation and eluates were analyzed by Western blotting (Figure 1B). In this manner, we could observe a co-purification of the N- terminal tagged version of OXA1L (^{FLAG}OXA1L) with subunits of the mitochondrial ribosome in addition to the assembly factors MITRAC12 and C12ORF73 (Figure 1B, lane 6). In contrast, our C-terminal tagged constructs seem to be unfunctional in this regard, since the expression was very weak and no interaction with the mitochondrial ribosome could be observed (Figure 1B, lane 7 and 8). The interaction of ^{FLAG}OXA1L with a number of proteins could be visualized when eluates of the FLAG-immunoprecipitation were analyzed by SDS-PAGE and colloidal Coomassie staining (Figure 1C). To identify individual protein bands within the SDS-PAGE, a mass spectrometry analysis was performed (Figure 1C).

To comprehensively identify the components of the OXA1L-containing complex, we undertook a quantitative affinity purification mass spectrometry analysis combined with a stable isotope labeling with amino acids (SILAC) (Figure 1D). Therefore, ^{FLAG}OXA1L and wildtype cells were cultured in media containing either heavy or light amino acids. Subsequently, solubilized mitochondria underwent FLAG-immunoisolation and enriched constituents were determined by mass spectrometry analysis by means of different amino acid incorporation. As expected, we found an enrichment of ribosomal subunits as well as proteins involved in the respiratory chain assembly (Figure 1D), which was confirmed by Western blot analysis (Figure 1E). Moreover, the analysis uncovered the enrichment of TMEM126A, a protein recently reported to be involved in complex I assembly (D'Angelo *et al.*, 2021; Formosa *et al.*, 2021). Like OXA1L, TMEM126A represents a multi-spanning inner membrane protein

by MitoCarta3.0 (Rath *et al.*, 2021) and its C- and N- terminus is exposed to the mitochondrial intermembrane space (Supplementary Figure 1).

Because of the close interaction between OXA1L and the mitochondrial ribosome, we hypothesized that TMEM126A could be isolated with the mitochondrial ribosome, as well. Thus, mL62^{FLAG} containing mitochondria were subjected to immunoisolation and eluates were analyzed again by Western blotting (Figure 1F). Clearly, besides the interaction of OXA1L with the mitochondrial ribosome, the TMEM126A association could be validated. This was further confirmed by performing the experiment vice versa, using an antibody, raised against the endogenous TMEM126A protein, for affinity purifications (Figure 1G). TMEM126A isolated OXA1L and uL1m, which represents the 39S-subunit of the mitochondrial ribosome. Furthermore, we confirmed its interaction with NDUFA5, NDUFB10 and NDUFB11 – proteins involved in the early assembly steps of the ND4 and ND1-module of complex I.

While current studies suggested that TMEM126A is exclusively involved in complex I biogenesis, we were surprised that COX2 was isolated as well, but only marginal amounts of COX1 (Figure 1G). Because COX2 is one of the core components of the cytochrome *c* oxidase, we decided to further investigate on the role of TMEM126A in the context of the OXA1L insertase machinery.

2.2.2.2. Absence of TMEM126A leads to decrease in OXA1L and complex I

To study the function of TMEM126A in detail we utilized two different methods to deplete TMEM126A in HEK293T cells. First, we used siRNA-mediated knockdowns of TMEM126A for 72 hours, secondly a knockout cell line was generated using the standard CRISPR/Cas9 technology (Wiedenheft *et al.*, 2011). For the knockout cell lines, we selected two clones with best survival, which are denotated as AA1 and AB1 in all illustrated experiments. To determine the effects on cell division under knockdown or knockout conditions, we determined the cell number at defined time points in glucose as well as in galactose media, to enhance mitochondrial metabolism (Aguer *et al.*, 2011). The knockdown (siTMEM126A) and the knockout of TMEM126A (TMEM126A$^{-/-}$) affected cell growth in glucose and galactose media compared to wildtype. After siRNA application, the number of cells was reduced by 30% compared to the wildtype control (Figure 2A, left panel). The same was observed for clone AA1

in glucose and galactose media, while clone AB1 showed a stronger growth defect in glucose media (65% of WT), which was even more pronounced in galactose media (27% of WT). These observations prompted us to investigate the steady state levels of mitochondrial proteins during siRNA application and in the TMEM126A$^{-/-}$ clones (Figure 2B, 2C). Under knockdown conditions, we observed a decrease in OXA1L and subunits from complex I (NDUFB8) and complex II (SDHA). However, subunits from complex III (UQCC2), complex IV (COX1, COX6A) and complex V (ATP5B) remained unaffected. In contrast, we could not detect any differences on the steady state levels of OXPHOS structural subunits in TMEM126A$^{-/-}$ mitochondria, except for complex I (NDUFA5; Figure 2C). Even OXA1L was not affected in the knockout which could be explained by a long-term adaptation of the cells.

To correlate the observed growth and the alterations in the steady state levels of mitochondrial proteins, we analyzed mitochondrial complexes on BN-PAGE. Therefore, mitochondria from siRNA treated TMEM126A cells were solubilized in DDM and subjected to native gel electrophoresis, followed by Western blot analysis (Figure 2D). As predicted from the previous protein steady state analysis (Figure 2B) complex I indicated the strongest phenotype (Figure 2D, lane 1-4). However, besides the decrease in complex I, we could further detect a slight decrease in complex IV and complex V. The only complexes which were not influenced by the knockdown of TMEM126A were complex II and complex III. In addition, complex I and IV activity measurements certified the decrease in complex I in siTMEM126A cells (Supplementary Figure 2).

When we inspected OXPHOS complexes from TMEM126A$^{-/-}$ mitochondria, solubilized in DDM, we observed a decrease of complex I on BN-PAGE (Figure 2E, lane 1-3). Interestingly, marginal differences between the two investigated knockout clones could be observed. For TMEM126A$^{-/-}$ AA1 sub-complexes for complex V were visible (Figure 2E, lane 14), which were not observed in clone AB1. Furthermore, both TMEM126A$^{-/-}$ clones seem to be affected regarding super-complex formation (Figure 2E, lane 8 and 9). Using an antibody against the complex III core-subunit cytochrome *b* a shift of complex III to the monomeric form was observed (Figure 2E, lane 8 and 9). Indeed, complex II (SDHA) and complex IV (COX1) were comparable to the wildtype.

Concluding, our results demonstrate that the depletion of TMEM126A leads to a decrease in complex I, both on protein and complex levels. The decrease of OXA1L after

siRNA-mediated knockdown of TMEM126A corroborated the hypothesis of TMEM126A being an interactor of OXA1L.

2.2.2.3. TMEM126A interacts with newly synthesized translation products

Because we identified an interaction between TMEM126A and COX2 (Figure 1G), we wondered if TMEM126A also interacts with newly synthesized mitochondrial encoded proteins, similar to OXA1L. For this purpose, we generated a stable HEK293T cell line, expressing an inducible TMEM126A-FLAG at the C-terminal tail. To address whether TMEM126A associates with newly mitochondrial translation products, $TMEM126A^{FLAG}$ expressing cells were incubated with radioactive [^{35}S] methionine after inhibition of cytosolic protein synthesis. Afterwards, solubilized $TMEM126A^{FLAG}$ cells were applied to FLAG-immunoprecipitation and eluates were analyzed by SDS-PAGE, followed by autoradiography. Unfortunately, the FLAG construct seemed to be dysfunctional because no mitochondrial translation products could be isolated compared to the positive control $C12ORF62^{FLAG}$ (Richter-Dennerlein *et al.*, 2016; Supplementary Figure 3). For this reason, we used two endogenous antibodies from different rabbits against the TMEM126A protein (a and b), and subjected radiolabeled wildtype cells to affinity purification (Figure 3A). As expected, TMEM126A co-purifies predominantly with newly synthesized COX2, but also other mitochondrial translation products could be visualized from the eluates (Figure 3A, lane 3 and 4). Interestingly, the pattern of isolated translation products in the eluate looked similar in comparison to the endogenous antibody purification with OXA1L (Figure 3A, lane 9).

Our next goal was to gain insight into mitochondrial translation in the absence of TMEM126A. First, we used a siRNA-mediated knockdown of TMEM126A and incubated cells for different time points with radiolabeled [^{35}S] methionine. Afterwards, cell lysates were analyzed by SDS-PAGE and visualized by autoradiography and immunodetection (Figure 3B). Compared to the non-targeting control, the mitochondrial translation was overall reduced in the knockdown cells. The most affected translation product is ND1, which reaches merely 40% of the wildtype ND1-level. The translation defect was further intensified when performing the same experiment in $TMEM126A^{-/-}$ cells (Figure 3C, lane 2 and 3). In both knockout clones, the overall translation was reduced to 20% compared to wildtype cells.

To further affirm that the translation defect is not triggered by a reduction of the mitochondrial ribosome, steady state levels of ribosomal subunit proteins were analyzed within isolated mitochondria using Western blot analysis (Figure 3D). Both, the large ribosomal subunit (uL23m, uL12m) and the small ribosomal subunit (mS39, mS40) were comparable to the levels in wildtype mitochondria. Accordingly, the translation deficiency is caused directly by the loss of TMEM126A.

2.2.2.4. TMEM126A - OXA1L interaction is independent from active translation

From studies in the model organism *S. cerevisiae,* it is well known that Oxa1 exports N- terminal domains from mitochondrial encoded membrane proteins across the IMM and helps with the membrane insertion of hydrophobic segments co-translationally. To do so, Oxa1 needs to be bound to the mitochondrial ribosome during the exposition of nascent chains from the ribosome exit tunnel even before these polypeptides are fully synthesized. To investigate this interaction with nascent chains for the human OXA1L as well, HEK293T wildtype cells were treated with puromycin, to induce prematurely termination, additional to radioactive labeling with [^{35}S] methionine. The released nascent chains from the ribosome could further be identified when whole cell lysates were used for affinity purification using an endogenous antibody against OXA1L (Figure 4A). Using this approach, we could clearly show that the human OXA1L copurifies nascent chains in a co-translational manner (Figure 4A, lane 8).

To demonstrate under which conditions TMEM126A is bound to OXA1L, we inhibited the mitochondrial translation for 24 hours by adding thiamphenicol to ^{FLAG}OXA1L expressing cells. Afterwards, isolated mitochondria were used to perform a FLAG-immunoisolation and eluates were analyzed by SDS-PAGE and Western blotting (Figure 4B). Even when mitochondrial translation is inhibited, ^{FLAG}OXA1L copurifies equal amounts of the mitochondrial ribosome (mL45, uL23m, mL62, uS14m and mS39) compared to the non-treated sample. Moreover, TMEM126A could be identified in the eluate when translation was inactivated (Figure 4B, lane 6).

Next, we asked ourselves if the TMEM126A-OXA1L interactions depend on the presence of the mitochondrial ribosome at all. Thus, ^{FLAG}OXA1L mitochondria were incubated with RNase/EDTA before FLAG-immunoisolation to remove mitochondrial ribosomes bound to ^{FLAG}OXA1L (Figure 4C). The Western blot analysis could clarify that

the amounts of co -purified TMEM126A decrease in the eluate when the mitochondrial ribosome dissociates from ^{FLAG}OXA1L (Figure 4C, lane 8). To explore whether TMEM126A is a key component of the human mitochondrial insertase machinery and therefore only present as a fixed component of the OXA1L-complex, we applied a double-immunoprecipitation approach. First, ^{FLAG}OXA1L mitochondria were subjected to FLAG-immunoisolation and subsequently, 90% of the eluate was used for affinity purification using the endogenous TMEM126A antibody (Figure 4D). By this, we were able to analyze the stoichiometrically association of OXA1L with TMEM126A. As shown in the Western blot analysis (Figure 4D), very little amounts of OXA1L could be identified in the unbound fraction which indicate that the majority of OXA1L could be co-purified with TMEM126A.

In summary, our study shows that the interaction between OXA1L and TMEM126A is independent from an active mitochondrial translation but needs the association of a fully assembled mitochondrial ribosome. Additionally, we determined that the majority of ^{FLAG}OXA1L is bound to TMEM126A which leads us to the assumption that TMEM126A is a permanent component of the OXA1L-complex.

2.2.2.5. Figures Manuscript 2

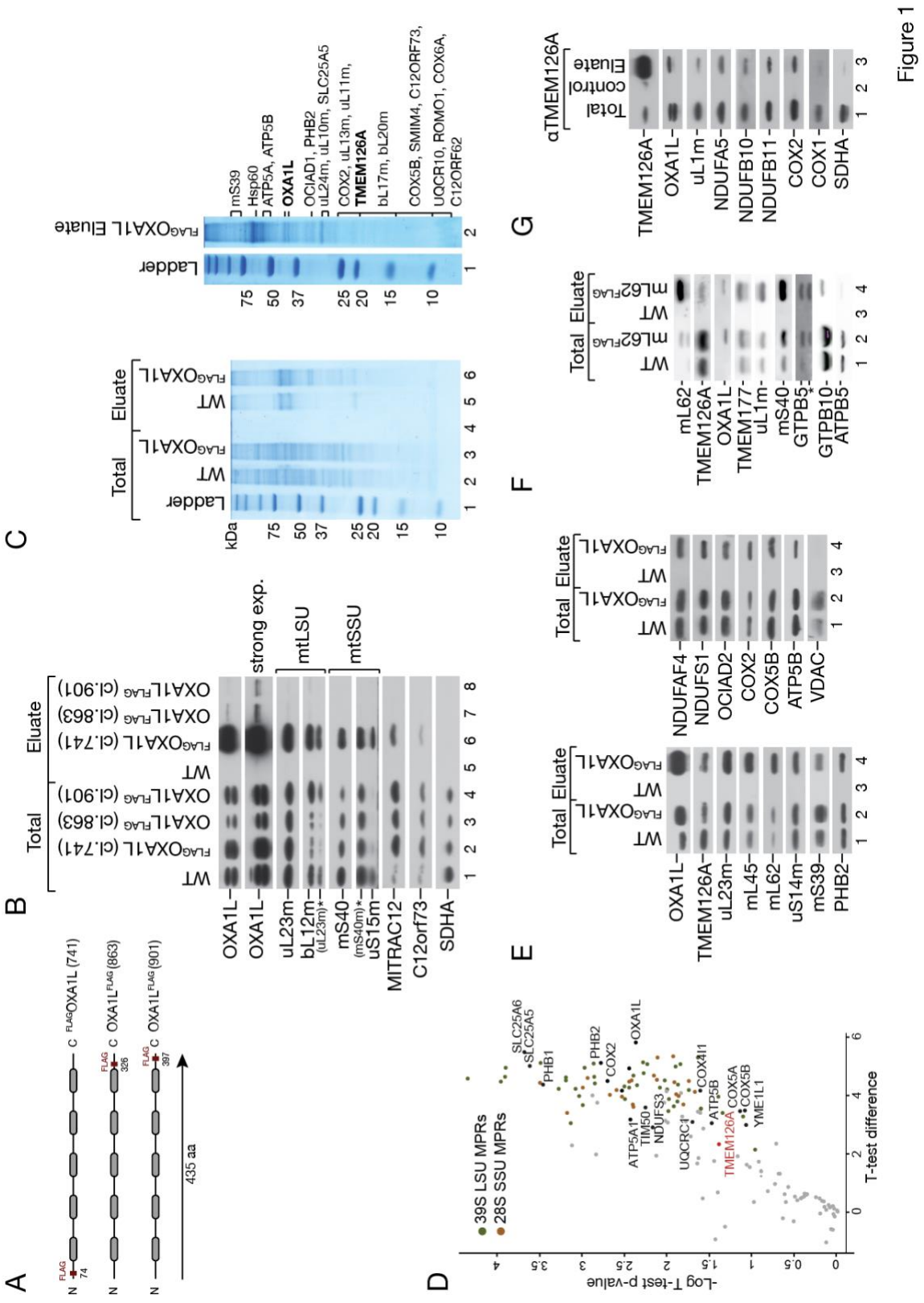

Figure 1

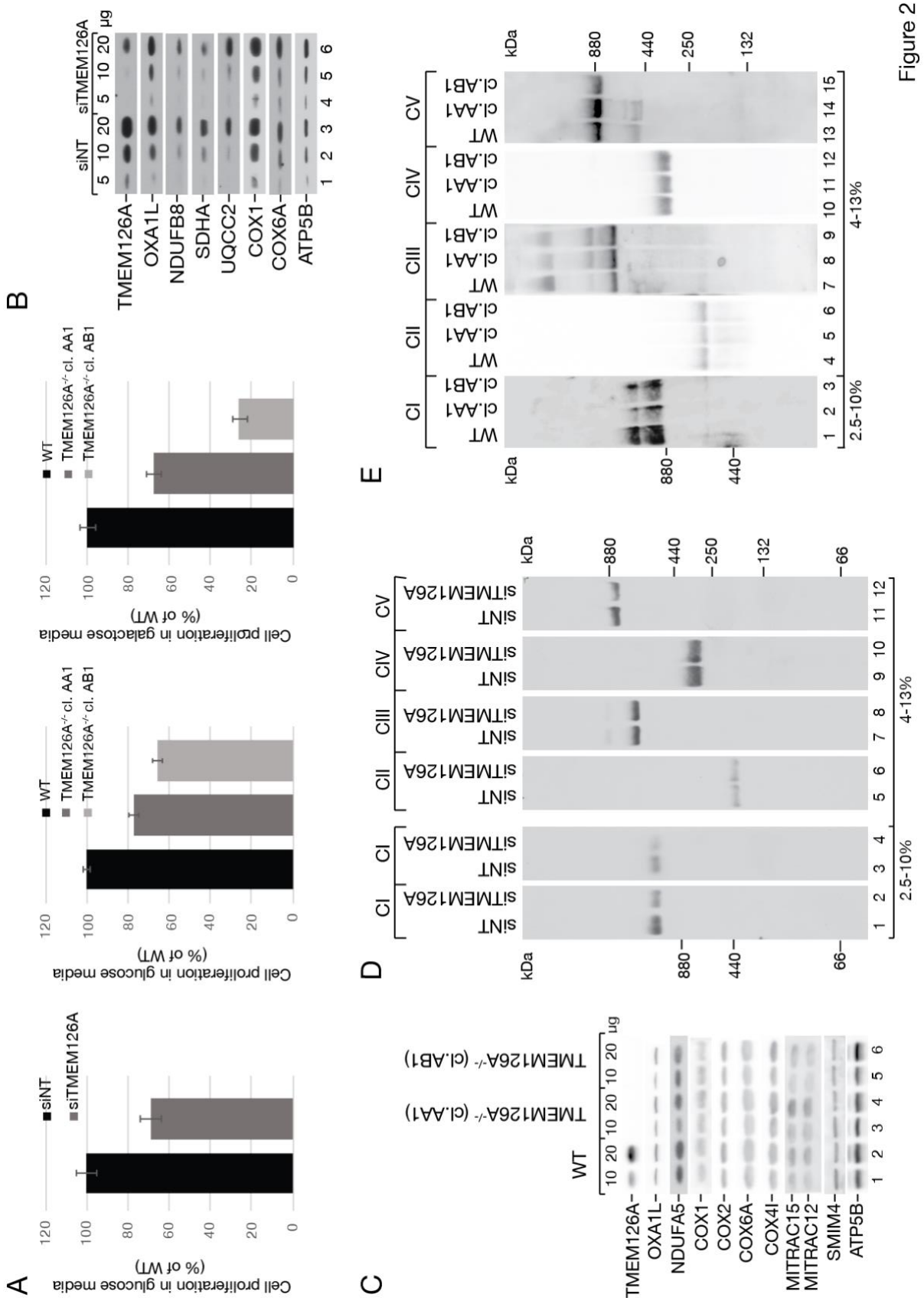
A
Cell proliferation in glucose media (% of WT)
siNT
siTMEM126A
Cell proliferation in glucose media (% of WT)
WT
TMEM126A-/- cl. AA1
TMEM126A-/- cl. AB1
Cell proliferation in galactose media (% of WT)
B
siNT
siTMEM126A
5 10 20 5 10 20 µg
1 2 3 4 5 6
TMEM126A
OXA1L
NDUFB8
SDHA
UQCC2
COX1
COX6A
ATP5B
C
WT
TMEM126A-/- (cl.AA1)
TMEM126A-/- (cl.AB1)
10 20 10 20 10 20 µg
1 2 3 4 5 6
TMEM126A
OXA1L
NDUFA5
COX1
COX2
COX6A
COX4I
MITRAC15
MITRAC12
SMIM4
ATP5B
D
CI CII CIII CIV CV
siNT siTMEM126A
1 2 3 4 5 6 7 8 9 10 11 12
2.5-10%
4-13%
kDa
880
440
66
E
CI CII CIII CIV CV
WT cl.AA1 cl.AB1
1 2 3 4 5 6 7 8 9 10 11 12 13 14 15
2.5-10%
4-13%
kDa
880
440
250
132

Figure 2

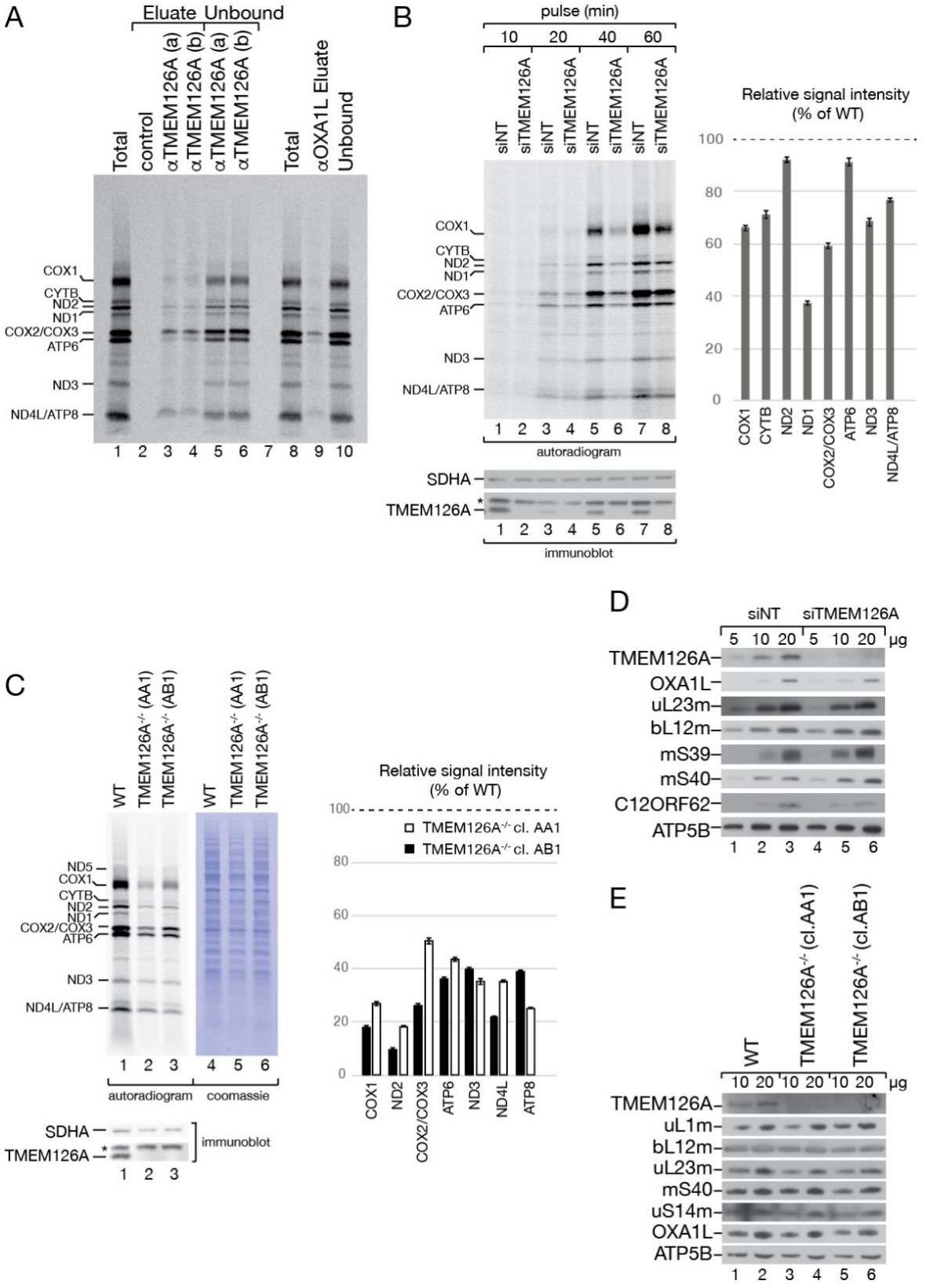
A
Eluate
Unbound
Total
control
αTMEM126A (a)
αTMEM126A (b)
αTMEM126A (a)
αTMEM126A (b)
Total
αOXA1L Eluate
Unbound
COX1
CYTB
ND2
ND1
COX2/COX3
ATP6
ND3
ND4L/ATP8
1 2 3 4 5 6 7 8 9 10
B
pulse (min)
10 20 40 60
siNT siTMEM126A siNT siTMEM126A siNT siTMEM126A siNT siTMEM126A
COX1
CYTB
ND2
ND1
COX2/COX3
ATP6
ND3
ND4L/ATP8
1 2 3 4 5 6 7 8
autoradiogram
SDHA
TMEM126A *
1 2 3 4 5 6 7 8
immunoblot
Relative signal intensity
(% of WT)
100
80
60
40
20
0
COX1 CYTB ND2 ND1 COX2/COX3 ATP6 ND3 ND4L/ATP8
C
WT
TMEM126A-/- (AA1)
TMEM126A-/- (AB1)
WT
TMEM126A-/- (AA1)
TMEM126A-/- (AB1)
ND5
COX1
CYTB
ND2
ND1
COX2/COX3
ATP6
ND3
ND4L/ATP8
1 2 3 4 5 6
autoradiogram coomassie
SDHA
TMEM126A *
immunoblot
1 2 3
Relative signal intensity
(% of WT)
100
80
60
40
20
0
TMEM126A-/- cl. AA1
TMEM126A-/- cl. AB1
COX1 ND2 COX2/COX3 ATP6 ND3 ND4L ATP8
D
siNT siTMEM126A
5 10 20 5 10 20 µg
TMEM126A
OXA1L
uL23m
bL12m
mS39
mS40
C12ORF62
ATP5B
1 2 3 4 5 6
E
WT
TMEM126A-/- (cl.AA1)
TMEM126A-/- (cl.AB1)
10 20 10 20 10 20 µg
TMEM126A
uL1m
bL12m
uL23m
mS40
uS14m
OXA1L
ATP5B
1 2 3 4 5 6

Figure 3

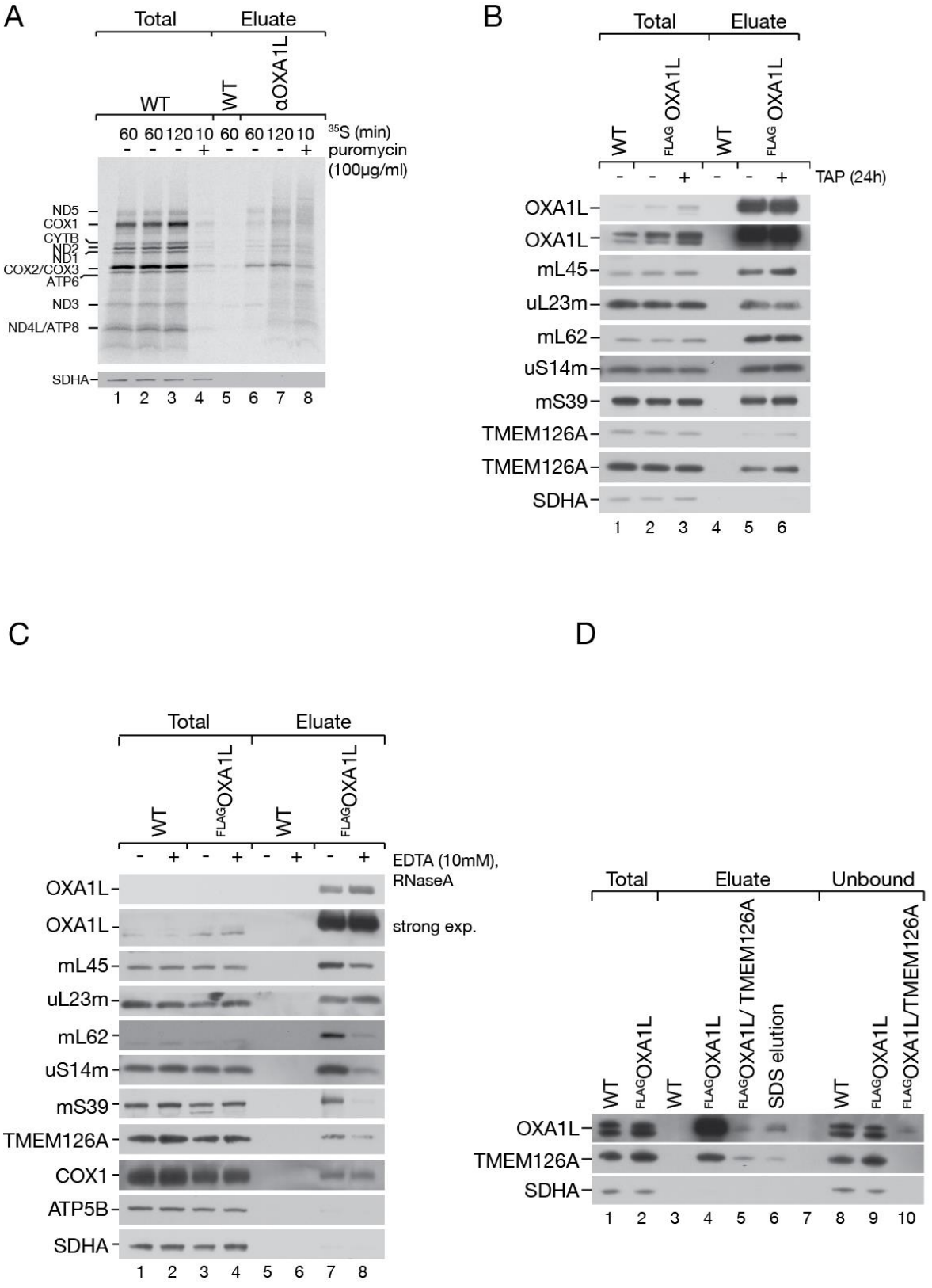
A
Total
Eluate
WT
WT
αOXA1L
60 60 120 10 60 60 120 10 35S (min)
- - - + - - - + puromycin
(100µg/ml)
ND5
COX1
CYTB
ND2
ND1
COX2/COX3
ATP6
ND3
ND4L/ATP8
SDHA
1 2 3 4 5 6 7 8
B
Total
Eluate
WT
FLAG OXA1L
WT
FLAG OXA1L
- - + - - + TAP (24h)
OXA1L
OXA1L
mL45
uL23m
mL62
uS14m
mS39
TMEM126A
TMEM126A
SDHA
1 2 3 4 5 6
C
Total
Eluate
WT
FLAGOXA1L
WT
FLAGOXA1L
- + - + - + - + EDTA (10mM), RNaseA
OXA1L
OXA1L
strong exp.
mL45
uL23m
mL62
uS14m
mS39
TMEM126A
COX1
ATP5B
SDHA
1 2 3 4 5 6 7 8
D
Total
Eluate
Unbound
WT
FLAGOXA1L
WT
FLAGOXA1L
FLAGOXA1L/ TMEM126A
SDS elution
WT
FLAGOXA1L
FLAGOXA1L/TMEM126A
OXA1L
TMEM126A
SDHA
1 2 3 4 5 6 7 8 9 10

Figure 4

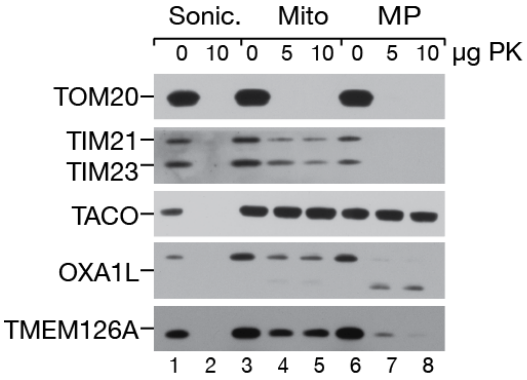

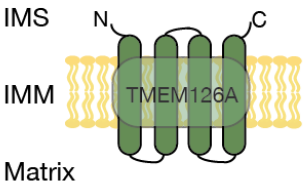

Supplementary Figure 1

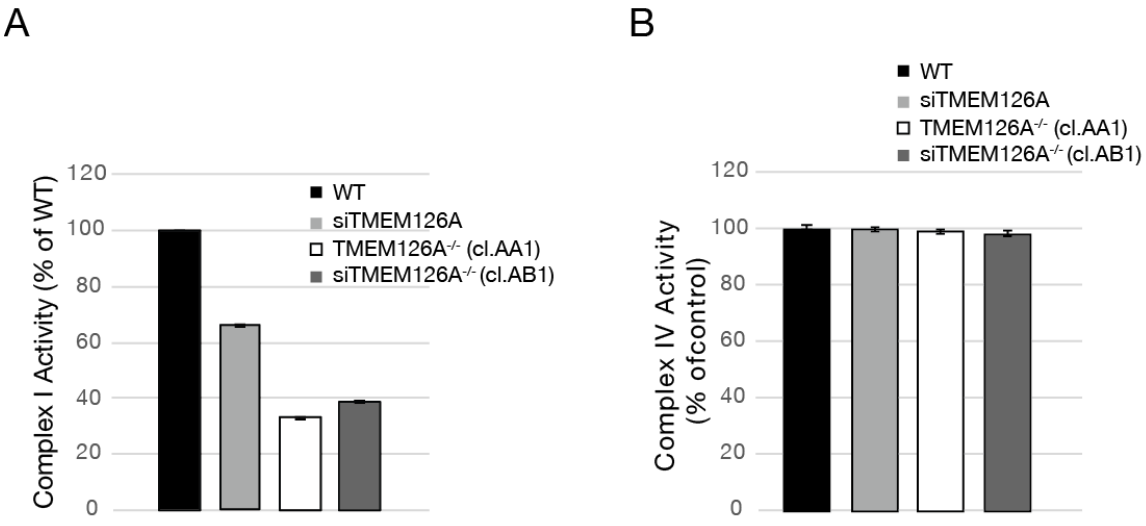

Supplementary Figure 2

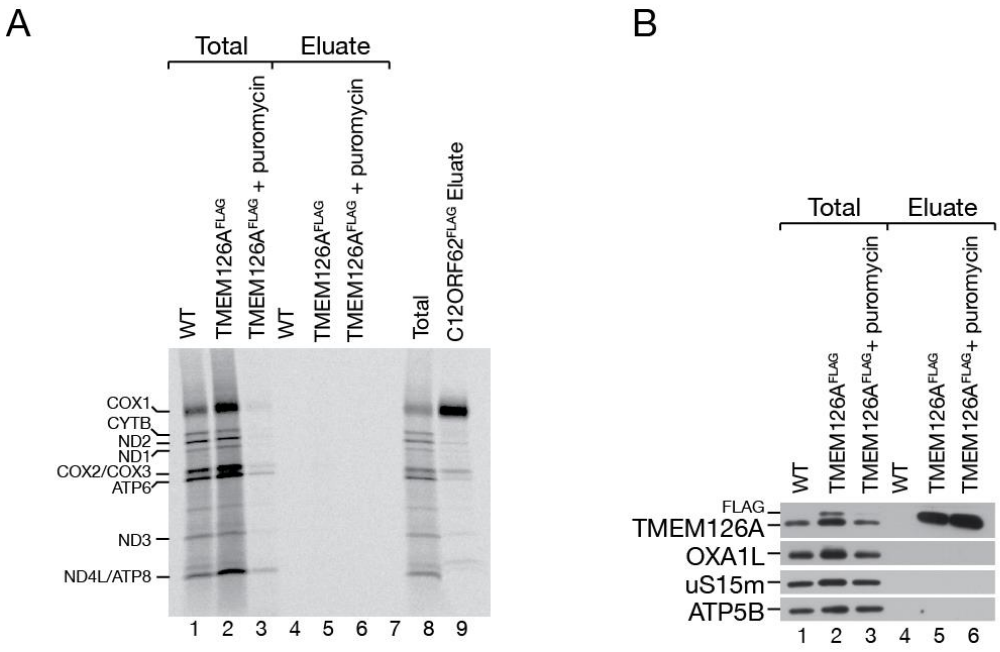

Supplementary Figure 3

2.2.2.6. Figure Legend

Figure 1 OXA1L interacts with the mitochondrial ribosome and TMEM126A. (A) Generation of different stable OXA1L-FLAG expressing HEK293T cell lines. **(B)** FLAG-immunoprecipitation was performed using isolated mitochondria from HEK293T cells expressing FLAG tagged OXA1L. Total 1%; eluates 100%. **(C)** Equal amounts of isolated mitochondria from wildtype HEK293T cells and ^{FLAG}OXA1L cells were subjected to FLAG-immunoprecipitation after SILAC-labeling for at least two weeks. Liquid eluates were used for mass spectrometry analyses (n=4) and additional visualized by SDS-PAGE following colloidal Coomassie staining. **(D)** ^{FLAG}OXA1L eluate was subjected to SDS-PAGE and individual slices were analyzed by mass spectrometry analysis (n=2). **(E)** FLAG-immunoisolation of isolated mitochondria from HEK293T cells expressing ^{FLAG}OXA1L. Total 1%; eluate 100%. **(F)** Isolated mitochondria from HEK293T cells expressing C12ORF62^{FLAG} were subjected to FLAG-immunoprecipitation. Total 1%, eluate 100%. **(G)** Isolated mitochondria from wildtype HEK293T cells were used to perform an immunoisolation using endogenous antibody for TMEM126A. Total 3%, eluate 100%.

Supplementary Figure 1 TMEM126A is an inner membrane protein. Isolated wildtype mitochondria were subjected to swelling experiment to investigate localization of TMEM126A. Sonic. = sonication; Mito = mitochondria; MP = mitoplast; PK = proteinase K. The C-terminus of TMEM126A is exposed to the intermembrane space (IMS).

Figure 2 The absence of TMEM126A leads to decrease in complex I. (A) Cell growth from non-targeted HEK293T cells (siNT) were compared with cell growth of HEK293T cells treated with TMEM126A specific siRNA (siTMEM126A). Wildtype (WT) HEK293T cells and TMEM126A$^{-/-}$ (cl.AA1 and cl. AB1) were cultured for seven days in DMEM media either containing glucose or galactose. Cell counts of a six-well plate were measured using a hemocytometer. Data are shown as the percentage of the control (mean ± SEM, n=3). **(B)** Protein steady state analysis of isolated mitochondria after depletion of TMEM126A (siTMEM126A). siRNA treatment was performed for 72 hours and analyzed with SDS-PAGE and Western Blot analyses. **(C)** Isolated mitochondria from TMEM126A$^{-/-}$ (cl.AA1 and AB1) were analyzed by SDS-PAGE and Western blotting to check protein steady state levels. **(D)** Mitochondrial complexes were analyzed by 4-13% BN-PAGE with isolated mitochondria from siTMEM126A compared with non-targeting control. Mitochondria were solubilized in 0.4% DDM. **(E)** Isolated mitochondria from TMEM126A$^{-/-}$ (cl.AA1 and cl.AB1) cells were solubilized in 0.4% DDM and subjected to BN-PAGE analyses and compared to WT samples. Complexes were detected using appropriate antibodies.

Supplementary Figure 2 TMEM126A depletion affects respiratory chain activity of complex I. Enzymatic activity of complex I **(A)** and complex IV **(B)** were measured using a plate reader assay from Abcam. Solubilized siTMEM126A cells and TMEM126A$^{-/-}$ cells were compared to wildtype and non-targeting samples. Data are shown as percentage of the control (mean ± SEM, n=3).

Figure 3 TMEM126A interacts with newly synthesized mitochondrial translation products. (A) Solubilized HEK293T cells were subjected to immunoisolation using indicated antibodies following radioactive labeling using [^{35}S] methionine for one hour. Samples were analyzed by SDS-PAGE and autoradiography **(B)** Mitochondrial translation of non-targeted (siNT) and siRNA-treated (siTMEM126A) cells were analyzed after [^{35}S] labeling using SDS-PAGE and autoradiography. Radioactive methionine was applied to cells for 10, 20, 40 and 60 minutes (min). Signal intensities of mitochondrial translation products were quantified according to percentage of non-targeting control (mean ± SEM, n=3). **(C)** Quantification of the amount of newly synthesized mitochondrial translation products within TMEM126A$^{-/-}$ cells (cl.AA1 and cl.AB1) after radioactive labeling for one hour (mean ± SEM, n=3). **(D)** Protein steady state analysis of ribosomal subunits from isolated mitochondria of control (siNT) and siTMEM126A cells. **(E)** Steady state analysis of ribosomal proteins within the knockouts of TMEM126A.

Supplementary Figure 3 Immunoisolation of TMEM126A^{FLAG} mitochondria. (A) HEK293T cells expressing TMEM126A^{FLAG} were subjected to FLAG-immunoprecipitation after labeling of mitochondrial translation products with [^{35}S] methionine and puromycin. C12ORF62^{FLAG} cells were used as positive control. **(B)** Western Blot analyses of samples from Suppl. Fig. 3A.

Figure 4 TMEM126A interaction with OXA1L is independent from active translation. (A) Radiolabeled wildtype HEK293T cells were subjected to immuoisolation with indicated antibodies. Nascent chain polypeptides were labeled with puromycin. Samples were analyzed with SDS-PAGE and autoradiography. **(B)** Mitochondria from HEK29T cells expressing ^{FLAG}OXA1L were used to perform FLAG-immunoprecipitation. Mitochondrial translation was inhibited in half of the samples by addition of thiamphenicol for 24 hours. **(C)** Isolated mitochondria were subjected to FLAG-immunoisolation after RNaseA and EDTA treatment and analyzed by Western blotting. **(D)** Double-immunoisolation using isolated mitochondria from ^{FLAG}OXA1L expressing HEK293T cells. 90% of ^{FLAG}OXA1L eluate was used for immunoisolation using an antibody against TMEM126A.

.

2.2.3. Discussion

In this study, we examined the unique relationship between the human insertase OXA1L and the inner membrane protein TMEM126A which has been primarily described as complex I assembly factor (D'Angelo *et al.*, 2021; Formosa *et al.*, 2021).

OXA1L is defined as the mitochondrial insertase machinery, responsible for membrane insertion of the 13 mitochondrial-encoded polypeptides (Haque *et al.*, 2010). By using an inducible ^{FLAG}OXA1L expressing HEK293T cell line we determined the interactome of OXA1L. As expected, subunits from the mitochondrial ribosome (100% of the 28S subunit and 92% of the 39S subunit) as well as proteins from the OXPHOS machinery could be identified. Moreover, we found TMEM126A as a novel OXA1L-associated factor, which is also bound to the mitochondrial ribosome.

A few studies have examined TMEM126A as membrane protein of the IMM (Hanein *et al.*, 2013; Meyer *et al.*, 2010). TMEM126A is conserved within metazoa, while its paralog TMEM126B only seems to exists in human (Andrews *et al.*, 2013; Formosa *et al.*, 2021; Heide *et al.*, 2012). TMEM126A and TMEM126AB were already described as complex I assembly factors, specifically involved in the biogenesis of the mitochondrial complex I intermediate assembly (MCIA) complex (Alston *et al.*, 2016; Andrews *et al.*, 2013; D'Angelo *et al.*, 2021; Formosa *et al.*, 2021). Additionally, recent studies have explored the role of TMEM126A in the assembly of complex I in more detail. TMEM126A was described to be crucial for the biogenesis of the ND4-module, which is the central constituent of the hydrophobic complex I arm in the IMM (Formosa *et al.*, 2021). Furthermore, the repression of the complex I core subunit NDUFS3 in an osteosarcoma 143B$^{-/-}$ cell line (Kurelac *et al.*, 2019) leads to an accumulation of TMEM126A. The aggregated TMEM126A was identified in the ND4-module together with NDUFB6, indicating that TMEM126A acts as an early complex I assembly factor (D'Angelo *et al.*, 2021).

When we used siRNA-mediated knockdowns of TMEM126A, the most obvious defect could be observed in complex I as well. Other complexes from the OXPHOS machinery remained stable, except for complex V where we observed a slight decrease. However, in steady state protein levels from isolated siTMEM126A mitochondria we could further detect a slight decrease in OXA1L. In addition, we could confirm the deficiency in complex I by using CRISPR/Cas9-generated knockout cell lines for our analyses.

Due to the sequence similarities between TMEM126A and TMEM126B, speculations arose if both proteins could compensate each other in case of mutations or dysfunctionality. But recently it was shown that the complex I deficiency, caused by the deletion of TMEM126A, is irreparable by the overexpression of TMEM126B^{FLAG} (Formosa *et al.*, 2021). Therefore, the role of TMEM126A is potentially independent from TMEM126B and needs a more detailed investigation, especially because of its unique feature to bind to OXA1L.

Interestingly, by labeling mitochondrial translation products, the immunoprecipitations with the endogenous TMEM126A antibody showed an interaction with all newly synthesized mitochondrial-encoded translation products, similar to OXA1L. This provides us an indication of its overlapping function as a general interacting partner of the human OXA1L- complex apart from its complex I association. As a consequence, the deletion of TMEM126A, using either siRNA or knockout cell lines, caused a general mitochondrial translation defect. This translation defect was not provoked by the reduction of the mitochondrial ribosome which could be confirmed by steady state protein analysis. Rather, it could be explained by the decreased protein levels of OXA1L while TMEM126A was reduced. The role of OXA1L in the assembly of the NADH:ubiquinone oxidoreductase was already explored in recent studies (Stiburek *et al.*, 2007). During the absence of OXA1L in HEK293T cells, a considerably decrease in the steady state levels as well as in the activity of complex I was reported (Stiburek *et al.*, 2007). However, a reduction of OXA1L was not detectable in both knockout clones of the TMEM126A protein, which argues against a direct effect caused by the decrease of OXA1L.

From studies in *S. cerevisiae* it is known that Oxa1 interacts with nascent polypeptide chains during their mitochondrial translation (Szyrach *et al.*, 2003). To investigate this in cultured human cells we used the endogenous antibody against the human OXA1L protein for immunoprecipitations. Thus, we could determine that OXA1L interacts with nascent chains, even when they are released from the mitochondrial ribosome after puromycin treatment. Furthermore, it was shown that the presence of mitochondrial translation products on ribosomes are not crucial for the interaction of Oxa1/OXA1L with the mitochondrial ribosome (Richter-Dennerlein *et al.*, 2016; Szyrach *et al.*, 2003). In this present study, we addressed this interaction for TMEM126A as well. After inhibition of the mitochondrial translation by thiamphenicol, the interaction between

OXA1L and TMEM126A seems to be unaffected, indicating that this interaction is independent from an active mitochondrial translation. To clarify if the OXA1L-TMEM126A interaction relies on the association of the mitochondrial ribosome in general, isolated mitochondria were incubated with RNase to degrade single-stranded RNA and EDTA to destabilize the mitochondrial ribosome. Consequently, the interaction between TMEM126A and OXA1L was disturbed which as well speaks for a ribosome-associated cooperation. Nevertheless, the interaction between TMEM126A and OXA1L is independent from an active translation process.

Finally, it was of importance to clarify the stoichiometric interaction of TMEM126A to OXA1L. Assuming that TMEM126A only exists in a defined complex I specific pool, it would be expected that a large amount of OXA1L is not associated with TMEM126A. Thus, we isolated the ^{FLAG}OXA1L-complex, following by a second immunoprecipitation using an endogenous antibody against TMEM126A. Our experiment shows that the majority of isolated ^{FLAG}OXA1L was bound to TMEM126A and only little amounts of OXA1L could be detected in the 'unbound' fraction, representing OXA1L- complexes without TMEM126A.

Overall, these findings demonstrate that TMEM126A has a more extended function as assumed previously. It can be characterized by its role in the assembly of complex I as well as by its strong association with OXA1L, indicating that TMEM126A is a so far unknown constituent of the human OXA1L-complex.

3. Discussion

The outer as well as the inner mitochondrial membrane are characterized by their protein-rich environment. Proteins, either translated on cytosolic or mitochondrial ribosomes, are integrated into the mitochondrial membranes in a highly controlled process resulting in the formation of macromolecular complexes function for example as translocases or as OXPHOS complexes. This process is assisted by dedicated chaperones and so- called assembly factors, often proteins of small molecular weight, which are necessary for the guidance of individual subunits and to stabilize assembly intermediates (Pfanner *et al.*, 2019).

The OXPHOS complexes are harbored in the inner mitochondrial membrane and are required to transfer electrons for the concluding step of ATP production by the ATP synthase (complex V). During assembly of these complexes, the balance between nuclear- and mitochondrial-encoded subunits is of particular importance and it is still unclear how the mitochondrial translation is adjusted in concern to the influx of nuclear-encoded precursor proteins (Priesnitz and Becker, 2018; Richter-Dennerlein *et al.*, 2016). It is suggested that a disturbed assembly procedure in one of these complexes can lead to far- reaching consequences, resulting in a dysfunctional OXPHOS machinery. Hence it is not surprising, that many human diseases are associated with such dysfunctionalities, e.g. inherited neurometabolic disorders, cardiovascular diseases or cancer (Friedrich *et al.*, 2021; Hock *et al.*, 2020; Ng *et al.*, 2021).

Over the years, an enormous amount of research investigated the detailed mechanisms of the individual assembly steps of each OXPHOS complex, especially by using the model organism *S. cerevisiae.* During the last decade, it became evident that the mechanisms and involved proteins in yeast are not entirely conserved in metazoan and require further investigation. Particularly our knowledge about assembly regulators and different assembly steps in human cells is still limited.

Since high-end mass spectrometry is an opportunity to gain insights into complex constituents, protein-protein interactions or protein modifications, we used this approach to define and further investigate uncharacterized proteins involved in the assembly of the respiratory chain complex III and IV as well as regulators bound to the mitochondrial ribosome, focusing on their interactions with the insertase machinery OXA1L, responsible for insertion of mitochondrial-encoded proteins into the IMM.

3.1. C12ORF73 and SMIM4 are proteins involved in the early assembly of the cytochrome *bc1* complex

The human cytochrome *bc1* complex is composed of eleven subunits, whereas only one subunit, namely cytochrome *b*, is encoded by the mitochondrial genome. The only difference between the mammalian complex III and the one in yeast, is the presence of one additional subunit (Fernández-Vizarra and Zeviani, 2015). These investigations were already made almost two decades ago using crystal-structure analysis (Hunte *et al.*, 2000; Iwata *et al.*, 1998). Nevertheless, the assembly of complex III has been studied mainly in *S. cerevisiae* and experimental data, on how the biogenesis of complex III intermediates takes place in the mammalian system are missing (Fernandez-Vizarra and Zeviani, 2018). To date, only a few orthologs of human assembly factors, such as UQCC1 and UQCC2 (Ubiquinol-Cytochrome *c* Reductase Complex Assembly Factor) have been investigated (Crofts, 2004; Gil-Borlado *et al.*, 2009; Tucker *et al.*, 2013; Wanschers *et al.*, 2014). During the initial assembly step, UQCC1 and UQCC2 are needed to insert cytochrome *b* into the inner mitochondrial membrane co-translationally (Tucker *et al.*, 2013; for detailed schema, see page 10). Additionally, one of the last steps known from recent studies in human cell lines is the incorporation of the RIESKE protein (UQCRFS1) into a dimeric, but inactive pre-complex III (Fernández-Vizarra *et al.*, 2009; Gil-Borlado *et al.*, 2009).

In this present study, we investigated and defined the role of two novel, so far uncharacterized assembly factors, involved in the biogenesis of the early complex III assembly intermediates in human. SMIM4 (small integral membrane protein 4) and C12ORF73, the two identified proteins, are conserved in vertebrates but not in yeast. SMIM4 was already explored *in vivo* as potential ribosome-associated factor in proteomic analysis of the mitochondrial ribosome in different murine tissues (Busch *et al.*, 2019). Interestingly, in parallel to our studies the function of C12ORF73 was examined in the model organism zebrafish (*Danio rerio*) and different human cell lines as well (Zhang *et al.*, 2020).

In agreement with our results, Zhang and colleagues explored the interaction of C12ORF73 exclusively with subunits of complex III, which was confirmed using a C12ORF73-FLAG expressing HEK293T cell line and isolated mitochondria from mouse heart expressing a C12ORF73-FLAG construct. Additionally, *in vivo* experiments showed that the C12ORF73 protein is highly expressed in skeletal and cardiac muscle

cells of zebrafish larvae. In C12ORF73 knockout animals, a dramatic growth phenotype could be detected by 65 dpf (days post fertilization). The low body weight of the knockout zebrafish could be explained by the food intake, which was significantly less compared to wildtype animals. Besides, the activity of the C12ORF73 knockout larvae were reduced compared to the healthy wildtype. The phenotype was further aggravated in the F_2 generation, resulting in death already after 42 dpf. Furthermore, biochemically analyses were performed to investigate the role of C12ORF73 in context with the OXPHOS machinery. Zhang and colleagues (2020) could detect a drastic decrease of complex III subunits (UQCRC1 and UQCRC2) when C12ORF73 was absent. In addition, isolated adult skeletal muscle mitochondria showed a decreased relative respiratory chain activity in mainly all complexes, which was most prominent in complex III causing a reduction of 50%. This could be detected in BN- PAGE analyses as well, where a 90% reduction of the mature complex III dimer was visible (Zhang *et al.*, 2020).

Moreover, this presented study provides detailed information about the timeframe when C12ORF73 and SMIM4 act as so-called assembly factors (Figure 3.1). In addition to the previous described data, we defined in more detail the interaction of C12ORF73 and SMIM4 with proteins involved in the very early assembly of the cytochrome *bc1* complex (Figure 4F and 5A, Manuscript 1). Zhang and colleagues (2020) explored the interaction between C12ORF73, UQCRC1 and UQCRC2 (Fernandez-Vizarra and Zeviani, 2018). Both proteins did not join the complex III intermediate until the haemylation occurred. In our immunoprecipitations we could show, that C12ORF73^{FLAG} as well as SMIM4^{FLAG} already interact with newly synthesized cytochrome *b* (Figure 6D, Manuscript 1). Additionally, we explored the interaction of C12ORF73 and SMIM4 with UQCC1 and UQCC2 (Figure 6C, Manuscript 1), prior to the incorporation of haeme b_L and haeme b_H. At the same time, the investigation of SMIM4 in the proteome analysis of the mitochondrial ribosome is a strong indication of its interaction with cytochrome *b* in a co-translational manner. Its dependency on C12ORF73, shown in our siRNA experiments (Figure 5B, Manuscript 1), leads to the assumption that C12ORF73 also binds to the cytochrome *b* polypeptide and interacts together with SMIM4 in a cooperative manner.

Whether SMIM4 and C12ORF73 have a secondary function within the translational process cannot be concluded from this study. Another possible role could lie in the

participation during the import of nuclear-encoded subunits from complex III, but this hypothesis needs further investigation.

Overall, the observations of this present study and the work from Zhang *et al.* (2020) are in line and provide an experimental basis for a better understanding of the complex III assembly pathway in higher eukaryotes (Figure 3.1).

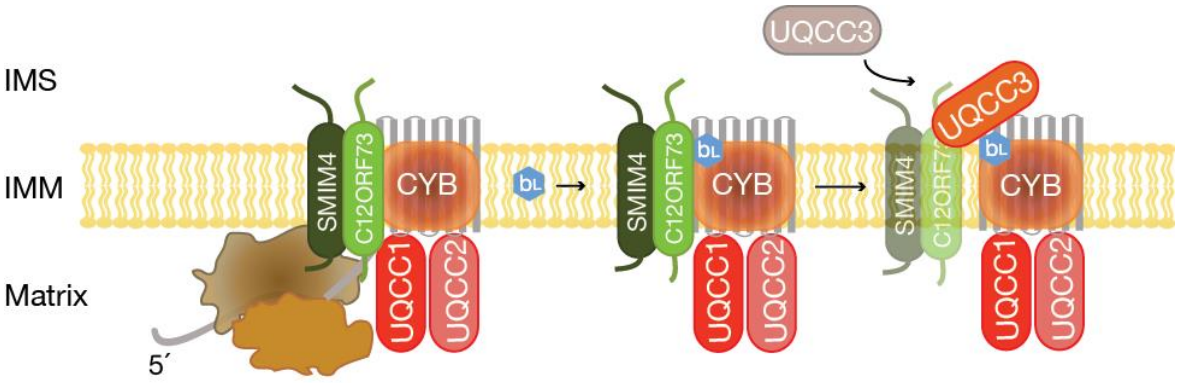

Figure 3.1 Model of early complex III assembly considering the presence of SMIM4 and C12ORF73. The co-translationally insertion of cytochrome *b* (CYTB) into the inner mitochondrial membrane (IMM) is accompanied by UQCC1 and UQCC2, which initiate the translation on mitochondrial ribosomes. SMIM4 and C12ORF73 are associated to the newly synthesized CYTB and assist during the first steps of complex III assembly.

3.2. Is Complex III a checkpoint for respiratory chain maturation?

We identified C12ORF73 as a protein involved in the early assembly of complex III, due to its exclusive interaction with subunits from this individual complex and newly- synthesized cytochrome *b* (Figure 5A and 6D, Manuscript 1). Nevertheless, in the absence of C12ORF73 we detected a slight decrease of complex I and IV by analyzing protein complexes on BN- PAGE in siC12ORF73 treated mitochondria (Figure 5E, Manuscript 1). Even there is no obvious interaction of C12ORF73 with other subunits apart from complex III (Figure 5A, Manuscript 1), its absence has a secondary effect on different respiratory chain complexes. This observation leads to the question how deficiencies in one individual complex can influence the overall OXPHOS machinery?

Because of its central position in the respiratory chain and its role in supercomplex-formation by binding to complex I and IV ($cI+cIII_2+cIV_n$), a more pleiotropic function

for complex III has been hypothesized (Protasoni *et al.*, 2020). Past studies have hinted at a link between assembly of complex III and the complex III-mediated maturation of complex I and IV (Protasoni *et al.*, 2020; Schägger and Pfeiffer, 2001). Protasoni *et al.* (2020) reported that the absence of complex III's enzymatic activity in osteosarcoma-derived cybrid cells with mutated *cytochrome b* leads to a decreased activity of complex I as well. Furthermore, they provided data that a mutation in the mitochondrial-encoded cytochrome *b* (Rana *et al.*, 2000) causes the accumulation of complex III intermediates which supposedly promotes the stalling of complex I during its assembly. Similar observations were made in complex III-deficient mouse cell lines (Acín-Pérez *et al.*, 2004). Astonishingly, the loss of complex I does not significantly influence the assembly or activity of complex III in the same degree (Acín-Pérez *et al.*, 2004; DiMauro and Schon, 2003; Kruse *et al.*, 2008). *NDUFS4* knockout mice, with a complex I deficiency, showed a slight reduction in complex III activity, but indeed the oxygen consumption and ATP-levels were similar to control animals (Kruse *et al.*, 2008).

These finding, therefore, provide evidence for the unique impact of complex III on respiratory chain biogenesis. Further research should be undertaken to ascertain how complex III acts as a platform for the assembly of complex I and IV, especially considering the function of supercomplexes within mitochondria.

3.3. SMIM4 and C12ORF73 are potential interactors of the mitochondrial quality control system

In the complex isolation of SMIM4^{FLAG} and C12ROF73^{FLAG} we identified different proteases and prohibitins as potential interacting candidates beside proteins involved in the assembly of complex III (Figure 4F, Manuscript 1; for C12ORF73 data not shown). In the mass spectrometry analysis of SMIM4^{FLAG} isolations, we determined the association of SMIM4^{FLAG} with mAAA-proteases, like AFG3L2 (Ehses *et al.*, 2009) and SPG7 (Almontashiri *et al.*, 2014), and the membrane-anchored iAAA-protease YME1L (Shi *et al.*, 2016). In addition, prohibitins PHB1 and PHB2 (Signorile *et al.*, 2019), were identified in SMIM4^{FLAG} immunoprecipitations as well. These interactions were confirmed by Western blot analysis using the endogenous antibodies (Figure 4E and 4F, Manuscript 1).

Interestingly, unpublished data from this study showed an increase of proteins of the mitochondrial quality control system in the absence of SMIM4 and C12ORF73 (data not shown). In isolated mitochondria from the knockdown of SMIM4 and C12ORF73, we observed increased steady state levels of SLP2 and PARL. An in-depth analysis of the interaction between SMIM4 and C12ROF73 with the mitochondrial proteases is not within the scope of this study, therefore it can be just speculated that both proteins are likewise involved in the mitochondrial quality control. Considering the increase of proteases associated with early complex III assembly factors, it could be hypothesized that SMIM4 and/or C12ORF73 act as a protective shield against different proteases during co-translationally insertion of cytochrome *b* into the IMM (Figure 3.2.). The increase of SLP2 and PARL in siRNA treated mitochondria and the interaction with YME1L provide a first evidence that SMIM4 and C12ORF73 are in close contact with the so-called SPY complex (for SLP2-PARL-YME1L) of the IMM, which is necessary for the processing of kinases (e.g. PINK1) and the regulation of stress-response within mitochondria (Song *et al.*, 2021; Steglich *et al.*, 1999; Wai *et al.*, 2016).

The pivotal functions of proteases within mitochondria are known from several studies (Steglich *et al.*, 1999; Wai *et al.*, 2016). Under stress conditions, mitochondrial proteases function according to the respiration, fission and fusion, and overall cell survival (Wai *et al.*, 2016). As a corollary, the interaction between assembly factors and the quality machinery is therefore of vital importance, on one hand, to protect assembly intermediates from degradation and, on the other hand, to remove dysfunctional, damaged protein-complexes from the IMM even before the complexes are fully assembled.

For example, the interplay between the assembly factor OCIAD1 (ovarian carcinoma immunoreactive antigen domain-containing protein 1) and prohibitins was explored in a recent study (Le Vasseur *et al.*, 2021). OCIAD1, an inner membrane protein, was identified as a novel assembly factor of complex III, involved in the proteolytic processing of the catalytic core subunit cytochrome c_1 (CYC1). Furthermore, subunits of the prohibitin complex, PHB1 and PHB2, were investigated in the same complex as OCIAD1. Le Vasseur and colleagues (2021) therefore supposed its function to be a stabilizer for complex III assembly intermediates and a chaperone for CYC1, in conjunction with the prohibitins (Le Vasseur *et al.*, 2021).

In conclusion, these data give an example that respiratory chain assembly factors can also act in the mitochondrial quality control system. If the activity of the SPY-complex is regulated by a negative feedback loop in the absence of SMIM4 or C12ORF73 needs further investigations.

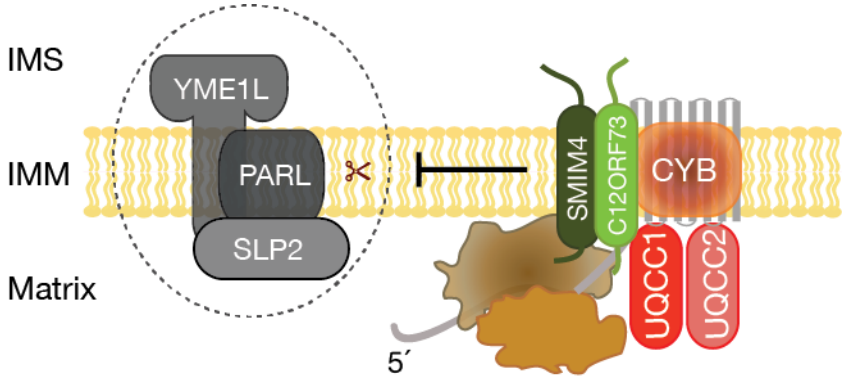

Figure 3.2 Model for the Complex III intermediate being protected from the SPY-complex. The protease activity of the SPY-complex (SLP2-PARL-YME1L) is inactivated and the complex III assembly intermediate is protected from the SPY-complex in the presence of SMIM4 and C12ORF73.

3.4. TMEM223 – a novel assembly factor of complex IV

Mitochondria contain a large number of low molecular weight proteins, which mainly function as so-called assembly factors for respiratory chain biogenesis. Several studies in the field of mitochondrial biogenesis have sought to examine the participation of these proteins. Mitochondrial assembly factors are often part of a conserved protein family, e.g. the transmembrane protein family – TMEM (Marx *et al.*, 2020). Previous studies investigated, for example, the role of TMEM70 and TMEM242 in the assembly of complex I and V (Carroll *et al.*, 2021; Sánchez-Caballero *et al.*, 2020), TMEM126B as assembly factor for complex I (Alston *et al.*, 2016; Formosa *et al.*, 2020; Fuhrmann *et al.*, 2019) or the association of TMEM177 during the COX2 biogenesis of complex IV assembly (Lorenzi *et al.*, 2018).

By defining the interactome of the large mitochondrial ribosome subunit mL62, we could identify TMEM223 as ribosome-associated protein (Figure 1B and 1D, Manuscript 1). Furthermore, we investigated its localization within the inner mitochondrial membrane, although an N-terminal presequence is not predicted for the TMEM223 protein (Figure 2A-C, Manuscript 1). By genome editing using CRISPR/Cas9,

we explored the influence on the respiratory chain during its absence. The most prominent effect was observable in complex IV constituents, where we could detect a decrease in early complex IV assembly factors, like C12ORF62 and MITRAC12, and in the structural subunits COX6A and COX4-1 (Figure 2D, Manuscript 1). Because of its exclusively impact on complex IV biogenesis, we suggested that TMEM223 is a protein involved in the assembly of complex IV by binding to the MITRAC complex (Mick *et al.*, 2012; Richter-Dennerlein *et al.*, 2016).

3.5. Interactome analyses of ^{FLAG}OXA1L identified TMEM126A as potential interactor

During the translational process in mitochondria, the co-translational insertion of newly synthesized proteins reflects an essential step. OXA1L is considered to be the insertase of mitochondrial-encoded proteins into the IMM. To define the interactome of the human OXA1L-complex, we generated a stable N-terminal OXA1L-FLAG tagged HEK293T cell line (^{FLAG}OXA1L). Because of its known interaction with the mitochondrial ribosome via its C-terminal tail (Haque *et al.*, 2010; Itoh *et al.*, 2021; Jia *et al.*, 2003), the FLAG-tag was introduced in a way so that it does not interfere with the ribosome interplay (Figure 1B, Manuscript 2). By mass spectrometry analysis from SILAC-labeled ^{FLAG}OXA1L HEK293T cells and extracted protein bands from colloidal-Coomassie stained SDS-PAGE, potential interacting partners of the OXA1L-complex could be identified (Figure 1C and 1D, Manuscript 2). As expected, mitochondrial-encoded proteins, such as COX1 and COX2, were identified together with 95% of the mitochondrial ribosomal subunits. In these analyses we discovered the inner membrane protein TMEM126A (Hanein *et al.*, 2013). Contemporaneously to this present study, TMEM126A was examined as a complex I assembly factor, which acts in the biogenesis of the ND4- module of complex I (D'Angelo *et al.*, 2021; Formosa *et al.*, 2021). In line with these studies, we confirmed its interaction with complex I subunits and its potential influence on the assembly of complex I. By using siRNA treated cells and CRISPR/Cas9-generated knockout cell lines for the TMEM126A protein, we observed a significant decrease in complex I activity and a defect in the assembly of complex I on BN-PAGE (Figure 2D and 2E, Manuscript 2). Supplementary, our siRNA analyses showed a slight decrease of complex II subunits on steady state protein levels (Figure 2B, Manuscript 2) and a reduced respiratory chain complex IV and complex V

on BN-PAGE. The complex V reduction could be observed in isolated mitochondria from the knockout of TMEM126A, as well (Figure 2D and 2E, Manuscript 2).

These observations stand in conflict with the previously described data from Formosa *et al.* (2021), since there was no further phenotype beside the complex I deficiency. One possible reason could be the usage of different experimental tools, for example, the different cell lines or the different ways to deplete TMEM126A in the cells. Formosa and colleagues solely used a knockout cell line for their analyses (Formosa *et al.*, 2021). In addition to the TMEM126A knockout cell lines, the study presented here used siRNA against TMEM126A for 72 hours. Because siRNA is carried out by transient transfections, potentially not all mRNAs, encoding TMEM126A, are degraded. Therefore, a small amount of TMEM126A protein is still available in the cells and able to fulfill its task. Further, by generating a knockout cell line, the adaption of the cells cannot be excluded over time, which can lead to slight differences compared to siRNA treated cells.

3.6. The functions of TMEM126A in mitochondrial homeostasis

Our analyses demonstrated that the interaction between OXA1L and TMEM126A is a unique feature regarding the paralog of TMEM126A. The paralog, TMEM126B, was also described as an assembly factor of complex I (Elurbe and Huynen, 2016; Formosa *et al.*, 2020; Heide *et al.*, 2012), but was not identified in our mass spectrometry analyses of ^{FLAG}OXA1L. The missing interaction between TMEM126B and OXA1L was confirmed by immunoisolation and Western Blot analyses (data not shown). Formosa *et al.* (2021) further investigated the independent role of TMEM126A by overexpressing TMEM126B^{FLAG} in TMEM126A knockout cell lines, which does not compensate the phenotypes of this cell line.

Overall, this study suggests a model of TMEM126A as a novel constituent of the human OXA1L-complex in consideration to its global function in the assembly of complex IV and V as well. A strong hint towards its participation in the OXA1L-complex is the negative effect on the mitochondrial translation in the absence of TMEM126A. All newly synthetized mitochondrial translation product levels were decreased during siRNA mediated depletion of TMEM126A and in the TMEM126A$^{-/-}$ cells (Figure 3B and 3C, Manuscript 2). In comparison with other known respiratory chain assembly

factors, such as MITRAC15 or C12ORF62, which affect the mitochondrial translation only for one mitochondrial-encoded protein (Mohanraj *et al.*, 2019; Richter-Dennerlein *et al.*, 2016; C. Wang *et al.*, 2020), TMEM126A seems to have influence on all newly-synthesized mitochondrial proteins and on the overall mitochondrial translation. Therefore, TMEM126A can be considered as a mitochondrial factor of diverse function, on one hand as an assembly factor for complex I, and on the other hand as a more general interactor for the human insertase machinery (Figure 3.3).

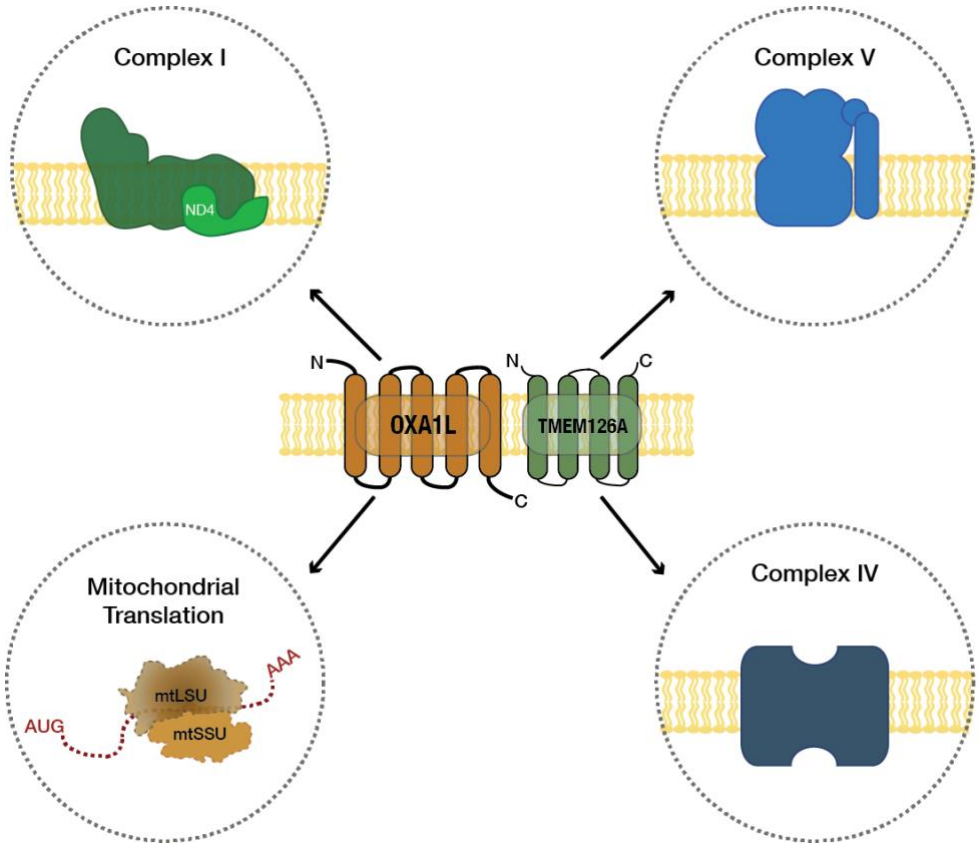

Figure 3.3 The role of TMEM126A in mitochondrial homoeostasis. In this study different potential functions of the membrane proteinTMEM126A were explored. TMEM126A interacts with the human insertase OXA1L in close cooperation and influences mitochondrial translation and the assembly of complex I, IV and V.

3.7. Does OXA1L exist in multiple complexes?

An interesting side finding was that both OXA1L and TMEM126A copurified with higher amounts of newly synthesized COX2/COX3 in relation to the other mitochondrial-encoded protein signals (Figure 3A, Manuscript 2). This observation leads to the pressing question if OXA1L maybe exists in separate complexes together with COX2 and COX3 or if the amounts of COX2/COX3 proteins in human cells are higher compared to the rest of mitochondrial-encoded proteins?

From studies in *Arabidopsis thaliana*, it is reported that mitochondria contain four OXA homologs, of which one is exclusively responsible for the biogenesis of Cox2 (Kolli *et al.*, 2020, 2019). In *S. cerevisiae*, two proteins are needed for the translocation of Cox2 into the IMM: Oxa1 and its paralog Cox18 (Fiumera *et al.*, 2009; Gaisne and Bonnefoy, 2006; Herrmann *et al.*, 1995). In *Neurospora crassa*, the insertion of Cox2 demands on Oxa2, a second Oxa homolog which complements the loss of Cox18 in yeast cells, as well (Funes *et al.*, 2004). All these examples demonstrate that the biogenesis of Cox2 requires the presence of members from the Oxa1/YidC/Alb3-protein subfamily. The yeast Cox18 is not conserved from yeast to human, but due to evolutionary events, it cannot be ruled out that the human OXA1L protein exists in distinct complexes, of which one solely interacts with COX2 or COX3.

Why we observed higher amounts of newly synthesized COX2/COX3 signals than other mitochondrial-encoded proteins (Figure 3A, Manuscript 2) could be explained by taking into consideration the assembly steps within the cytochrome *c* oxidase biogenesis. The assembly takes place in different modules and starts with the catalytic core subunit COX1. The COX2- and COX3-modules are assembled separately and added to the COX1-module in following steps. This implies a longer interaction of OXA1L with COX2 and COX3 polypeptides at the mitochondrial ribosome and a release not till the COX holoenzyme is properly assembled.

Our data provide preliminary evidence for this theory descripted above, but further research will have to clarify whether human cells contain different OXA1L-complexes and if the OXA1L protein is split into pools of diverse function.

4. Conclusion and Perspectives

The presented study provides insights into the mechanistical and biochemical steps of the assembly of the respiratory chain complex III and IV by the investigation of novel assembly factors SMIM4, C12ORF73 and TMEM223.

By binding to the mitochondrial ribosome and newly synthesized cytochrome *b*, SMIM4 and C12ORF73 are part of the early assembly intermediates of the ubiquinol-cytochrome *c* oxidoreductase. We could show, that in the absence of SMIM4 or C12ORF73 the assembly of complex III is disturbed and early complex III assembly intermediates accumulate in human cells. In mammals, the different assembly steps of complex III biogenesis are barely evaluated and are referred to as orthologous proteins known from studies in *S. cerevisiae*. This study examined the interaction of SMIM4 and C12ORF73 with the human assembly factors UQCC1 and UQCC2, which mediate the expression of cytochrome *b* and hence the initiation of complex III assembly (Crofts, 2004; Tucker *et al.*, 2013). Interestingly, SMIM4 and C12ORF73 are not conserved in *S. cerevisiae* which shine a light on the importance of this research and the to be clarified variations between yeast and human.

The best investigated human OXPHOS complex is the cytochrome *c* oxidase. Nevertheless, we identified TMEM223 and its association with the mitochondrial-encoded core subunit COX1. Further, our analyses showed an interaction between TMEM223 and early assembly MITRAC intermediates together with C12ORF62, which was previously described as a complex IV assembly factor (Dennerlein *et al.*, 2015; Richter-Dennerlein *et al.*, 2016).

Over and above, we defined the interactome of the human OXA1L-complex by mass spectrometry analyses to investigate proteins which are in close contact with the OXA1L protein. In addition, this study clarified the association of the human OXA1L protein with nascent polypeptide chains on the mitochondrial ribosome, which was only published for the model organism *S. cerevisiae* so far.

One of the central claims of this presented research was the biochemical characterization of the identified membrane protein TMEM126A (Hanein *et al.*, 2013), which interacts with OXA1L in the same complex. The data provide preliminary evidence that TMEM126A has a more extended function than previously assumed in a limited number of studies published in parallel (D'Angelo *et al.*, 2021; Formosa *et al.*,

2021). Our analyses demonstrated the negative effect on the respiratory chain complex I as well as complex V in the absence of TMEM126A. Additionally, knockdown experiments using siRNA against TMEM126A showed a decrease of protein steady state levels of OXA1L, which is a strong indication for their interdependency.

Further research will have to address the issue of the mitochondrial translation defect, which was investigated in the absence of TMEM126A. Our dataset in this direction was limited and we only analyzed the protein steady state levels of mitochondrial ribosomal subunits. Therefore, future studies will have to continue to explore the impact of TMEM126A as a translation regulator.

5. Material and Methods

Because the manuscripts contain condensed material and methods, the following section depicts a more detailed execution.

5.1. Material

5.1.1. Buffers and Solutions

In Table 5.1 all buffers are listed which were used in this present study. For the preparation, autoclaved deionized water was used.

Table 5.1 Buffers and solutions

Buffers	Components
Blotting buffer	20mM Tris, 150mM glycine, 0.02% SDS, 20% ethanol
BN-PAGE anode buffer	50mM Bis-Tris/ HCl pH 7.0
BN-PAGE cathode buffer	50mM Tricine, 15mM Bis-Tris, pH 7.0, with or without 0.02% Coomassie Brilliant Blue G-250
BN-PAGE 3x gel buffer	66.67mM 6-aminocaproic acid, 50mM Bis-Tris/ HCl pH 7.0
BN-PAGE loading dye (10x)	0.5% Coomassie Brilliant Blue G-250, 50mM 6-aminocaproic acid, 10mM Bis-Tris, pH 7.0
BN-PAGE solubilization buffer	20mM Tris/HCl, pH 7.4, 0.1mM EDTA, pH 8.0, 50mM NaCl, 10% glycerol, 1mM PMSF, 0.4% DDM or 1% digitonin
Cell culture medium	Dulbeccos's Modified Eagle Medium (DMEM) containing 10% (v/v) fetal calf serum (FCS), 1mM sodium pyruvate, 2mM L-glutamine, 50µg/ml uridine

Buffer	Components
Cell lysis buffer	50mM Tris/HCl, pH 7.4, 14mM NaCl, 10mM MgCl, 10% NP40, 5mM PMSF, 10mM protease inhibitor from Roche
Coomassie staining solution	2.5g/l Coomassie Brilliant Blue R-250, 40% ethanol, 10% acetic acid
Coomassie destaining solution	40% ethanol, 10% acetic acid
Homemade ECL substrate	250mM Luminol disodium salt in 0.1M Tris pH 8.8, 90mM 4-Iodophenyl boronic acid in DMSO, 30%H_2O_2
Hypertonic buffer (P3)	1.25mM sucrose, 10mM MOPS, pH 7.2
Hypotonic buffer (P2)	100mM sucrose, 10mM MOPS, 1mM EGTA, pH 7.2
Import buffer	250mM sucrose, 5mM magnesium acetate, 80mM potassium acetate, 5mM ATP, 20mM HEPES, pH 7.4
Isolation buffer (P1)	75mM mannitol, 225mM sucrose, 1mM EGTA, 10mM MOPS/KOH, pH7.2
PBS (phosphate-buffered saline)	137mM NaCl, 2.7mM KCl, 10mM Na_2HPO_4, 1.8mM KH_2PO_4
SDS-running buffer	25mM Tris, 192mM glycine, 0.1% SDS
SDS sample buffer	10% glycerol, 2% SDS, 0.01% bromophenol blue, 60mM Tris/HCl pH 6.8, 1% beta-mercaptoethanol or 1mM DTT
SEM buffer	250mM sucrose, 10mM EDTA, pH 7.2
Solubilization buffer	50mM Tris/HCl, pH 7.4, 150mM NaCl, 2mM PMSF, 1% digitonin, 1x Halt Protease Inhibitor mix (Thermo), 10% glycerol, 20mM $MgCl_2$
TAE buffer	40mM Tris/acetate pH 8.0, 2mM EDTA

Buffer	**Components**
TBS (Tris-buffered saline)	20mM Tris/HCl, pH 7.5, 125mM NaCl
TBT-T	20mM Tris/HCl, pH 7.5, 125mM NaCl, 0.1% Tween-20
Tris-Tricine anode buffer	0.2M Tris, pH 8.9
Tris-Tricine cathode buffer	0.1M Tricine, 0.1M Tris, 0.1% SDS, pH 8.25
Tris-Tricine gel buffer	1M Tris, 0.1% SDS, pH 8.45
VOA mixture	0.8mM antimycin, 0.1mM valomycin, 2mM oligomycin, in ethanol
Wash buffer for immunoprecipitation	50mM Tris/HCl, pH 7.4, 150mM NaCl, 10% glycerol, 20mM glycerol, 0.3% digitonin, 1mM PMSF
^{35}S labeling media	DMEM with or without fetal calf serum, without sodium pyruvate, without L- glutamine, without L-methionine, without L-cysteine

5.1.2. List of Chemicals

Standard chemicals, used in this thesis, can be found in Table 5.2.

Table 5.2 List of chemicals

Chemical	Manufacturer	Catalog number
Acetone	Roth	9372.5
Adenosine-5´-triphosphate	Roche	44504128
Agarose NEEO ultra quality	Roth	2267.3
Ammonium persulfate	Roth	9592.1
Ammonium chloride	Merck	12125-02-9
Ammonium acetate	Roth	7869.2
Ammonium sulfate	Roth	3746.1
6-Aminocaproic acid	Sigma-Aldrich	A2504-100G
Anisomycin from Streptomyces griseolus	Sigma-Aldrich	A9789-25MG
L-Arginine	Cambridge Isotope Laboratories	CNLM-539-H-1
L-Arginine	Serva	13940
Bis-Tris	Roth	9140.3
Bovine Serum Albumin	Sigma-Aldrich	A6003-100G
Brilliant Blue G250	Roth	9598.2
Brilliant Blue R250	Roth	3862.2
Creatine kinase	Roche	47716222
Creatine phosphate	Roche	23001332
Dimethyl sulfoxide	Merck	1.02952.1000
1,4-Dithiothreitol	Roth	6908.2
DMEM High Glucose w/ sodium pyruvate	Capricorn Scientific	DMEM-HPSTA
EGTA	Roth	3054.2
Emetine dihydrochloride	Merck	324693-250MG
Ethanol	Roth	9065.4

Chemical	Manufacturer	Catalog number
Fetal Bovine Serum	Biochrom AG	S 0115
Fetal Bovine Serum	Hyclone Laboratories	SG30070.03
D (+)-Galactose	Sigma-Aldrich	G5388-100G
GeneJuice® Transfection Reagent	Novagen	70967-3
L-Glutamine	Gibco	25030-024
Glycine	Roth	3187.4
Halt Protease inhibitor cocktail, EDTA- free	Thermo Fisher Scientific	78425
HEPES	Roth	HN78.3
Hydrogen peroxide 30%	Roth	8070.2
Hygromycin B	Invitrogen	10687010
Immobilon® Forte Western HRP Substrate	Merck	WBLUFO500
Instant skimmed milk powder	Frema	0202V01
Lipofectamine® RNAiMAX	Invitrogen	13778-150
Lipofectamine® 3000 Transfection Kit	Invitrogen	L3000-015
Luminol sodium salt	Sigma-Aldrich	A4685-5G
L-Lysine	Serva	28220
L-Lysine	Cambridge Isotope Laboratories	CNLM-291-H-1
Potassium acetate	Merck	127-08-01
Potassium chloride	Roth	6781.1
Potassium dihydrogen phosphate	Roth	3904.1
Potassium hydroxide	Roth	6751.1
L-Proline	Biomol Feinchemikalien GmbH	07010
Puromycin	Invivogen	ant-pr-1
D (-)-Mannitol	Roth	4175.1

Chemical	Manufacturer	Catalog number
Magnesium hydroxide carbonate	Merck	5827
Methanol	Roth	4627.5
MOPS	Roth	6979.4
NADH disodium salt	Roth	AE12.3
Nonidet™ P 40 substitute	Sigma-Aldrich	74385-1L
Pen Strep	Gibco	15140-122
Pierce™ ECL Western Blotting Substrate	Thermo Fisher Scientific	32106
2-Propanol	Roth	6752.4
Protein A Sepharose™ CL-4B	GE Healthcare	17-0963-03
Proteinase inhibitor cocktail tablets	Roche	45148300
Proteinase K	Roth	7528.2
Pure Link™ RNase A	Invitrogen	12091-021
Rotiphorese® Gel 30 (37, 5:1)	Roth	2029.1
Roti® Quant 5x	Roth	K015.1
SILAC DMEM High Glucose w/o L-Glutamine, w/o Arginine, w/o Lysine, w/ sodium pyruvate	Anprotec	AO-LM-0065
Sodium acetate	Roth	6773.2
Sodium bicarbonate	Sigma-Aldrich	56297-1KG
Sodium carbonate	Merck	1.06398.1000
Sodium hydrogen carbonate	Merck	1.06329.1000
Sodium hydroxide	Roth	6771.1
Sodium dithionite	Fluka Analytica	71699
Sodium pyruvate solution	Sigma	S8636-100ML
SDS pellets	Roth	CN30.3
D (+)-Saccharose	Roth	9286.2
Tag Man® Universal PCR Master Mix	Applied Biosystems	4304437
Thiamphenicol	Sigma-Aldrich	TO261-1G

Chemical	Manufacturer	Catalog number
D (+)-Trehalose dihydrate	Roth	5151.3
Tricine	Roth	6977.3
Tris	Roth	5429.2
Triton® X-100	Merck	1.08643.1000
TRIzol® Reagent	Ambion	15596018
Tween® 20	Roth	9127.2
0.05% Trypsin-EDTA	Gibco	25300-054
Urea	Roth	3941.1

5.1.3. Antibodies

In Table 5.3 the primary antibodies are listed which were used within this study.

Table 5.3 Primary antibodies

Antibody	Source
Mouse monoclonal ANTI-OXA1L	Proteintech Europe, Cat.No: 66126-1-Ig
Rabbit polyclonal ANTI-TMEM126A	Sigma Prestige Antibodies, HPA046648
Rabbit polyclonal ANTI-MRPL12	Proteintech, Cat.No: 14795-1-AP
Rabbit polyclonal ANTI-PTCD3	Proteintech, Cat.No: 25158-1-AP
Rabbit polyclonal ANTI-SDHA	Cell Signaling, 5839
Rabbit polyclonal ANTI-UQCC	Novus Biologicals, NBP1-90766
Rabbit polyclonal ANTI-MNF1	Novus Biologicals, NBP2-14240
Rabbit polyclonal ANTI-UQCC3	Novus Biologicals, NBP2-14579
Rabbit polyclonal ANTI-NDUFAF4	Proteintech, Cat.No: 26003-1-AP
Rabbit polyclonal ANTI-NDUFA5	Proteintech, Cat.No: 16640-1-AP
Rabbit polyclonal ANTI-NDUFB10	Abcam, ab196019
Rabbit polyclonal ANTI-NDUFB11	Abcam, ab183716
Rabbit monoclonal ANTI-NDUFS1	Invitrogen, 459130
Rabbit polyclonal ANTI-bL12m	Proteintech, Cat.No: 14795-1-AP
Rabbit polyclonal ANTI-uS15m	Proteintech, Cat.No: 17006-1-AP
Rabbit polyclonal ANTI-GTPB5	Proteintech, Cat.No: 13220-1-AP
Rabbit polyclonal ANTI-GTPB10	Proteintech, Cat.No: 20133-1-AP
Rabbit polyclonal ANTI-AFG3L2	AG Rehling
Rabbit polyclonal ANTI-ATP5B	AG Rehling
Rabbit polyclonal ANTI-C12ORF73	AG Rehling
Rabbit polyclonal ANTI-C12ORF62	AG Rehling
Rabbit polyclonal ANTI-COX1	AG Rehling
Rabbit polyclonal ANTI-COX2	AG Rehling
Rabbit polyclonal ANTI-COX6A	AG Rehling

Antibody	Source
Rabbit polyclonal ANTI-COX5B	AG Rehling
Rabbit polyclonal ANTI-COX4I-1	AG Rehling
Rabbit polyclonal ANTI-CYTB	AG Rehling
Rabbit polyclonal ANTI-mL45	AG Rehling
Rabbit polyclonal ANTI-mL62	AG Rehling
Rabbit polyclonal ANTI-mS40	AG Rehling
Rabbit polyclonal ANTI-mS39	AG Rehling
Rabbit polyclonal ANTI-MITRAC7	AG Rehling
Rabbit polyclonal ANTI-MITRAC12	AG Rehling
Rabbit polyclonal ANTI-MITRAC15	AG Rehling
Rabbit polyclonal ANTI-NDUFB8	AG Rehling
Rabbit polyclonal ANTI-NDUFA9	AG Rehling
Rabbit polyclonal ANTI-OXA1L	AG Rehling
Rabbit polyclonal ANTI-OCIAD2	AG Rehling
Rabbit polyclonal ANTI-PHB1	AG Rehling
Rabbit polyclonal ANTI-PHB2	AG Rehling
Rabbit polyclonal ANTI-RIESKE	AG Rehling
Rabbit polyclonal ANTI-SLIRP	AG Rehling
Rabbit polyclonal ANTI-SMIM4	AG Rehling
Rabbit polyclonal ANTI-TACO1	AG Rehling
Rabbit polyclonal ANTI-TIM21	AG Rehling
Rabbit polyclonal ANTI-TIM23	AG Rehling
Rabbit polyclonal ANTI-TIM44	AG Rehling
Rabbit polyclonal ANTI-TMEM126A	AG Rehling
Rabbit polyclonal ANTI-TMEM177	AG Rehling
Rabbit polyclonal ANTI-TMEM223	AG Rehling
Rabbit polyclonal ANTI-TOM20	AG Rehling
Rabbit polyclonal ANTI-TOM70	AG Rehling

Antibody	Source
Rabbit polyclonal ANTI-uL1m	AG Rehling
Rabbit polyclonal ANTI-uL23m	AG Rehling
Rabbit polyclonal ANTI-uS14m	AG Rehling
Rabbit polyclonal ANTI-VDAC	AG Rehling
Rabbit polyclonal ANTI-YME1L	AG Rehling

Table 5.4 Secondary antibodies

Antibody	Source
Goat-anti rabbit HRP	Dianova, Hamburg, Germany
Goat-anti mouse HRP	Dianova, Hamburg, Germany
Goat-anti rabbit IR880	LI-COR, Lincoln, NE, USA
Goat-anti mouse IR880	LI-COR, Lincoln, NE, USA

5.1.4. Cell lines

Cell lines used in this present study are listed in Table 5.5.

Table 5.5 Human embryo kidney cell lines

Cell line	Source
HEK293-Flp-In T-Rex WT	Thermo Fisher Scientific, R78007
HEK293-Flp-In T-Rex-C12ORF73^{FLAG}	AG Rehling
HEK293-Flp-In T-Rex-SMIM4^{FLAG}	AG Rehling
HEK293-Flp-In T-Rex-TMEM223^{FLAG}	AG Rehling
HEK293-Flp-In T-Rex-UQCC1^{FLAG}	AG Rehling
HEK293-Flp-In T-Rex-UQCC2^{FLAG}	AG Rehling
HEK293-Flp-In T-Rex-UQCC3^{FLAG}	AG Rehling
HEK293-Flp-In T-Rex-TMEM126A^{FLAG}	AG Rehling
HEK293-Flp-In T-Rex-OXA1L^{FLAG}	AG Rehling
HEK293-Flp-In T-Rex-^{FLAG}OXA1L	AG Rehling
HEK293-Flp-In T-Rex-C12ORF62^{LAG}	Richter-Dennerlein *et al.,* 2016
HEK293-Flp-In T-Rex-MITRAC12^{FLAG}	Mick *et al.*, 2012
HEK293-Flp-In T-Rex-TMEM223$^{-/-}$	AG Rehling
HEK293-Flp-In T-Rex-TMEM126A$^{-/-}$	AG Rehling

5.1.5. Plasmids and oligonucleotides

Plasmids used in this study are listed in Table 5.6 and were propagated in *E. coli* XL1 Blue. Under section 5.2.3.5, the cloning process is described in detail. Oligonucleotides for siRNA treatment and generation of CRISPR/Cas9-knockout cell lines are listed in Table 5.7.

Table 5.6 Plasmids

Name	Purpose	Features	Marker	Reference
pOG44	Flp-Recombinase-Expression Vector	CMV promoter	Ampicillin	Thermo Fisher Scientific
pcDNA5/FRT/TO	Genomic integration vector for tetracycline-inducible expression	CMV promoter	Ampicillin, Hygromycin	

Table 5.7 Oligonucleotides

Oligonucleotide	Sequence	Target and Function
siC12orf73	ACA-CAA-ACC-UCA-AGU-UUC-U	Sense siRNA for transiently silencing of C12ORF73 (33nM)
siTMEM126A	GGU-GAU-UUG-GAU-UGU-GAA-A	Sense siRNA for transiently silencing of TMEM126A (33nM)
siSMIM4	GCA-GUC-AAU-AAA-GUC-AAU-A	Sense siRNA for transiently silencing of SMIM4 (33nM)
siUQCC1	GAU-GCC-UGA-UAC-AUU-CAA-U	Sense siRNA for transiently silencing of UQCC1 (33nM)
siUQCC2	CUC-CAU-UCA-AAC-UAC-UAC-A	Sense siRNA for transiently silencing of UQCC2 (33nM)
siUQCC3	GGA-AGC-AGG-AAA-UGC-UAA-A	Sense siRNA for transiently silencing of UQCC3 (33nM)
HS.Cas9. TMEM126A.1.AA	AltR1/AGUCAGUCCACUCCGUGUUA GUUUUAGAGCUAUGCU/AltR2	Guide sequence for CRISPR/Cas9 targeting TMEM126A (cl.AA1)
HS.Cas9. TMEM126A.1.AB	AltR1/GCUGCUAGACCACCAUUUAC GUUUUAGAGCUAUGCU/AltR2	Guide sequence for CRISPR/Cas9 targeting TMEM126A (cl.AB1)

5.2. Methods

5.2.1. Cell culture methods

5.2.1.1. Cultivation of mammalian cells

Mammalian cell lines were cultured at 37°C under 5% of CO_2 and increased humidity in Dulbecco's modified eagle media (DMEM) containing high glucose or galactose supplemented with 10% (v/v) FBS, 1mM sodium pyruvate, 2mM L-glutamine and 50µg/ml uridine. Handling has been done under a laminar hood, using sterile disposals. On regular basis, cells were tested for mycoplasma contaminations using GATC Services by eurofins Genomic. For this study human kidney cell lines (HEK293-Flp-In T-Rex; HEK293T) were used exclusively. For passaging cells, growth media were removed and attached cells were rinsed with PBS. For further separation of cells, equal amount of growth medium was added, and cells were centrifuged for five minutes at 1500 rpm at room temperature. Afterwards, a desired number of cells was added back to the cell culture flask. In case of exact calculations of the cell number, a hemocytometer (*Neubauer* improved) was prepared. Cells were used in a dilution of 1:10 and 10µl of this cell suspension was introduced to the chamber. The cell number in 1ml medium was calculated according to the following equation:

$$\frac{\text{cells}}{\text{ml}} = \frac{\text{number of cells}}{4\ (\text{number of squares})} \text{x dilution factor x } 10\text{^}4$$

5.2.1.2. Determination of cell growth

To ascertain differences in cell growth between wild-type and knockdown/knockout cell lines two methods were performed. Either cell growth was measured with trypan blue exclusion test using Countess™ automated cell counter (Thermo Scientific)(Strober, 2015) or by applying cells to a hemocytometer (*Neubauer* improved). Therefore, 200.000 cells were seeded to 6-well tissue cell culture plate and after three days, cells were harvested with 1x PBS to determine cell number per milliliter.

5.2.1.3. Generation of stable HEK293T cell lines

To generate stable mammalian expression cell lines, we used Flp recombinase-mediated DNA integration as described previously (Dennerlein *et al.*, 2010; O'Gorman *et al.*, 1991). All Flp-In™ T-REx™ 293 cell lines were engendered with a FLAG-tag under the control of a tetracycline-inducible promotor. For the purpose of transfection, cells were seeded to a six-well plate until confluency reach 60-70 percentage. GeneJuice®, the transfection reagent of choice, was used according to manufacturer's introductions and 5µl were added to 100µl Opti-Mem into sterile round bottom tube. Together with 400ng of pcDNA5/FRT/TO plasmid and 1.2µg of pOG44 recombinase transfection mixture was incubated for ten minutes at room temperature under sterile conditions. Additionally, 900µl of growth medium without antibiotics were supplemented to the transfection reagent. After removing growth medium from prepared cells, transfection medium was added gently to cells and pre-incubated for two hours at 37°C. Afterwards, cells were covered again with 3ml growth medium. The selection for cells which incorporated the expression construct was conferred by addition of hygromycin (100µg/ml). Growth medium containing hygromycin was changes periodically and after two weeks single clones were selected and enlarged until expression of the protein of interest could be screened by immunoblotting. Due to the tetracycline-inducible promotor, expression was provoked by treating cells with 2µg/5ml of tetracycline 24 hours prior harvesting.

5.2.1.4. Generation of knockout cell lines by CRISPR/Cas9

To generate HEK293T cells lacking TMEM126A, I used Alt-R CRISPR-Cas9 system from IDT (Integrated DNA Technologies)(Ran *et al.*, 2013; Vakulskas *et al.*, 2018). The appropriate oligonucleotides used for this approach are listed in Table 5.68 and were used according to manufacturer's protocol. Two-part guide RNA was ordered, consists of crRNA and tracRNA which must be combined before to create a functional, targeting ribonucleoprotein (RNP) with Cas9. Therefore, crRNA and tracRNA were combined at equimolar ratio and incubated at 95°C for five minutes followed by cooling down at room temperature. Guide RNA (1µM) and provided Alt-R S.p. Cas9 (1µM) were mixed in nuclease-free duplex buffer to set up the RNP complex and incubated for additional five minutes at room temperature. For final transfection, 40.000cells/well were seeded to a standard 96-well tissue culture plate using growth media without antibiotics.

Then, 25µl of RNP complex were incubated with 1.2µl RNAiMAX transfection reagent in 23.8µl Opti-Mem. After twenty minutes incubation at room temperature, 50µl of transfection complex was added to each well. Cells were incubated at 37°C for two days.

In due time, transfected HEK293T cells were harvested from the 96-well tissue culture plate with PBS containing 1% of FBS. For further FACS sorting we collaborated with Sandra Becker of the University Medical Center Göttingen, Cell Sorting Facility. Single clones were sorted with the help of the fluorescence marker ATTO 550 at 540-565nm. After expansion of single clones, loss of TMEM126A was screened via western blot method using whole cell lysates (5.2.2.3) and sequencing (SEQLAB Göttingen, Germany).

5.2.1.5. siRNA treatment to knockdown protein of interest

Prior siRNA treatment HEK293T cells were harvested as described before (5.2.1.1) and passaged in the way that cells ensure exponential growth phase during siRNA treatment the day after.

Briefly, 1ml Opti-Mem were incubated in sterile glass-tube together with 8µl Lipofectamine RNAiMAX and 16µl siRNA oligonucleotides (final concentration 33nM) for twenty minutes under sterile conditions at room temperature. Meanwhile, the appropriate number of HEK293T cells needed for efficient knockdown (1×10^6) were counted after harvesting with PBS and DMEM growth media as described in 1.1.1. Subsequently, calculated number of cells were added together with siRNA mixture to 25cm^2 cell culture flask prepared with 5ml growth media and incubated for 72 hours at 37°C with 5% CO_2.

5.2.1.6. Inhibition of mitochondrial translation

To inhibit mitochondrial translation cells were treated with thiamphenicol in a concentration of 50µg/ml for individual time points. Thiamphenicol was dissolved in ethanol (≥99.8% p.a.) and incubated for thirty minutes at 37°C. The concentration was measured using spectrophotometry at a wavelength of 273nM and freshly prepared thiamphenicol was applied to growth media.

5.2.1.7. *In vivo* labeling of mitochondrial translation products

To investigate mitochondrial translation, translation products were labeled with ^{35}S-methionine. Therefore, cells were split into a 25cm^2 tissue culture flask one day before. Next day, growth media was replaced by 2ml of FBS-free media (w/o methionine) and incubated two times for ten minutes at 37°C. Afterwards, cytosolic translation was inhibited by addition of emetine (100µg/ml) to labeling media (plus FBS, but w/o methionine; Table 5.1) and cells were incubated again for ten minutes at 37°C. In case of pulse-chase experiments, cytosolic translation was inhibited reversible with anisomycin (100µg/ml). To label mitochondrial translation products exclusively, 200µCi radioactive methionine was added to cells and incubated for individual time points. After incubation, cells were harvested using PBS and kept on ice until further use or frozen at -80°C. Samples were detected via SDS-PAGE and digital autoradiography as described in section 5.2.4.2 and 5.2.4.7.

5.2.2. Preparation of mitochondria and cell lysates

5.2.2.1. Mitochondria isolation with TH-buffer

As previous described (Callegari *et al.*, 2017) mammalian cells were resuspended in cold TH-buffer (Table 5.1) containing 0.1% BSA and 2mM PMSF. Following, suspension was transferred to a Dounce homogenizer and homogenized 30 times at 800U/min. To remove cell debris and intact cells suspension was centrifuged for ten minutes at 400 x g. The supernatant, containing mitochondria, was transferred to a fresh tube and the remaining cell pellet was homogenized once again to increase the yield. After the first centrifugation step supernatants were pooled and centrifuged for additional ten minutes at 800 x g to finally remove remaining debris. Afterwards, mitochondria were isolated by a centrifugation step at 12.000 x g for ten minutes and collected in 1.5ml tubes. Isolated mitochondria were resuspended again in TH-buffer without BSA and without PMSF and directly used for experiments or frozen at -80°C after shock freezing with liquid nitrogen.

5.2.2.2. Isolation of mitochondria for import experiments

To isolate mitochondria under more mild conditions and in smaller amounts for import reactions, cells were treated as descripted previously based on Panov, 2013. Therefore, cells were harvested with PBS and centrifuged at 1000 x g for ten minutes. Cell pellets were resuspended again in 5ml cold isolation buffer P1 (Table 5.1) and the centrifugation step was repeated at same speed. Subsequently, cell pellets were incubated with cold hypotonic buffer P2 (5ml/1g cells) containing 2mM PMSF for seven minutes to initiate swelling of cell membrane. Cell suspension was gently homogenized 20-30 times using a glass-glass Dounce homogenizer to disrupt cells. Ice-cold hypertonic buffer P3 (1.1ml/5ml) was added into the homogenizer and the volume of the suspension was doubled or tripled by addition of cold isolation buffer P1 (+ 2mM PMSF, + 2mg/ml BSA). To remove cell debris from intact cells, suspension was centrifuged at 1000 x g for ten minutes and supernatant transferred to 1.5ml tubes. After a spin down at 10.000 x g for additional ten minutes, pelleted mitochondria were pooled with isolation buffer. The protein concentration was determined using Bradford method (5.2.4.1) and mitochondria were used immediately for experiments.

5.2.2.3. Preparation of lysates from whole cells

Mammalian cells were harvested with PBS and centrifuged at 1000 x g for ten minutes. Cell pellets were resuspended in cell lysis buffer (Table 5.1) containing NP40 as detergent. For an optimal lysis, suspension was vortexed for thirty seconds at maximum speed followed by centrifugation at 2600 rpm for five minutes. The supernatant was transferred to a new 1.5ml tube and protein concentrations were measured as described in section 5.2.4.1.

5.2.3. Molecular biology methods

5.2.3.1. Transformation of competent *E. coli*

For transformation, 100-300µl of competent cells were thawed on ice and incubated for fifteen minutes on ice with 10-100ng of plasmid DNA. After a heat shock at 42°C for two minutes, cells were placed again on ice for three minutes. Next, 1ml of warm and antibiotic-free LB media was added to cells and mixture incubated for another 30-60 minutes at 37°C under shaking. Finally, cells were centrifuged for two minutes at 5000 x g and cell pellet was resuspended in remaining media and plated on agar plates

with appropriate selection antibiotics. Incubation of plates took place at 37°C overnight until colonies were visible.

5.2.3.2. Isolation of plasmid DNA

Plasmid DNA was isolated using the Wizard® Plus SV Miniprep DNA Purification Kit (Promega) according to manufacturer's protocol. Briefly, 2-5ml of overnight *E. coli* culture was centrifuged for five minutes at 5000 x g at room temperature. Cells were resuspended in 250µl cell resuspension buffer and 250µl cell lysis buffer, and incubated for five minutes after supplementation of 10µl alkaline protease solution. After addition of 350µl neutralization buffer cells were mixed and immediately centrifuged for ten minutes at 16.000 x g. The lysate was decanted into provided spin columns and centrifuged again for one minute at maximum speed. After two washing steps with 750µl and 250µl of wash solution columns were centrifuged for 2 minutes at maximum speed and finally transferred to a sterile 1.5ml tube for elution. The eluate (plasmid DNA) was extracted by adding 25-50µl of nuclease-free water to the filter of the column. After an incubation of 1-2 minutes columns were centrifuged for one minute to collect plasmid DNA. The concentration of DNA was measured using a NanoDrop™ One/One^{C} Mikrovolume UV-VIS spectrophotometer (Thermo Fisher) and stored at -20°C.

5.2.3.3. Polymerase chain reaction (PCR)

To amplify DNA segments from plasmid DNA (Saiki *et al.*, 1988) the KOD Hot Start DNA Polymerase Kit was used according to manufacturer's introductions (Merck). For a reaction of 50µl, 10-100ng of cDNA or plasmid DNA was used as template. Additionally, the reaction contained 0.2mM dNTPs, 1.5mM MgSo4, 1x KOD reaction buffer, 0.3µM forward and reverse primers and 1U KOD Hot Start Polymerase. Cycling conditions were 2 minutes at 95°C followed by 35 cycles at 95°C for 30 seconds for initial denaturation of DNA, annealing for 10 seconds at 48-55°C (depending on template and primers used) and 2 minutes at 70°C for elongation. At the end, PCR products were stored at 4°C until further use. After PCR amplification, PCR products were analyzed by agarose gel electrophoresis (Mullis *et al.*, 1986). Therefore, 1% agarose was dissolved in 1x TAE buffer (Table 5.1) under heating. After cooling-down ethidium bromide (1µg/ml) was added to liquid agarose and applied to appliance. 5µl of PCR product was

loaded onto gel after mixing with 5µl 50% glycerol. To identify size of PCR products GeneRuler DNA ladder (Thermo Scientific) was loaded beside the samples. Finally, DNA fragments were visualized by UV-light.

5.2.3.4. Purification of PCR products

Following electrophoresis, PCR products were purified with the Wizard® Plus SV Gel and PCR Purification System (Promega). Therefore, DNA bands were cut out from agarose gel and completely dissolved in the presence of provided membrane binding solution (10µl/10mg) at 50-65°C. The gel mixture was transferred to the provided SV columns and incubated for one minute at room temperature. Afterwards, columns were centrifuged for one minute at 16.000 x g and washed twice with 700µl and 500 µl of provided membrane wash buffer. After additional spinning step at 16.000 x g for another minute DNA was eluted from the column by adding 25-50µl of nuclease-free water. The concentration of DNA was measured using a NanoDrop™ One/One^{C} Mikrovolume UV-VIS spectrophotometer (Thermo Fisher) and stored at -20°C.

5.2.3.5. Molecular cloning

PCR products were inserted into vector plasmids with the aid of restriction enzymes as published before (Deininger, 1983). Briefly, both plasmids were treated with FastDigest restriction enzymes (Thermo Scientific). Therefore, 16µl PCR product, 1µl of each enzyme and 1x FastDigest buffer were incubated for 30 minutes at 37°C. Alkaline phosphatase (1µl) was used for the dephosphorylation of digested plasmid and incubated for 45 minutes at 37°C under agitation (450rpm). For ligation of digested PCR product with the vector plasmid the Rapid DNA Ligation Kit (Thermo Scientific) was used. In a total volume of 20µl, 60ng of PCR insert were mixed with 1.5-2µl of vector plasmid together with provided 1x ligation buffer and 1µl T4 DNA ligase. The mixture was incubated for 30 minutes at room temperature or overnight at 4°C. At last, ligation product was transformed into competent *E. coli* cells (5.2.3.1), isolated (5.2.3.2) and analyzed by sequencing (SEQLAB Göttingen, Germany).

5.2.3.6. Isolation of RNA from mammalian cells

HEK293T cells were seeded to 75cm^2 tissue culture flask and harvested upon reaching a confluence of 80% with PBS and centrifuged four minutes at 1740rpm at 4°C. Samples were incubated with 0.5ml TRIzol for five minutes at room temperature. Afterwards, 0.1ml chloroform per 0.5ml TRIzol were added and mixture was incubated for additional three minutes after mixing samples properly for 15 seconds by hand. The upper aqueous phase containing RNA was transferred to fresh tube after separation at 12.000 x g for 15 minutes at 4°C. Then, isopropanol was added to samples (0.25ml/0.5ml TRIzol) and incubated for ten minutes at room temperature followed by centrifugation at 12.000 x g for ten minutes. After removing the supernatant, samples were washed twice with 75% and 100% ethanol and briefly centrifuged to get rid of remaining liquid. RNA pellets were dried at room temperature for 5-10 minutes and resuspended in 20µl RNase free water. To resolve pellet completely, samples were stored on ice overnight at 4°C. Next day, RNA concentration was determined with the help of a NanoDrop™ One/One^C Microvolume-UV/VIS-Spectrophotometer (Thermo Scientific). RNA was stored at -80°C.

5.2.3.7. Isolation of genomic DNA

Genomic DNA (gDNA) was isolated for HEK293T TMEM126A$^{-/-}$ cells. Therefore, cells were harvested from a 6-well tissue culture plate and pelleted at 5000 x g for five minutes at 4°C. Cell pellet was resuspended in 500µl TRIzol™ (Thermo Scientific) and incubated at 28°C for five minutes under mild agitation. After addition of 0.2ml chloroform samples were mixed properly and incubated for three minutes at 28°C. Then, samples were centrifuged at 12.000 x g for 15 minutes at 4°C and top aqueous phase was removed carefully and transferred to a new 1.5ml tube. 500µl of 2-propanol was added and samples were incubated for 10 minutes at 28°C following by a centrifugation step at 12.000 x g for 10 minutes at 4°C. Supernatants were removed and pellets were washed with 70% ethanol and again centrifuged for five minutes at 7500 x g at 4°C. Pellets were dried after removing supernatant on thermal heater at 28°C for 5-10 minutes. Finally, RNA-pellet was resuspended in nuclease free water, dissolved at 60°C for ten minutes and concentration was measured using a NanoDrop™ One/One^C Microvolume-UV/VIS-Spectrophotometer (Thermo Scientific). Samples were stored at -80°C.

5.2.3.8. In vitro mRNA synthesis

The SP6 mMESSAGE mMACHINE®Kit (Ambion) was used to synthesize *in vitro* mRNA from purified PCR products containing a SP6 promoter. The manufacturer's protocol was followed by adding 1µg of purified PCR product (5.2.3.4) to provided 1x NTP/CAP, 1x reaction buffer and 2µl of enzyme mix in a total volume of 20µl. After incubation for 90 minutes at 37°C, 1µl of provided Turbo DNase was added, mixed gently and incubated for another 15 minutes at 37°C to remove template DNA. Following, recovery of RNA was performed by addition of 30µl nuclease free water and 30µl LiCl precipitation solution (7.5M lithium chloride, 50mM EDTA). Samples were incubated at -20°C for at least one hour or overnight and afterwards RNA was pelleted for 15 minutes at 16.000 x g. After washing with 70% ethanol, pellet was left to dry at room temperature to get rid of remaining ethanol. At the end, RNA pellet was resuspended in nuclease free water, incubated on ice for 30 minutes and RNA concentration was determined using a NanoDrop™ One/One^{C} Microvolume-UV/VIS-Spectrophotometer (Thermo Scientific).

5.2.3.9. *In vitro* transcription and translation

To perform accelerated transcription and translation for precursor proteins *in vitro*, the TnT® Quick coupled Transcription/Translation System (Promega) was used. Hence, 0.5-1µg of plasmid, containing either T7 or SP6 promotor, were incubated with 50µl of TNT® Quick Master Mix in the presence of 50µCi ^{35}S-methionine and incubated for 90 minutes under mild agitation (450rpm) at 30°C. After incubation, unlabeled methionine was added in same amounts to reaction mixture and incubated for another minute at 30°C. Precursor proteins were stored immediately on ice until further use.

The Flexi® Rabbit Reticulocyte Lysate System (Promega) was used to synthesize precursor proteins from mRNA (5.2.3.8). 100-200ng of mRNA was incubated in 33µl of Flexi® Rabbit Reticulocyte Lysate with 1µl of 1mM amino acid mix without methionine, 70-120mM KCl (depending on mRNA), 25mM magnesium acetate and 50µCi ^{35}S-methionine. Mixture was incubated for 90 minutes at 30°C under mild agitation and afterwards kept on ice until further use.

5.2.4. Protein analysis

5.2.4.1. Determination of protein concentration

The concentration of isolated mitochondria or whole cells were determined by using the Roti®-Quant assay solution (Roth). As standard curve bovine immunoglobin was used in following concentrations: 0, 7.5, 15, 30 and 60µg/µl. 5, 10 and 20µl of diluted mitochondria/cells (1:10) were mixed with water in a final volume of 86µl. The optical density of each solution was measured after supplementation of 1ml Roti®-Quant reagent using a Cary® 50 Bio UV Visible spectrophotometer (Agilent Technologies). The concentration of the samples was calculated by means of the calibration curve.

5.2.4.2. SDS-PAGE

As reported by Laemmli, 1970, proteins were separated according to their molecular size using a sodium dodecyl sulphate-polyacrylamide gel electrophoresis (SDS-PAGE). The overall percentage of 0.8%/30% acrylamide/bis-acrylamide solution (Roth) in the gel were chosen according to the molecular size of proteins of interest. For cross-linking experiments a 4-20% gradient SDS gel were used with following components: 5ml acrylamide/bis-acrylamide solution, 1.5ml 1.875M Tris/HCL (pH 8.8), 0.75ml 50% glycerol, 0.075ml 10% SDS and 0.175ml water for a 20% gel. Polymerization were initiate by adding APS (10%) and TEMED. As stacking gel, a 4% SDS gel was cast on top of resolving gel and electrophoresis was performed at 20-25mA/gel and 250V in SDS-running buffer (Table 5.1) using a custom-made midi gel system.

5.2.4.3. Tris-Tricine-SDS-PAGE

Tris-Tricine-SDS-PAGE was used to separate bigger proteins as well as smaller proteins in the same range (Schägger, 2006). Therefore, resolving gels were cast as gradient gels with a concentration of 10% and 18% acrylamide. For the 10% gel the following components were used: 1.65ml acrylamide/bis-acrylamide, 2.67ml 3x gel buffer (Table 5.1), 3.68ml water. For the 18% gel, 2.97ml acrylamide/bis-acrylamide were mixed with 2.67ml 3x gel buffer, 1.25ml 80% glycerol and 1.11ml water. As stacking gel, a 4% acrylamide gel was cast on top of the resolving gel. Electrophoretic separation took place overnight for 14-16 hours at 20-25mA/gel under application of Tris-Tricine cathode and anode buffer (Table 5.1)

5.2.4.4. Blue-Native-PAGE

Protein complexes in its native state were separated using a Blue Native acrylamide gel electrophoresis (BN-PAGE) as described before (Schägger and von Jagow, 1991; Wittig *et al.*, 2006). For separation of complexes II-IV of the OXPHOS complex, a standard 4-13% gradient gel was used whereas a 2.5-10% gradient was used for complex I isolation. For a 13% acrylamide gel following components were mixed together: 3ml 3x gel buffer for BN-PAPGE (Table 5.1), 2.53ml of 49.5%/3% acrylamide/bis-acrylamide, 2.16ml of glycerol (80%) and 1.45ml water. As stacking gel, a 4% acrylamide gel was cast on top of resolving gradient gel and polymerization was induced by adding APS and TEMED to acrylamide mixture. Isolated mitochondria were solubilized on ice in solubilization buffer with either 1% digitonin or 0.6% DMM (Table 5.1; 1µg protein/1µl buffer) and incubated for 20 minutes. After centrifugation at 16.000 x g for 15 minutes lysates were mixed with 10x BN-PAGE loading dye (Table 5.1) and loaded onto BN-PAGE and separated either overnight at 80V and 15mA/gel or for 4-5 hours at 600V and 15mA/gel. Electrophoresis was performed in the presence of anode and cathode buffer (Table 5.1). All described steps were done at 4°C.

5.2.4.5. Coomassie Brilliant Blue staining

To stain separated protein bands on PVDF membranes or on acrylamide gels Coomassie staining solution (Table 5.1) was used containing 1.5% Coomassie Brilliant-Blue R250. Acrylamide gels or PVDF membranes were either incubated for one hour or ten minutes under mild movement at room temperature. Afterwards, staining solution was replaced with destaining solution (Table 5.1) until protein bands were visible. To entirely destain protein bands, PVDF membranes were washed with methanol (≥ 99%) and used subsequently for immunodetection.

5.2.4.6. Western Blot and immunodetection

After gel electrophoresis, macromolecules were transferred to a second matrix – the polyvinylidene difluoride (PVDF) membrane (Merck) using a semi-dry transfer method (Levey *et al.*, 1982; Mahmood and Yang, 2012). Therefore, PEQLAB chambers were used. First, PVDF membranes were activated with methanol, blotting paper (Heinemann Labortechnik, Sartorius) were incubated in blotting buffer (Table 5.1) to

fill itself up with liquid and the gel was reassembled. Subsequently, blotting layers were assembled as follows: three blotting papers, the activated PVDF membrane, the gel and again three blotting papers. The transfer was performed at 25V, 250mA/gel for 2.5 hours for SDS-PAGE and for BN-PAGE at 25V, 400mA/gel for 3 hours. To visualize protein bands, PVDF membrane was stained with Coomassie Brilliant Blue solution as described above (5.2.4.5) and prestained protein standard (BIO-RAD) was marked before membrane was cut into slices needed for immunodetection. After destaining the membrane completely with destaining solution (Table 5.1) and methanol, membrane was prepared for incubation with primary antibodies. Therefore, PVDF membrane was washed twice with TBS-T (Table 5.1) under agitation for 10 minutes and incubated for one hour in blocking solution (TBS-T containing 5-10% milk powder). Before antibody incubation, membranes were washed again three times for 15 minutes with TBS-T to remove remaining blocking solution. Finally, incubation with primary antibodies (Table 5.3) were performed either overnight at 4°C or for one hour at room temperature under mild agitation. Secondary HRP-conjugated antibodies (Table 5.4) were applied to the membrane after three washing steps for 15 minutes with TBS-T. Secondary antibodies were used in a concentration of 1:10.000 in TBS-T and incubated for 1-2 hours at room temperature. In the end, unbound secondary antibodies were washed out with TBS-T with the same washing procedure as describe before. Protein signals were visualized by using either a homemade ECL substrate (Table 5.1) or the Pierce® ECL Western Blotting Detection Reagent (Thermo Scientific) on X-ray films (FUJI Medical X-RAY Film, FUJIFILM Corporation).

5.2.4.7. Digital autoradiography

To visualize radioactive-labeled proteins which were separated by gel electrophoresis a digital autoradiography was used. After electrophoresis, gels were either dried immediately or transferred to a PVDF membrane as described above (5.2.4.6). In case of drying, gel was transferred to Coomassie Brilliant Blue staining solution (5.2.4.5) for at least 30 minutes and afterwards destained with fresh destaining solution (Table 5.1) until proteins bands were visible. On a sheet of filter paper gel was placed on a vacuum gel dryer (Gel Dryer UG 3545, LTF Labortechnik), covered with a plastic foil and dried for 2-4 hours at 65°C. In the other case, PVDF membranes were dried at room temperature after staining and destaining (5.2.4.5). Both, dried gels and PVDF

membranes were exposed on storage phosphor screens (GE Healthcare) for at least 24 hours and signals were visualized using an Amersham Thypoon laser-scanner (GE Healthcare).

5.2.5. Specialized Assays

5.2.5.1. Import and assembly of radiolabeled precursor proteins

Radiolabeled precursor proteins were synthesized *in vitro* (5.2.3.9) and imported into isolated mitochondria (5.2.2.2) as described previously (Lazarou *et al.*, 2009; Mohanraj *et al.*, 2019). Briefly, isolated mitochondria were incubated with import buffer (Table 5.1) supplemented with 5mM ATP in a final concentration of 1µg/µl for two minutes at 30°C at 450rpm. Samples selected for negative control were additional incubated with VOA mixture (Table 5.1) to dissipate the membrane potential. After pre-incubation, radiolabeled precursor proteins (2-10% (v/v)) were added to each sample to initiate the import reaction and incubated at 30°C. After individual time points, reaction was stopped by addition of VOA mix and samples were stored immediately on ice. To remove unimported precursor proteins, samples were treated afterwards with 20µg/ml proteinase K for ten minutes. To stop proteinase activity, 2mM PMSF were added to each reaction and again incubated for 15 minutes on ice. Finally, mitochondria were harvested by a centrifugation step at 12.000 x g for ten minutes and resuspended in SDS sample buffer (Table 5.1) After heating at 95°C for five minutes samples were separated on SDS-PAGE (5.2.4.2) and analyzed by digital autoradiography (5.2.4.7). For assembly analysis, pelleted mitochondria were incubated after the import with BN solubilization buffer (Table 5.1) for 20 minutes as described in 5.2.4.4 and separated on BN-PAGE to visualize the incorporation of radiolabeled precursor proteins into complexes of the respiratory chain.

5.2.5.2. Stability assay for imported precursor proteins

The stability of imported precursor proteins were monitored by an pulse/chase-import assay (Reinhold *et al.*, 2011; Röttgers *et al.*, 2002). Therefore, precursor proteins were imported into isolated mitochondria as described above. After import reaction, pelleted mitochondria were washed with SEM buffer (Table 5.1) re-isolated for ten minutes at 12.000 x g, resuspended again in import buffer without ATP and stored on ice at indicated time points. At the end, mitochondria were centrifuged for

ten minutes at 12.000 x g, incubated in SDS sample buffer and used for analysis on SDS-PAGE and autoradiography as described before.

5.2.5.3. Co-immunoprecipitation for FLAG-tagged samples

Co-immunoprecipitations for C- or N-terminally tagged cells or mitochondria were performed as descripted before (Dennerlein *et al.*, 2015) with modifications. 24 hours prior affinity purification, expression of respective protein was induced by adding tetracycline (2µg/5ml media) to cells (5.2.1.3). Next day, cells were either used for mitochondria isolation as described in section 5.2.2.1 or whole cell lysates were used for co-immunoprecipitation (5.2.2.3). In case of isolated mitochondria, samples were lysed in solubilization buffer (Table 5.1) containing 1% digitonin (1µg protein/µl) and incubated for 30 minutes at 4°C (850rpm). To remove non-solubilized material lysates were centrifuged for 15 minutes at 16.000 x g at 4°C. Cleared lysates were transferred onto equilibrated anti-FLAG Affinity Gel (SIGMA) and incubated for one hour on an overhead rotor at 4°C. Subsequently, FLAG-beads were washed with wash buffer (Table 5.1) containing 0.3% digitonin ten times by centrifugation for 30 seconds at 4°C and 200 x g. Proteins bound to FLAG-beads were eluted with FLAG peptide (4mg/ml) diluted 1:10 in wash buffer. Instead, samples were incubated for 30 minutes at 850rpm at 4°C and eluate was gained by centrifugation for one minute at 200 x g at 4°C. Samples were either used for further experiments (double-IP) or analyzed by SDS-PAGE/BN-PAGE and immunoblotting (5.2.4.6) after addition of sample buffer.

5.2.5.4. Affinity purification using Protein A Sepharose

To observe covalent and non-covalent protein-protein interactions Protein A Sepharose™ CL-4B (GE Healthcare) was conjugated with endogenous antibodies as described previously (Mick *et al.*, 2012; Richter-Dennerlein *et al.*, 2016). As negative control the yeast antibody for Pam18 was used in regard of experiments with human samples. Specific or control antibodies were crosslinked onto Protein A Sepharose beads with the help of dimethyl-pimelindiimidat dihydrochloride for 30 minutes at room temperature or overnight at 4°C using specific purification Mobicol columns (MoBiTec). Isolated mitochondria or cells were lysed in solubilization buffer (section 5.2.5.3) in the presence of 1% digitonin for 30 minutes at 4°C (850rpm) and supernatants (16.000 x g, 15 minutes, 4°C) were applied onto corresponding antibody

columns. The incubation took place for one hour at 4°C on an overhead rotor. Prior elution, affinity resins were washed with wash buffer (Table 5.1) ten times (200 x g, 30 seconds) and eluate was obtained by pH shift using 0.1M glycine (pH 2.8) for 5-6 minutes at room temperature under shaking (450 rpm). Finally, SDS sample buffer was enclosed to eluates and used for SDS-PAGE (5.2.4.2) and immunoblotting (5.2.4.6).

5.2.5.5. Cytochrome *c* oxidase activity assay

The complex IV Human Enzyme Activity Microplate Assay Kit (abcam) was used to determine the activity of cytochrome *c* oxidase in human samples according to the manufacturer's protocol. In short, cells were harvested and resuspended in "Solution 1" which was provided by the kit. Afterwards, protein concentration was measured as described in section 5.2.4.1 and adjusted for all samples to a concentration of 5µg/µl. To solubilize samples 1/10 of the provided detergent was added, mixed and incubated for 30 minutes on ice. After centrifugation at 16.000 x g for 20 minutes at 4°C, protein concentrations of all samples were determined again and adapted to a concentration of 15µg/200µl. Samples were transferred to provided 96-well microplate in triplicates and incubated for three hours at room temperature. After washing for three times with "Solution 1" the "Assay Solution" was prepared by adding appropriate amounts of cytochrome c to "Solution 1". Immediately after addition, optical density was measured at 550nm at 30°C for two hours. For measurement a Synergy H1 microplate reader (BioTek) was used. Since the rate of activity is expressed as the initial rate of oxidation of cytochrome *c* the absorbance was used to calculate the slope.

5.2.5.6. NADH:ubiquinone reductase activity assay

Mitochondrial OXPHOS complex I enzyme activity was measured using the Complex I Enzyme Activity Assay Kit (abcam) and instructions of producer were followed. After harvesting of cells, protein concentration was measured as described in section 5.2.4.1 and adapt oneself to a concentration at 5.5mg/ml. Samples were solubilized by adding 1/10 of provided detergent solution and incubated for 30 minutes on ice. Cell lysates were cleared by centrifugation at 16.000 g x for 20 minutes at 4°C and supernatants diluted in provided incubation solution according to manufacturer's protocol. 200µl of each sample was load on provided 96-well microplate in triplicates and incubated for three hours at room temperature. The wells were washed with 300µl "Wash Buffer"

and provided "Assay solution" containing 2mM NADH was added to each well. Immediately afterwards, absorbance was measured at 450nm in a kinetic mode for 30 minutes at room temperature. Complex I activity was calculated using the linear rate of increase in absorbance over the time.

5.2.5.7. *In vivo* radiolabeling of ribosome-nascent chain complex

To visualize nascent chains during mitochondrial translation cells were treated with puromycin in a concentration of 2µg/ml (Richter-Dennerlein *et al.*, 2016). Labeling was performed as described in section 5.2.1.7 with modifications. Cells were incubated with FBS/methionine-free DMEM media for 20 minutes at 37°C. Afterwards, media was changed into methionine-free DMEM media but with FBS and cytosolic translation was inhibited by adding 100µg/ml emetine to cells for 10 minutes. Mitochondrial translation products were labeled radioactively by addition of 200µCi/ml of ^{35}S-methionine for 10 minutes at 37°C. To inhibit mitochondrial translation, cells were incubated subsequently with puromycin for another 20 minutes at 37°C. Finally, cells were harvested with PBS and centrifugation at 5000 x g for two minutes at room temperature. Samples were either stored at -80°C or immediately on ice for following experiments and analyzed via SDS-PAGE (5.2.4.2) and autoradiography (5.2.4.7).

5.2.5.8. Stable isotope labeling by amino acids in cell culture

Stable isotope labeling by amino acids in cell culture (SILAC) was used for *in vivo* incorporation of specific amino acids (Ong *et al.*, 2002). Wildtype HEK293T cells and FLAG-tagged HEK293T cells were cultured in equal amounts in SILAC medium (Table 5.2) containing heavy amino acids, L-arginine (U-13C6, 99%; U-15N4 99%) and L-lysine (U-13C6, 99%; U-15N2, 99%; Cambridge Isotope Laboratories) as well as in light SILAC medium. For each experiment ^{FLAG}OXA1L cells were grown in heavy SILAC media and wildtype cells in light SILAC media and vice versa for the reverse experiment. Cells were cultured as described in section 5.2.1.1 and incorporation of amino acids in the cells were performed in collaboration with Dr. Silke Oeljeklaus and Dr. Alexander Schendzielorz from the group of Prof. Bettina Warscheid at the Institute of Biology II at the University of Freiburg.

5.2.5.9. Mass spectrometric analysis of SILAC labeled proteins

^{FLAG}OXA1L cells were used for mass spectrometry analysis in collaboration with the group of Prof. Bettina Warscheid (Institute of Biology II, University of Freiburg). Therefore, ^{FLAG}OXA1L and wildtype HEK293T cells were cultured in SILAC medium as described above (5.2.5.8). Isolated mitochondria from these cell lines (5.2.2.1) were mixed in a ratio of 1:1 in the combination of heavy labeled wildtype together with light labeled ^{FLAG}OXA1L samples and vice versa for the reverse setup. Protein complexes were isolated using affinity purification with anti-FLAG M2 Affinity Gel (5.2.5.3). Each experiment was done in two replicates, sent to Freiburg and analyzed by Dr. Alexander Schendzielorz and Dr. Silke Oeljeklaus.

The eluates of the IP were precipitated by addition of 4-fold volume of acetone and incubated at -20 °C for two hours. Samples were centrifuged for 15 min at 21.000xg, 4 °C and the supernatant was carefully removed. The pellet was denatured using 8M urea, 50mM ammonium bicarbonate, reduced for 30 min at 37 °C using 5 mM TCEP and alkylated for 30 minutes at room temperature in the dark using 50 mM IAA. Samples were digested overnight using Trypsin at 37 °C and desalted using C18 StageTips. One replicate of control and TAP treated samples was analyzed using a LTQ Orbitrap XL (Thermo Fisher Scientific, Bremen, Germany) coupled to an UltiMate 3000 RSLCnano HPLC system (Thermo Fisher Scientific, Dreieich, Germany). The other three replicates were analyzed using a Q Exactive Plus mass spectrometer (Thermo Fisher Scientific, Bremen, Germany). The RSLC systems for the LTQ was operated with C18 pre-columns (5 cm) and a C18 analytical column (50 cm column, both Thermo Fisher Scientific) and C18 pre-columns (2 cm) and C18 analytical column (25 cm, both Waters) for the Q Exactive Plus instrument. Peptides were eluted during a 50 minute linear gradient of increasing acetonitrile concentration (4% - 42% in 0.1% formic acid; v/v each) for the Q Exactive Plus and during a 60 minutes gradient (1%-65% in 0.1% formic acid; v/v each) for the LTQ Orbitrap XL system.

Proteins were identified using MaxQuant/Andromeda (version 1.6.0.1; Cox and Mann, 2008; Cox *et al.*, 2011) and the UniProt human ProteomeSet including isoforms (downloaded 09/2018). The database search was performed with MaxQuant default settings. After correcting for the label switch, $\log_2$ transformed MaxQuant ratios were used for a student's t-test (one sample, two sided).

6. Bibliography

Abe, Y., Shodai, T., Muto, T., Mihara, K., Torii, H., Nishikawa, S., Endo, T., Kohda, D., 2000. Structural Basis of Presequence Recognition by the Mitochondrial Protein Import Receptor Tom20. *Cell* 100, 551–560.

Acín-Pérez, R., Bayona-Bafaluy, M.P., Fernández-Silva, P., Moreno-Loshuertos, R., Pérez-Martos, A., Bruno, C., Moraes, C.T., Enríquez, J.A., 2004. Respiratory complex III is required to maintain complex I in mammalian mitochondria. *Mol*. *Cell* 13, 805–815.

Aguer, C., Gambarotta, D., Mailloux, R.J., Moffat, C., Dent, R., McPherson, R., Harper, M.-E., 2011. Galactose Enhances Oxidative Metabolism and Reveals Mitochondrial Dysfunction in Human Primary Muscle Cells. *PLoS ONE* 6, e28536.

Almontashiri, N.A.M., Chen, H.-H., Mailloux, R.J., Tatsuta, T., Teng, A.C.T., Mahmoud, A.B., Ho, T., Stewart, N.A.S., Rippstein, P., Harper, M.E., Roberts, R., Willenborg, C., Erdmann, J., Pastore, A., McBride, H.M., Langer, T., Stewart, A.F.R., 2014. SPG7 variant escapes phosphorylation-regulated processing by AFG3L2, elevates mitochondrial ROS, and is associated with multiple clinical phenotypes. *Cell Rep.* 7, 834–847.

Alston, C.L., Compton, A.G., Formosa, L.E., Strecker, V., Oláhová, M., Haack, T.B., Smet, J., Stouffs, K., Diakumis, P., Ciara, E., Cassiman, D., Romain, N., Yarham, J.W., He, L., De Paepe, B., Vanlander, A.V., Seneca, S., Feichtinger, R.G., Płoski, R., Rokicki, D., Pronicka, E., Haller, R.G., Van Hove, J.L.K., Bahlo, M., Mayr, J.A., Van Coster, R., Prokisch, H., Wittig, I., Ryan, M.T., Thorburn, D.R., Taylor, R.W., 2016. Biallelic Mutations in TMEM126B Cause Severe Complex I Deficiency with a Variable Clinical Phenotype. *Am. J. Hum. Genet*. 99, 217–227.

Altamura, N., Capitanio, N., Bonnefoy, N., Papa, S., Dujardin, G., 1996. The *Saccharomyces cerevisiae* OXA1 gene is required for the correct assembly of cytochrome *c* oxidase and oligomycin-sensitive ATP synthase. *FEBS Lett*. 382, 111–115.

Anand, R., Reichert, A.S., Kondadi, A.K., 2021. Emerging Roles of the MICOS Complex in Cristae Dynamics and Biogenesis. *Biology* 10, 600.

Andrews, B., Carroll, J., Ding, S., Fearnley, I.M., Walker, J.E., 2013. Assembly factors for the membrane arm of human complex I. *Proc. Natl. Acad. Sci. U. S. A*. 110, 18934–18939.

Barrientos, A., Gouget, K., Horn, D., Soto, I.C., Fontanesi, F., 2009. Suppression mechanisms of COX assembly defects in yeast and human: insights into the COX assembly process. *Biochim. Biophys. Acta* 1793, 97–107.

Bauer, M., Behrens, M., Esser, K., Michaelis, G., Pratje, E., 1994. PET1402, a nuclear gene required for proteolytic processing of cytochrome oxidase subunit 2 in yeast. *Mol. Gen. Genet. MGG* 245, 272–278.

Bausewein, T., Naveed, H., Liang, J., Nussberger, S., 2020. The structure of the TOM core complex in the mitochondrial outer membrane. *Biol. Chem*. 401, 687–697.

Bhangoo, M.K., Tzankov, S., Fan, A.C.Y., Dejgaard, K., Thomas, D.Y., Young, J.C., 2007. Multiple 40-kDa Heat-Shock Protein Chaperones Function in Tom70-dependent Mitochondrial Import. *Mol. Biol. Ce*ll 18, 3414–3428.

Bohnert, M., Pfanner, N., van der Laan, M., 2007. A dynamic machinery for import of mitochondrial precursor proteins. *FEBS Lett*. 581, 2802–2810.

Bohnert, M., Rehling, P., Guiard, B., Herrmann, J.M., Pfanner, N., van der Laan, M., 2010. Cooperation of stop-transfer and conservative sorting mechanisms in mitochondrial protein transport. *Curr. Biol. CB* 20, 1227–1232.

Bonnefoy, N., Chalvet, F., Hamel, P., Slonimski, P.P., Dujardin, G., 1994. OXA1, a *Saccharomyces cerevisiae* nuclear gene whose sequence is conserved from prokaryotes to eukaryotes controls cytochrome oxidase biogenesis. *J. Mol. Biol*. 239, 201–212.

Brandt, U., 2006. Energy converting NADH:quinone oxidoreductase (complex I). *Annu. Rev. Biochem.* 75, 69–92.

Brzezinski, P., Moe, A., Ädelroth, P., 2021. Structure and Mechanism of Respiratory III-IV Supercomplexes in Bioenergetic Membranes. *Chem. Rev.*

Busch, J.D., Cipullo, M., Atanassov, I., Bratic, A., Silva Ramos, E., Schöndorf, T., Li, X., Pearce, S.F., Milenkovic, D., Rorbach, J., Larsson, N.-G., 2019. MitoRibo-Tag Mice Provide a Tool for *In Vivo* Studies of Mitoribosome Composition. *Cell Rep*. 29, 1728-1738.

Callegari, S., Cruz-Zaragoza, L.D., Rehling, P., 2020. From TOM to the TIM23 complex - handing over of a precursor. *Biol. Chem*. 401, 709–721.

Callegari, S., Müller, T., Schulz, C., Lenz, C., Jans, D.C., Wissel, M., Opazo, F., Rizzoli, S.O., Jakobs, S., Urlaub, H., Rehling, P., Deckers, M., 2019. A MICOS-TIM22 Association Promotes Carrier Import into Human Mitochondria. *J. Mol. Biol*. 431, 2835–2851.

Callegari, S., Oeljeklaus, S., Warscheid, B., Dennerlein, S., Thumm, M., Rehling, P., Dudek, J., 2017. Phospho-ubiquitin-PARK2 complex as a marker for mitophagy defects. *Autophagy* 13, 201–211.

Carroll, J., He, J., Ding, S., Fearnley, I.M., Walker, J.E., 2021. TMEM70 and TMEM242 help to assemble the rotor ring of human ATP synthase and interact with assembly factors for complex I. *Proc. Natl. Acad. Sci. U. S. A.* 118, e2100558118.

Ceh-Pavia, E., Spiller, M.P., Lu, H., 2013. Folding and biogenesis of mitochondrial small Tim proteins. *Int. J. Mol. Sci.* 14, 16685–16705.

Chacinska, A., Guiard, B., Müller, J.M., Schulze-Specking, A., Gabriel, K., Kutik, S., Pfanner, N., 2008. Mitochondrial Biogenesis, Switching the Sorting Pathway of the Intermembrane Space Receptor Mia40. *J. Biol. Chem*. 283, 29723–29729.

Chacinska, A., Koehler, C.M., Milenkovic, D., Lithgow, T., Pfanner, N., 2009. Importing Mitochondrial Proteins: Machineries and Mechanisms. *Cell* 138, 628–644.

Chatzi, A., Sideris, D.P., Katrakili, N., Pozidis, C., Tokatlidis, K., 2013. Biogenesis of yeast Mia40 – uncoupling folding from import and atypical recognition features. *FEBS J*. 280, 4960–4969.

Chaudhuri, M., Darden, C., Gonzalez, F.S., Singha, U.K., Quinones, L., Tripathi, A., 2020. Tim17 Updates: A Comprehensive Review of an Ancient Mitochondrial Protein Translocator. *Biomolecules* 10.

Crofts, A.R., 2004. The cytochrome *bc1* complex: function in the context of structure. *Annu. Rev. Physiol*. 66, 689–733.

Dang, Q.-C.L., Phan, D.H., Johnson, A.N., Pasapuleti, M., Alkhaldi, H.A., Zhang, F., Vik, S.B., 2020. Analysis of Human Mutations in the Supernumerary Subunits of Complex *I. Life Basel Switz.* 10.

D'Angelo, L., Astro, E., De Luise, M., Kurelac, I., Umesh-Ganesh, N., Ding, S., Fearnley, I.M., Gasparre, G., Zeviani, M., Porcelli, A.M., Fernandez-Vizarra, E., Iommarini, L., 2021. NDUFS3 depletion permits complex I maturation and reveals TMEM126A/OPA7 as an assembly factor binding the ND4-module intermediate. *Cell Rep*. 35, 109002.

Deininger, P.L., 1983. Approaches to rapid DNA sequence analysis. *Anal. Biochem*. 135, 247–263.

Denkert, N., Schendzielorz, A.B., Barbot, M., Versemann, L., Richter, F., Rehling, P., Meinecke, M., 2017. Cation selectivity of the presequence translocase channel Tim23 is crucial for efficient protein import. *eLife* 6.

Dennerlein, S., Oeljeklaus, S., Jans, D., Hellwig, C., Bareth, B., Jakobs, S., Deckers, M., Warscheid, B., Rehling, P., 2015. MITRAC7 Acts as a COX1-Specific Chaperone and Reveals a Checkpoint during Cytochrome *c* Oxidase Assembly. *Cell Rep*. 12, 1644–1655.

Dennerlein, S., Rozanska, A., Wydro, M., Chrzanowska-Lightowlers, Z.M.A., Lightowlers, R.N., 2010. Human ERAL1 is a mitochondrial RNA chaperone involved in the assembly of the 28S small mitochondrial ribosomal subunit. *Biochem. J*. 430, 551–558.

Diederichs, K.A., Buchanan, S.K., Botos, I., 2021. Building Better Barrels – β-barrel Biogenesis and Insertion in Bacteria and Mitochondria. *J. Mol. Biol*. 166894.

Dietmeier, K., Hönlinger, A., Bömer, U., Dekker, P.J.T., Eckerskorn, C., Lottspeich, F., Kübrich, M., Pfanner, N., 1997. Tom5 functionally links mitochondrial preprotein receptors to the general import pore. *Nature* 388, 195–200.

DiMauro, S., Schon, E.A., 2003. Mitochondrial respiratory-chain diseases. *N. Engl. J. Med*. 348, 2656–2668.

Dudek, J., Rehling, P., van der Laan, M., 2013. Mitochondrial protein import: Common principles and physiological networks. *Biochim. Biophys. Acta BBA - Mol. Cell Res.*, Protein Import and Quality Control in Mitochondria and Plastids 1833, 274–285.

Eckl, E.-M., Ziegemann, O., Krumwiede, L., Fessler, E., Jae, L.T., 2021. Sensing, signaling and surviving mitochondrial stress. *Cell. Mol. Life Sci. CMLS*.

Ehses, S., Raschke, I., Mancuso, G., Bernacchia, A., Geimer, S., Tondera, D., Martinou, J.-C., Westermann, B., Rugarli, E.I., Langer, T., 2009. Regulation of OPA1 processing and mitochondrial fusion by m-AAA protease isoenzymes and OMA1. *J. Cell Biol*. 187, 1023–1036.

Elurbe, D.M., Huynen, M.A., 2016. The origin of the supernumerary subunits and assembly factors of complex I: A treasure trove of pathway evolution. *Biochim. Biophys. Acta* 1857, 971–979.

Endo, T., Yamano, K., 2010. Transport of proteins across or into the mitochondrial outer membrane. Biochim. Biophys. Acta BBA - *Mol. Cell Res.*, Molecular Chaperones and Intracellular Protein Transport 1803, 706–714.

Endo, T., Yamano, K., Kawano, S., 2011. Structural insight into the mitochondrial protein import system. *Biochim. Biophys. Acta BBA - Biomembr.*, Including the Special Section: Protein translocation across or insertion into membranes 1808, 955–970.

Fernández-Vizarra, E., Tiranti, V., Zeviani, M., 2009. Assembly of the oxidative phosphorylation system in humans: what we have learned by studying its defects. *Biochim. Biophys. Acta* 1793, 200–211.

Fernandez-Vizarra, E., Zeviani, M., 2021. Mitochondrial disorders of the OXPHOS system. *FEBS Lett.* 595, 1062–1106.

Fernandez-Vizarra, E., Zeviani, M., 2018. Mitochondrial complex III Rieske Fe-S protein processing and assembly. *Cell Cycle* 17, 681–687.

Fernández-Vizarra, E., Zeviani, M., 2015. Nuclear gene mutations as the cause of mitochondrial complex III deficiency. *Front. Genet.* 6, 134.

Fiumera, H.L., Dunham, M.J., Saracco, S.A., Butler, C.A., Kelly, J.A., Fox, T.D., 2009. Translocation and assembly of mitochondrially coded *Saccharomyces cerevisiae* cytochrome *c* oxidase subunit Cox2 by Oxa1 and Yme1 in the absence of Cox18. *Genetics* 182, 519–528.

Formosa, L.E., Muellner-Wong, L., Reljic, B., Sharpe, A.J., Jackson, T.D., Beilharz, T.H., Stojanovski, D., Lazarou, M., Stroud, D.A., Ryan, M.T., 2020. Dissecting the Roles of Mitochondrial Complex I Intermediate Assembly Complex Factors in the Biogenesis of Complex I. *Cell Rep*. 31, 107541.

Formosa, L.E., Reljic, B., Sharpe, A.J., Hock, D.H., Muellner-Wong, L., Stroud, D.A., Ryan, M.T., 2021. Optic atrophy-associated TMEM126A is an assembly factor for the ND4-module of mitochondrial complex I. *Proc. Natl. Acad. Sci. U. S. A*. 118.

Frazier, A.E., Dudek, J., Guiard, B., Voos, W., Li, Y., Lind, M., Meisinger, C., Geissler, A., Sickmann, A., Meyer, H.E., Bilanchone, V., Cumsky, M.G., Truscott, K.N., Pfanner, N., Rehling, P., 2004. Pam16 has an essential role in the mitochondrial protein import motor. *Nat. Struct. Mol. Biol*. 11, 226–233.

Friedrich, V.K., Rubel, M.A., Schurr, T.G., 2021. Mitochondrial genetic variation in human bioenergetics, adaptation, and adult disease. *Am. J. Hum. Biol. Off. J. Hum. Biol. Counc*. e23629.

Fuhrmann, D.C., Wittig, I., Brüne, B., 2019. TMEM126B deficiency reduces mitochondrial SDH oxidation by LPS, attenuating HIF-1α stabilization and IL-1β expression. *Redox Biol*. 20, 204–216.

Funes, S., Kauff, F., Sluis, E.O. van der, Ott, M., Herrmann, J.M., 2011. Evolution of YidC/Oxa1/Alb3 insertases: three independent gene duplications followed by functional specialization in bacteria, mitochondria and chloroplasts 392, 13–19.

Gabriel, K., Milenkovic, D., Chacinska, A., Müller, J., Guiard, B., Pfanner, N., Meisinger, C., 2007. Novel mitochondrial intermembrane space proteins as substrates of the MIA import pathway. *J. Mol. Biol.* 365, 612–620.

Gakh, O., Cavadini, P., Isaya, G., 2002. Mitochondrial processing peptidases. *Biochim. Biophys. Acta* 1592, 63–77.

Ghezzi, D., Zeviani, M., 2018. Human diseases associated with defects in assembly of OXPHOS complexes. *Essays Biochem*. 62, 271–286.

Giachin, G., Bouverot, R., Acajjaoui, S., Pantalone, S., Soler-López, M., 2016. Dynamics of Human Mitochondrial Complex I Assembly: Implications for Neurodegenerative Diseases. *Front. Mol. Biosci*. 3, 43.

Gil-Borlado, M.C., González-Hoyuela, M., Blázquez, A., García-Silva, M.T., Gabaldón, T., Manzanares, J., Vara, J., Martín, M.A., Seneca, S., Arenas, J., Ugalde, C., 2009. Pathogenic mutations in the 5' untranslated region of BCS1L mRNA in mitochondrial complex III deficiency. *Mitochondrion* 9, 299–305.

Glick, B.S., Brandt, A., Cunningham, K., Müller, S., Hallberg, R.L., Schatz, G., 1992. Cytochromes *c1* and *b2* are sorted to the intermembrane space of yeast mitochondria by a stop-transfer mechanism. *Cell* 69, 809–822.

Gomkale, R., Cruz-Zaragoza, L.D., Suppanz, I., Guiard, B., Montoya, J., Callegari, S., Pacheu-Grau, D., Warscheid, B., Rehling, P., 2020. Defining the Substrate Spectrum of the TIM22 Complex Identifies Pyruvate Carrier Subunits as Unconventional Cargos. *Curr. Biol*. 30, 1119-1127.

Grevel, A., Pfanner, N., Becker, T., 2020. Coupling of import and assembly pathways in mitochondrial protein biogenesis. *Biol. Chem*. 401, 117–129.

Gusic, M., Prokisch, H., 2021. Genetic basis of mitochondrial diseases. *FEBS Lett.* 595, 1132–1158.

Habib, S.J., Neupert, W., Rapaport, D., 2007. Analysis and prediction of mitochondrial targeting signals. *Methods Cell Biol.* 80, 761–781.

Hällberg, B.M., Larsson, N.-G., 2014. Making Proteins in the Powerhouse. *Cell Meta*b. 20, 226–240.

Hanein, S., Garcia, M., Fares-Taie, L., Serre, V., De Keyzer, Y., Delaveau, T., Perrault, I., Delphin, N., Gerber, S., Schmitt, A., Masse, J.-M., Munnich, A., Kaplan, J., Devaux, F., Rozet, J.-M., 2013. TMEM126A is a mitochondrial located mRNA (MLR) protein of the mitochondrial inner membrane. *Biochim. Biophys. Acta* 1830, 3719–3733.

Hansen, K.G., Herrmann, J.M., 2019. Transport of Proteins into Mitochondria. *Protein J*. 38, 330–342.

Haque, Md.E., Elmore, K.B., Tripathy, A., Koc, H., Koc, E.C., Spremulli, L.L., 2010. Properties of the C-terminal Tail of Human Mitochondrial Inner Membrane Protein Oxa1L and Its Interactions with Mammalian Mitochondrial Ribosomes. *J. Biol. Chem*. 285, 28353–28362.

Haque, M.E., Spremulli, L.L., Fecko, C.J., 2010. Identification of Protein-Protein and Protein-Ribosome Interacting Regions of the C-terminal Tail of Human Mitochondrial Inner Membrane Protein Oxa1L. *J. Biol. Chem.* 285, 34991–34998.

Harbauer, A.B., Zahedi, R.P., Sickmann, A., Pfanner, N., Meisinger, C., 2014. The Protein Import Machinery of Mitochondria—A Regulatory Hub in Metabolism, Stress, and Disease. *Cell Metab*. 19, 357–372.

Haucke, V., Lithgow, T., Rospert, S., Hahne, K., Schatz, G., 1995. The yeast mitochondrial protein import receptor Mas20p binds precursor proteins through electrostatic interaction with the positively charged presequence. *J. Biol. Chem*. 270, 5565–5570.

He, S., Fox, T.D., 1997. Membrane translocation of mitochondrially coded Cox2p: distinct requirements for export of N and C termini and dependence on the conserved protein Oxa1p. *Mol. Biol. Cel*l 8, 1449–1460.

Heide, H., Bleier, L., Steger, M., Ackermann, J., Dröse, S., Schwamb, B., Zörnig, M., Reichert, A.S., Koch, I., Wittig, I., Brandt, U., 2012. Complexome profiling identifies TMEM126B as a component of the mitochondrial complex I assembly complex. *Cell Metab*. 16, 538–549.

Hell, K., Herrmann, J.M., Pratje, E., Neupert, W., Stuart, R.A., 1998. Oxa1p, an essential component of the N-tail protein export machinery in mitochondria. *Proc. Natl. Acad. Sci. U. S. A*. 95, 2250–2255.

Hell, K., Neupert, W., Stuart, R.A., 2001. Oxa1p acts as a general membrane insertion machinery for proteins encoded by mitochondrial DNA. *EMBO J*. 20, 1281–1288.

Herrmann, J.M., Neupert, W., 2000. Protein transport into mitochondria. *Curr. Opin. Microbiol.* 3, 210–214.

Herrmann, J.M., Neupert, W., Stuart, R.A., 1997. Insertion into the mitochondrial inner membrane of a polytopic protein, the nuclear-encoded Oxa1p. *EMBO J*. 16, 2217–2226.

Hock, D.H., Robinson, D.R.L., Stroud, D.A., 2020. Blackout in the powerhouse: clinical phenotypes associated with defects in the assembly of OXPHOS complexes and the mitoribosome. *Biochem. J*. 477, 4085–4132.

Höhr, A.I.C., Lindau, C., Wirth, C., Qiu, J., Stroud, D.A., Kutik, S., Guiard, B., Hunte, C., Becker, T., Pfanner, N., Wiedemann, N., 2018. Membrane protein insertion through a mitochondrial β-barrel gate. *Science* 359.

Holt, I.J., Harding, A.E., Morgan-Hughes, J.A., 1988. Deletions of muscle mitochondrial DNA in patients with mitochondrial myopathies. *Nature* 331, 717–719.

Hunte, C., Koepke, J., Lange, C., Rossmanith, T., Michel, H., 2000. Structure at 2.3 A resolution of the cytochrome $bc_{(1)}$ complex from the yeast *Saccharomyces cerevisiae* co-crystallized with an antibody Fv fragment. Struct. Lond. Engl. 1993 8, 669–684.

Itoh, Y., Andréll, J., Choi, A., Richter, U., Maiti, P., Best, R.B., Barrientos, A., Battersby, B.J., Amunts, A., 2021. Mechanism of membrane-tethered mitochondrial protein synthesis. *Science* 371, 846–849.

Iwata, S., Lee, J.W., Okada, K., Lee, J.K., Iwata, M., Rasmussen, B., Link, T.A., Ramaswamy, S., Jap, B.K., 1998. Complete structure of the 11-subunit bovine mitochondrial cytochrome bc_1 complex. *Science* 281, 64–71.

Jackson, T.D., Hock, D.H., Fujihara, K.M., Palmer, C.S., Frazier, A.E., Low, Y.C., Kang, Y., Ang, C.-S., Clemons, N.J., Thorburn, D.R., Stroud, D.A., Stojanovski, D., 2021. The TIM22 complex mediates the import of sideroflexins and is required for efficient mitochondrial one-carbon metabolism. *Mol. Biol. Cell* 32, 475–491.

Jang, Y., Ahn, S.R., Shim, J., Lim, K., 2021. Engineering Genetic Systems for Treating Mitochondrial Diseases. *Pharmaceutics 13, 810.*

Jensen, R.E., Dunn, C.D., 2002. Protein import into and across the mitochondrial inner membrane: role of the TIM23 and TIM22 translocons. *Biochim. Biophys. Acta* 1592, 25–34.

Jia, L., Dienhart, M., Schramp, M., McCauley, M., Hell, K., Stuart, R.A., 2003. Yeast Oxa1 interacts with mitochondrial ribosomes: the importance of the C-terminal region of Oxa1. *EMBO J.* 22, 6438–6447.

Káldi, K., Bauer, M.F., Sirrenberg, C., Neupert, W., Brunner, M., 1998. Biogenesis of Tim23 and Tim17, integral components of the TIM machinery for matrix-targeted preproteins. *EMBO J*. 17, 1569–1576.

Kiebler, M., Becker, K., Pfanner, N., Neupert, W., 1993. Mitochondrial protein import: Specific recognition and membrane translocation of preproteins. *J. Membr. Biol*. 135.

Kohler, R., Boehringer, D., Greber, B., Bingel-Erlenmeyer, R., Collinson, I., Schaffitzel, C., Ban, N., 2009. YidC and Oxa1 form dimeric insertion pores on the translating ribosome. Mol. *Cell* 34, 344–353.

Krämer, L., Groh, C., Herrmann, J.M., 2021. The proteasome: friend and foe of mitochondrial biogenesis. *FEBS Lett.* 595, 1223–1238.

Krüger, V., Deckers, M., Hildenbeutel, M., van der Laan, M., Hellmers, M., Dreker, C., Preuss, M., Herrmann, J.M., Rehling, P., Wagner, R., Meinecke, M., 2012. The mitochondrial oxidase assembly protein 1 (Oxa1) insertase forms a membrane pore in lipid bilayers. *J. Biol. Chem*. 287, 33314–33326.

Kruse, S.E., Watt, W.C., Marcinek, D.J., Kapur, R.P., Schenkman, K.A., Palmiter, R.D., 2008. Mice with Mitochondrial Complex I Deficiency Develop a Fatal Encephalomyopathy. *Cell Metab*. 7, 312–320.

Künkele, K.-P., Heins, S., Dembowski, M., Nargang, F.E., Benz, R., Thieffry, M., Walz, J., Lill, R., Nussberger, S., Neupert, W., 1998. The Preprotein Translocation Channel of the Outer Membrane of Mitochondria. *Cell* 93, 1009–1019.

Kurelac, I., Iommarini, L., Vatrinet, R., Amato, L.B., De Luise, M., Leone, G., Girolimetti, G., Umesh Ganesh, N., Bridgeman, V.L., Ombrato, L., Columbaro, M., Ragazzi, M., Gibellini, L., Sollazzo, M., Feichtinger, R.G., Vidali, S., Baldassarre, M., Foriel, S., Vidone, M., Cossarizza, A., Grifoni, D., Kofler, B., Malanchi, I., Porcelli, A.M., Gasparre, G., 2019. Inducing cancer indolence by targeting mitochondrial Complex I is potentiated by blocking macrophage-mediated adaptive responses. *Nat. Commun.* 10, 903.

Laemmli, U.K., 1970. Cleavage of Structural Proteins during the Assembly of the Head of Bacteriophage T4. *Nature* 227, 680–685.

Lazarou, M., Smith, S.M., Thorburn, D.R., Ryan, M.T., McKenzie, M., 2009. Assembly of nuclear DNA-encoded subunits into mitochondrial complex IV, and their preferential integration into supercomplex forms in patient mitochondria. *FEBS J*. 276, 6701–6713.

Le Vasseur, M., Friedman, J., Jost, M., Xu, J., Yamada, J., Kampmann, M., Horlbeck, M.A., Salemi, M.R., Phinney, B.S., Weissman, J.S., Nunnari, J., 2021. Genome-wide CRISPRi screening identifies OCIAD1 as a prohibitin client and regulatory determinant of mitochondrial Complex III assembly in human cells. *eLife* 10, e67624.

Lee, S., Lee, H., Yoo, S., Ieva, R., van der Laan, M., von Heijne, G., Kim, H., 2020. The Mgr2 subunit of the TIM23 complex regulates membrane insertion of marginal stop-transfer signals in the mitochondrial inner membrane. *FEBS Lett.* 594, 1081–1087.

Letts, J.A., Sazanov, L.A., 2017. Clarifying the supercomplex: the higher-order organization of the mitochondrial electron transport chain. *Nat. Struct. Mol. Biol.* 24, 800–808.

Levey, A.I., Rye, D.B., Wainer, B.H., 1982. Immunochemical Studies of Bovine and Human Choline-O-Acetyltransferase Using Monoclonal Antibodie. *J. Neurochem.* 39, 1652–1659.

Lionello, S., Marzaro, G., Martinvalet, D., 2020. SAM50, a side door to the mitochondria: The case of cytotoxic proteases. *Pharmacol. Res*. 160, 105196.

Lithgow, T., Junne, T., Suda, K., Gratzer, S., Schatz, G., 1994. The mitochondrial outer membrane protein Mas22p is essential for protein import and viability of yeast. *Proc. Natl. Acad. Sci.* 91, 11973–11977.

Lorenzi, I., Oeljeklaus, S., Aich, A., Ronsör, C., Callegari, S., Dudek, J., Warscheid, B., Dennerlein, S., Rehling, P., 2018. The mitochondrial TMEM177 associates with COX20 during COX2 biogenesis. Biochim. Biophys. *Acta Mol. Cell Res.* 1865, 323–333.

Luirink, J., Samuelsson, T., de Gier, J.W., 2001. YidC/Oxa1p/Alb3: evolutionarily conserved mediators of membrane protein assembly. *FEBS Lett*. 501, 1–5.

Mahmood, T., Yang, P.-C., 2012. Western Blot: Technique, Theory, and Trouble Shooting. *North Am. J. Med. Sc*i. 4, 429–434.

Maity, S., Chakrabarti, O., 2021. Mitochondrial protein import as a quality control sensor. *Biol. Cell*. https://doi.org/10.1111/boc.202100002

Marom, M., Dayan, D., Demishtein-Zohary, K., Mokranjac, D., Neupert, W., Azem, A., 2011. Direct interaction of mitochondrial targeting presequences with purified components of the TIM23 protein complex. *J. Biol. Chem*. 286, 43809–43815.

Marx, S., Dal Maso, T., Chen, J.-W., Bury, M., Wouters, J., Michiels, C., Le Calvé, B., 2020. Transmembrane (TMEM) protein family members: Poorly characterized even if essential for the metastatic process. Semin. *Cancer Biol*. 60, 96–106.

Meinecke, M., Wagner, R., Kovermann, P., Guiard, B., Mick, D.U., Hutu, D.P., Voos, W., Truscott, K.N., Chacinska, A., Pfanner, N., Rehling, P., 2006. Tim50 maintains the permeability barrier of the mitochondrial inner membrane. *Science* 312, 1523–1526.

Meisinger, C., Sickmann, A., Pfanner, N., 2008. The mitochondrial proteome: from inventory to function. *Cell* 134, 22–24.

Meyer, E., Michaelides, M., Tee, L.J., Robson, A.G., Rahman, F., Pasha, S., Luxon, L.M., Moore, A.T., Maher, E.R., 2010. Nonsense mutation in TMEM126A causing autosomal recessive optic atrophy and auditory neuropathy. *Mol. Vis*. 16, 650–664.

Mick, D.U., Dennerlein, S., Wiese, H., Reinhold, R., Pacheu-Grau, D., Lorenzi, I., Sasarman, F., Weraarpachai, W., Shoubridge, E.A., Warscheid, B., Rehling, P., 2012. MITRAC Links Mitochondrial Protein Translocation to Respiratory-Chain Assembly and Translational Regulation. *Cell* 151, 1528–1541.

Mick, D.U., Wagner, K., van der Laan, M., Frazier, A.E., Perschil, I., Pawlas, M., Meyer, H.E., Warscheid, B., Rehling, P., 2007. Shy1 couples Cox1 translational regulation to cytochrome *c* oxidase assembly. *EMBO J.* 26, 4347–4358.

Mimaki, M., Wang, X., McKenzie, M., Thorburn, D.R., Ryan, M.T., 2012. Understanding mitochondrial complex I assembly in health and disease. *Biochim. Biophys. Act*a 1817, 851–862.

Mohanraj, K., Wasilewski, M., Benincá, C., Cysewski, D., Poznanski, J., Sakowska, P., Bugajska, Z., Deckers, M., Dennerlein, S., Fernandez-Vizarra, E., Rehling, P., Dadlez, M., Zeviani, M., Chacinska, A., 2019. Inhibition of proteasome rescues a pathogenic variant of respiratory chain assembly factor COA7. *EMBO Mol. Med*. 11.

Mokranjac, D., Neupert, W., 2005. Protein import into mitochondria. *Biochem. Soc. Trans*. 33, 1019–1023.

Mordas, A., Tokatlidis, K., 2015. The MIA Pathway: A Key Regulator of Mitochondrial Oxidative Protein Folding and Biogenesis. *Acc. Chem. Res*. 48, 2191–2199.

Mori, M., Terada, K., 1998. Mitochondrial protein import in animals. *Biochim. Biophys. Acta BBA - Mol. Cell Res.* 1403, 12–27.

Moulin, C., Caumont-Sarcos, A., Ieva, R., 2019. Mitochondrial presequence import: Multiple regulatory knobs fine-tune mitochondrial biogenesis and homeostasis. *Biochim. Biophys. Acta Mol. Cell Res.* 1866, 930–944.

Mullis, K., Faloona, F., Scharf, S., Saiki, R., Horn, G., Erlich, H., 1986. Specific Enzymatic Amplification of DNA *In Vitro*: The Polymerase Chain Reaction. *Cold Spring Harb. Symp. Quant. Biol*. 51, 263–273.

Nargang, F.E., Preuss, M., Neupert, W., Herrmann, J.M., 2002. The Oxa1 protein forms a homooligomeric complex and is an essential part of the mitochondrial export translocase in *Neurospora crassa*. *J. Biol. Chem*. 277, 12846–12853.

Ndi, M., Marin-Buera, L., Salvatori, R., Singh, A.P., Ott, M., 2018. Biogenesis of the bc_1 Complex of the Mitochondrial Respiratory Chain. *J. Mol. Biol*. 430, 3892–3905.

Neupert, W., Herrmann, J.M., 2007. Translocation of Proteins into Mitochondria. *Annu. Rev. Biochem*. 76, 723–749.

Ng, Y.S., Bindoff, L.A., Gorman, G.S., Klopstock, T., Kornblum, C., Mancuso, M., McFarland, R., Sue, C.M., Suomalainen, A., Taylor, R.W., Thorburn, D.R., Turnbull, D.M., 2021. Mitochondrial disease in adults: recent advances and future promise. *Lancet Neurol*. 20, 573–584.

Nunnari, J., Suomalainen, A., 2012. Mitochondria: In Sickness and in Health. *Cell* 148, 1145–1159.

O'Gorman, S., Fox, D.T., Wahl, G.M., 1991. Recombinase-mediated gene activation and site-specific integration in mammalian cells. *Science* 251, 1351–1355.

Ong, S.-E., Blagoev, B., Kratchmarova, I., Kristensen, D.B., Steen, H., Pandey, A., Mann, M., 2002. Stable Isotope Labeling by Amino Acids in Cell Culture, SILAC, as a Simple and Accurate Approach to Expression Proteomics. *Mol. Cell. Proteomic*s 1, 376–386.

Panov, A. (2013). Practical Mitochondriology. Createspace Independent Pub.

Paschen, S.A., Neupert, W., 2001. Protein Import Into Mitochondria. *IUBMB Life* 52, 101–112.

Pfanner, N., Warscheid, B., Wiedemann, N., 2019. Mitochondrial proteins: from biogenesis to functional networks. *Nat. Rev. Mol. Cell Biol*. 20, 267–284.

Potluri, P., Yadava, N., Scheffler, I.E., 2004. The role of the ESSS protein in the assembly of a functional and stable mammalian mitochondrial complex I (NADH-ubiquinone oxidoreductase). *Eur. J. Biochem*. 271, 3265–3273.

Preuss, M., Ott, M., Funes, S., Luirink, J., Herrmann, J.M., 2005. Evolution of mitochondrial oxa proteins from bacterial YidC. Inherited and acquired functions of a conserved protein insertion machinery. *J. Biol. Chem.* 280, 13004–13011.

Priesnitz, C., Becker, T., 2018. Pathways to balance mitochondrial translation and protein import. *Genes Dev.* 32, 1285–1296.

Protasoni, M., Pérez-Pérez, R., Lobo-Jarne, T., Harbour, M.E., Ding, S., Peñas, A., Diaz, F., Moraes, C.T., Fearnley, I.M., Zeviani, M., Ugalde, C., Fernández-Vizarra, E., 2020. Respiratory supercomplexes act as a platform for complex III -mediated maturation of human mitochondrial complexes I and IV. *EMBO J*. 39.

Rampelt, H., Sucec, I., Bersch, B., Horten, P., Perschil, I., Martinou, J.-C., van der Laan, M., Wiedemann, N., Schanda, P., Pfanner, N., 2020. The mitochondrial carrier pathway transports non-canonical substrates with an odd number of transmembrane segments. *BMC Biol.* 18, 2.

Ran, F.A., Hsu, P.D., Wright, J., Agarwala, V., Scott, D.A., Zhang, F., 2013. Genome engineering using the CRISPR-Cas9 system. *Nat. Protoc*. 8, 2281–2308.

Rana, M., Coo, I.D., Diaz, F., Smeets, H., Moraes, C.T., 2000. An out-of-frame cytochrome *b* gene deletion from a patient with parkinsonism is associated with impaired complex III assembly and an increase in free radical production. *Ann. Neurol.* 48, 774–781.

Rath, S., Sharma, R., Gupta, R., Ast, T., Chan, C., Durham, T.J., Goodman, R.P., Grabarek, Z., Haas, M.E., Hung, W.H.W., Joshi, P.R., Jourdain, A.A., Kim, S.H., Kotrys, A.V., Lam, S.S., McCoy, J.G., Meisel, J.D., Miranda, M., Panda, A., Patgiri, A., Rogers, R., Sadre, S., Shah, H., Skinner, O.S., To, T.-L., Walker, M.A., Wang, H., Ward, P.S., Wengrod, J., Yuan, C.-C., Calvo, S.E., Mootha, V.K., 2021. MitoCarta3.0: an updated mitochondrial proteome now with sub-organelle localization and pathway annotations. *Nucleic Acids Res.* 49, D1541–D1547.

Rehling, P., Model, K., Brandner, K., Kovermann, P., Sickmann, A., Meyer, H.E., Kühlbrandt, W., Wagner, R., Truscott, K.N., Pfanner, N., 2003. Protein insertion into the mitochondrial inner membrane by a twin-pore translocase. *Science* 299, 1747–1751.

Reif, S., Randelj, O., Domanska, G., Dian, E.A., Krimmer, T., Motz, C., Rassow, J., 2005. Conserved mechanism of Oxa1 insertion into the mitochondrial inner membrane. *J. Mol. Biol*. 354, 520–528.

Reinhold, R., Bareth, B., Balleininger, M., Wissel, M., Rehling, P., Mick, D.U., 2011. Mimicking a SURF1 allele reveals uncoupling of cytochrome *c* oxidase assembly from translational regulation in yeast. *Hum. Mol. Genet.* 20, 2379–2393.

Richter-Dennerlein, R., Oeljeklaus, S., Lorenzi, I., Ronsör, C., Bareth, B., Schendzielorz, A.B., Wang, C., Warscheid, B., Rehling, P., Dennerlein, S., 2016. Mitochondrial Protein Synthesis Adapts to Influx of Nuclear-Encoded Protein. *Cell* 167, 471-483.

Röttgers, K., Zufall, N., Guiard, B., Voos, W., 2002. The ClpB Homolog Hsp78 Is Required for the Efficient Degradation of Proteins in the Mitochondrial Matrix. *J. Biol. Chem.* 277, 45829–45837.

Saccone, C., Gissi, C., Lanave, C., Larizza, A., Pesole, G., Reyes, A., 2000. Evolution of the mitochondrial genetic system: an overview. *Gene* 261, 153–159.

Saiki, R.K., Gelfand, D.H., Stoffel, S., Scharf, S.J., Higuchi, R., Horn, G.T., Mullis, K.B., Erlich, H.A., 1988. Primer-directed enzymatic amplification of DNA with a thermostable DNA polymerase. *Science* 239, 487–491.

Sánchez-Caballero, L., Elurbe, D.M., Baertling, F., Guerrero-Castillo, S., van den Brand, M., van Strien, J., van Dam, T.J.P., Rodenburg, R., Brandt, U., Huynen, M.A., Nijtmans, L.G.J., 2020. TMEM70 functions in the assembly of complexes I and V. *Biochim. Biophys. Acta Bioenerg*. 1861, 148202.

Schägger, H., 2006. Tricine–SDS-PAGE. *Nat. Protoc.* 1, 16–22.

Schägger, H., 2002. Respiratory chain supercomplexes of mitochondria and bacteria. *Biochim. Biophys. Acta* 1555, 154–159.

Schägger, H., Pfeiffer, K., 2001. The ratio of oxidative phosphorylation complexes I-V in bovine heart mitochondria and the composition of respiratory chain supercomplexes. *J. Biol. Chem*. 276, 37861–37867.

Schägger, H., von Jagow, G., 1991. Blue native electrophoresis for isolation of membrane protein complexes in enzymatically active form. *Anal. Biochem*. 199, 223–231.

Schmitt, S., Ahting, U., Eichacker, L., Granvogl, B., Go, N.E., Nargang, F.E., Neupert, W., Nussberger, S., 2005. Role of Tom5 in Maintaining the Structural Stability of the TOM Complex of Mitochondria. *J. Biol. Chem*. 280, 14499–14506.

Schuler, M.-H., Di Bartolomeo, F., Böttinger, L., Horvath, S.E., Wenz, L.-S., Daum, G., Becker, T., 2015. Phosphatidylcholine Affects the Role of the Sorting and Assembly Machinery in the Biogenesis of Mitochondrial β-Barrel Proteins. *J. Biol. Chem*. 290, 26523–26532.

Schulz, C., Schendzielorz, A., Rehling, P., 2015. Unlocking the presequence import pathway. *Trends Cell Biol.* 25, 265–275.

Scotti, P.A., Urbanus, M.L., Brunner, J., de Gier, J.W., von Heijne, G., van der Does, C., Driessen, A.J., Oudega, B., Luirink, J., 2000. YidC, the Escherichia coli homologue of mitochondrial Oxa1p, is a component of the Sec translocase. *EMBO J*. 19, 542–549.

Shi, H., Rampello, A.J., Glynn, S.E., 2016. Engineered AAA+ proteases reveal principles of proteolysis at the mitochondrial inner membrane. *Nat. Commun*. 7, 13301.

Signes, A., Fernandez-Vizarra, E., 2018. Assembly of mammalian oxidative phosphorylation complexes I-V and supercomplexes. *Essays Biochem*. 62, 255–270.

Signorile, A., Sgaramella, G., Bellomo, F., De Rasmo, D., 2019. Prohibitins: A Critical Role in Mitochondrial Functions and Implication in Diseases. *Cells* 8, 71.

Smith, P.M., Fox, J.L., Winge, D.R., 2012. Biogenesis of the cytochrome $bc_{(1)}$ complex and role of assembly factors. *Biochim. Biophys. Acta* 1817, 276–286.

Sokol, A.M., Sztolsztener, M.E., Wasilewski, M., Heinz, E., Chacinska, A., 2014. Mitochondrial protein translocases for survival and wellbeing. *FEBS Lett*. 588, 2484–2495.

Söllner, T., Pfaller, R., Griffiths, G., Pfanner, N., Neupert, W., 1990. A mitochondrial import receptor for the ADP/ATP carrier. *Cell* 62, 107–115.

Song, J., Herrmann, J.M., Becker, T., 2021. Quality control of the mitochondrial proteome. *Nat. Rev. Mol. Cell Biol*. 22, 54–70.

Soto, I.C., Fontanesi, F., Liu, J., Barrientos, A., 2012. Biogenesis and assembly of eukaryotic cytochrome *c* oxidase catalytic core. *Biochim. Biophys. Acta* 1817, 883–897.

Steglich, G., Neupert, W., Langer, T., 1999. Prohibitins regulate membrane protein degradation by the m-AAA protease in mitochondria. *Mol. Cell. Biol.* 19, 3435–3442.

Stewart, J.B., Chinnery, P.F., 2021. Extreme heterogeneity of human mitochondrial DNA from organelles to populations. *Nat. Rev. Genet.* 22, 106–118.

Stiburek, L., Fornuskova, D., Wenchich, L., Pejznochova, M., Hansikova, H., Zeman, J., 2007. Knockdown of human Oxa1l impairs the biogenesis of F_1F_o-ATP synthase and NADH:ubiquinone oxidoreductase. *J. Mol. Biol.* 374, 506–516.

Stiller, S.B., Höpker, J., Oeljeklaus, S., Schütze, C., Schrempp, S.G., Vent-Schmidt, J., Horvath, S.E., Frazier, A.E., Gebert, N., van der Laan, M., Bohnert, M., Warscheid, B., Pfanner, N., Wiedemann, N., 2016. Mitochondrial OXA Translocase Plays a Major Role in Biogenesis of Inner-Membrane Proteins. *Cell Metab*. 23, 901–908.

Stoccoro, A., Coppedè, F., 2021. Mitochondrial DNA Methylation and Human Diseases. *Int. J. Mol. Sci.* 22. https://doi.org/10.3390/ijms22094594

Stojanovski, D., Guiard, B., Kozjak-Pavlovic, V., Pfanner, N., Meisinger, C., 2007. Alternative function for the mitochondrial SAM complex in biogenesis of alpha-helical TOM proteins. *J. Cell Bio*l. 179, 881–893.

Straub, S.P., Stiller, S.B., Wiedemann, N., Pfanner, N., 2016. Dynamic organization of the mitochondrial protein import machinery. *Biol. Chem*. 397, 1097–1114.

Strober, W., 2015. Trypan Blue Exclusion Test of Cell Viability. *Curr. Protoc. Immunol*. 111, A3.B.1-A3.B.3.

Stuart, R., 2002. Insertion of proteins into the inner membrane of mitochondria: the role of the Oxa1 complex. *Biochim. Biophys. Acta* 1592, 79–87.

Szczepanowska, K., Trifunovic, A., 2021. Mitochondrial matrix proteases: quality control and beyond. *FEBS J*. https://doi.org/10.1111/febs.15964

Sztolsztener, M.E., Brewinska, A., Guiard, B., Chacinska, A., 2013. Disulfide Bond Formation: Sulfhydryl Oxidase ALR Controls Mitochondrial Biogenesis of Human MIA40. *Traffic* 14, 309–320.

Szyrach, G., Ott, M., Bonnefoy, N., Neupert, W., Herrmann, J.M., 2003. Ribosome binding to the Oxa1 complex facilitates co-translational protein insertion in mitochondria. *EMBO J*. 22, 6448–6457.

Taanman, J.-W., 1999. The mitochondrial genome: structure, transcription, translation and replication. *Biochim. Biophys. Acta BBA - Bioenerg*. 1410, 103–123.

Takeda, H., Tsutsumi, A., Nishizawa, T., Lindau, C., Busto, J.V., Wenz, L.-S., Ellenrieder, L., Imai, K., Straub, S.P., Mossmann, W., Qiu, J., Yamamori, Y., Tomii, K., Suzuki, J., Murata, T., Ogasawara, S., Nureki, O., Becker, T., Pfanner, N., Wiedemann, N., Kikkawa, M., Endo, T., 2021. Mitochondrial sorting and assembly machinery operates by β-barrel switching. *Nature* 590, 163–169.

Tang, J.X., Thompson, K., Taylor, R.W., Oláhová, M., 2020. Mitochondrial OXPHOS Biogenesis: Co-Regulation of Protein Synthesis, Import, and Assembly Pathways. *Int. J. Mol. Sci*. 21.

Thompson, K., Mai, N., Oláhová, M., Scialó, F., Formosa, L.E., Stroud, D.A., Garrett, M., Lax, N.Z., Robertson, F.M., Jou, C., Nascimento, A., Ortez, C., Jimenez-Mallebrera, C., Hardy, S.A., He, L., Brown, G.K., Marttinen, P., McFarland, R., Sanz, A., Battersby, B.J., Bonnen, P.E., Ryan, M.T., Chrzanowska-Lightowlers, Z.M., Lightowlers, R.N., Taylor, R.W., 2018. OXA1L mutations cause mitochondrial encephalopathy and a combined oxidative phosphorylation defect. *EMBO Mol. Med.* 10, e9060.

Truscott, K.N., Brandner, K., Pfanner, N., 2003. Mechanisms of protein import into mitochondria. *Curr. Biol*. CB 13, R326-337.

Truscott, K.N., Voos, W., Frazier, A.E., Lind, M., Li, Y., Geissler, A., Dudek, J., Müller, H., Sickmann, A., Meyer, H.E., Meisinger, C., Guiard, B., Rehling, P., Pfanner, N., 2003. A J-protein is an essential subunit of the presequence translocase-associated protein import motor of mitochondria. *J. Cell Biol*. 163, 707–713.

Tucker, E.J., Wanschers, B.F.J., Szklarczyk, R., Mountford, H.S., Wijeyeratne, X.W., van den Brand, M.A.M., Leenders, A.M., Rodenburg, R.J., Reljić, B., Compton, A.G., Frazier, A.E., Bruno, D.L., Christodoulou, J., Endo, H., Ryan, M.T., Nijtmans, L.G., Huynen, M.A., Thorburn, D.R., 2013. Mutations in the UQCC1-interacting protein, UQCC2, cause human complex III deficiency associated with perturbed cytochrome b protein expression. *PLoS Genet*. 9, e1004034.

Vakulskas, C.A., Dever, D.P., Rettig, G.R., Turk, R., Jacobi, A.M., Collingwood, M.A., Bode, N.M., McNeill, M.S., Yan, S., Camarena, J., Lee, C.M., Park, S.H., Wiebking, V., Bak, R.O., Gomez-Ospina, N., Pavel-Dinu, M., Sun, W., Bao, G., Porteus, M.H., Behlke, M.A., 2018. A high-fidelity Cas9 mutant delivered as a ribonucleoprotein complex enables efficient gene editing in human haematopoietic stem and progenitor cells. *Nat. Med*. 24, 1216–1224.

van der Laan, M., Hutu, D.P., Rehling, P., 2010. On the mechanism of preprotein import by the mitochondrial presequence translocase. *Biochim. Biophys. Acta* 1803, 732–739.

van der Laan, M., Rissler, M., Rehling, P., 2006. Mitochondrial preprotein translocases as dynamic molecular machines. *FEMS Yeast Res*. 6, 849–861.

Vasiljev, A., Ahting, U., Nargang, F.E., Go, N.E., Habib, S.J., Kozany, C., Panneels, V., Sinning, I., Prokisch, H., Neupert, W., Nussberger, S., Rapaport, D., 2004. Reconstituted TOM core complex and Tim9/Tim10 complex of mitochondria are sufficient for translocation of the ADP/ATP carrier across membranes. *Mol. Biol. Cell* 15, 1445–1458.

Vogel, F., Bornhövd, C., Neupert, W., Reichert, A.S., 2006. Dynamic subcompartmentalization of the mitochondrial inner membrane. *J. Cell Biol*. 175, 237–247.

Vögtle, F.-N., Burkhart, J.M., Rao, S., Gerbeth, C., Hinrichs, J., Martinou, J.-C., Chacinska, A., Sickmann, A., Zahedi, R.P., Meisinger, C., 2012. Intermembrane space proteome of yeast mitochondria. *Mol. Cell. Proteomics MCP* 11, 1840–1852.

Wai, T., Saita, S., Nolte, H., Müller, S., König, T., Richter-Dennerlein, R., Sprenger, H.-G., Madrenas, J., Mühlmeister, M., Brandt, U., Krüger, M., Langer, T., 2016. The membrane scaffold SLP2 anchors a proteolytic hub in mitochondria containing PARL and the i-AAA protease YME1L. *EMBO Rep*. 17, 1844–1856.

Walther, D.M., Rapaport, D., 2009. Biogenesis of mitochondrial outer membrane proteins. *Biochim. Biophys. Acta BBA - Mol. Cell Res.*, Assembly of the Mitochondrial Respiratory Chain 1793, 42–51.

Wang, C., Richter-Dennerlein, R., Pacheu-Grau, D., Liu, F., Zhu, Y., Dennerlein, S., Rehling, P., 2020. MITRAC15/COA1 promotes mitochondrial translation in a ND2 ribosome-nascent chain complex. *EMBO Rep*. 21, e48833.

Wang, C., Youle, R.J., 2009. The Role of Mitochondria in Apoptosis. *Annu. Rev. Genet*. 43, 95–118.

Wang, W., Chen, X., Zhang, L., Yi, J., Ma, Q., Yin, J., Zhuo, W., Gu, J., Yang, M., 2020. Atomic structure of human TOM core complex. *Cell Discov.* 6, 67.

Wanschers, B.F.J., Szklarczyk, R., van den Brand, M.A.M., Jonckheere, A., Suijskens, J., Smeets, R., Rodenburg, R.J., Stephan, K., Helland, I.B., Elkamil, A., Rootwelt, T., Ott, M., van den Heuvel, L., Nijtmans, L.G., Huynen, M.A., 2014. A mutation in the human CBP4 ortholog UQCC3 impairs complex III assembly, activity and cytochrome b stability. *Hum. Mol. Genet*. 23, 6356–6365.

Wasilewski, M., Chojnacka, K., Chacinska, A., 2017. Protein trafficking at the crossroads to mitochondria. *Biochim. Biophys. Acta BBA - Mol. Cell Res.* 1864, 125–137.

Westermann, B., Prip-Buus, C., Neupert, W., Schwarz, E., 1995. The role of the GrpE homologue, Mge1p, in mediating protein import and protein folding in mitochondria. *EMBO J*. 14, 3452–3460.

Widmann, M., Christen, P., 1995. Differential effects of molecular chaperones on refolding of homologous proteins. *FEBS Lett*. 377, 481–484.

Wiedemann, N., Pfanner, N., 2017. Mitochondrial Machineries for Protein Import and Assembly. *Annu. Rev. Biochem*. 86, 685–714.

Wiedenheft, B., van Duijn, E., Bultema, J.B., Bultema, J., Waghmare, S.P., Waghmare, S., Zhou, K., Barendregt, A., Westphal, W., Heck, A.J.R., Heck, A., Boekema, E.J., Boekema, E., Dickman, M.J., Dickman, M., Doudna, J.A., 2011. RNA-guided complex from a bacterial immune system enhances target recognition through seed sequence interactions. *Proc. Natl. Acad. Sci. U. S. A*. 108, 10092–10097.

Wittig, I., Braun, H.-P., Schägger, H., 2006. Blue native PAGE. *Nat. Protoc.* 1, 418–428.

Wrobel, L., Trojanowska, A., Sztolsztener, M.E., Chacinska, A., 2013. Mitochondrial protein import: Mia40 facilitates Tim22 translocation into the inner membrane of mitochondria. *Mol. Biol. Cell* 24, 543–554.

Wu, Y., Sha, B., 2006. Crystal structure of yeast mitochondrial outer membrane translocon member Tom70p. *Nat. Struct. Mol. Biol*. 13, 589–593.

Yan, C., Duanmu, X., Zeng, L., Liu, B., Song, Z., 2019. Mitochondrial DNA: Distribution, Mutations, and Elimination. *Cells* 8.

Yasukawa, T., Kang, D., 2018. An overview of mammalian mitochondrial DNA replication mechanisms. *J. Biochem.* (Tokyo) 164, 183–193.

Zhang, S., Reljić, B., Liang, C., Kerouanton, B., Francisco, J.C., Peh, J.H., Mary, C., Jagannathan, N.S., Olexiouk, V., Tang, C., Fidelito, G., Nama, S., Cheng, R.-K., Wee, C.L., Wang, L.C., Duek Roggli, P., Sampath, P., Lane, L., Petretto, E., Sobota, R.M., Jesuthasan, S., Tucker-Kellogg, L., Reversade, B., Menschaert, G., Sun, L., Stroud, D.A., Ho, L., 2020. Mitochondrial peptide BRAWNIN is essential for vertebrate respiratory complex III assembly. *Nat. Commun*. 11, 1312.

Zhang, Y.-J., Tian, H.-F., Wen, J.-F., 2009. The evolution of YidC/Oxa/Alb3 family in the three domains of life: a phylogenomic analysis. *BMC Evol. Biol*. 9, 137.

Zhunina, O.A., Yabbarov, N.G., Grechko, A.V., Starodubova, A.V., Ivanova, E., Nikiforov, N.G., Orekhov, A.N., 2021. The Role of Mitochondrial Dysfunction in Vascular Disease, Tumorigenesis, and Diabetes. *Front. Mol. Biosci.* 8, 671908.

Zimmerman, R., Paluch, U., Sprinzl, M., Neupert, W., 1979. Cell-Free Synthesis of the Mitochondrial ADP/ATP Carrier Protein of *Neurospora crassa*. *Eur. J. Biochem.* 99, 247–252.

7. Acknowledgments

First and foremost, I would like to thank **Peter Rehling** for giving me the opportunity to work on these interesting projects in his group. I am grateful for his supervision, fruitful discussions and help during every step of my projects. Thank you for the trust in my competencies as well as in my organizational skills far from the daily experiments.

I would like to thank my thesis advisory committee members **Ralph Kehlenbach** and **Wolfgang Wintermeyer** for their time, suggestions during our meetings and support regarding upcoming questions in my projects. Moreover, I am thankful to my extended thesis advisory committee: **Sarah Adio, Henning Urlaub, and Alexander Stein**.

A big thank you to **Sven Dennerlein** for his close supervision on a daily basis. Especially during the last weeks of writing this thesis and the revision of the first manuscript. Without your engagement and support these things would have been impossible in parallel.

At his point, I would also thank **Agnieszka Chacinska**. She and her group members inspired me to continue with this interesting topic of mitochondrial biogenesis after my master's thesis. During the past years I benefited a lot from the knowledge and know- how I appropriated in her lab.

The start of this thesis would not have been successful without the support from **Isotta Lorenzi, Frank Richter** and **Christin Ronsör**, who introduced me to the experimental secrets of the lab. Even in struggling times Frank and Isotta were the best lab neighbors you can have, and I enjoyed the time together in our lab a lot.

Many thanks belonging to **Silke Oeljeklaus** and **Alexander Schenzielorz** from Bettina Warscheid's group for the mass spectrometry analyses and the wonderful explanations, especially from Silke.

I would like to show my greatest appreciation to **Mirjam, Carmen** and **Annette**. Without your tireless commitment the daily research would not be possible. It is not a given that we, the researchers, can perform their experiments without having to worry about the materials and maintenance.

A special thanks belongs to all current and former members of the Department of Cellular Biochemistry. I would like to mention **Bettina, Franzi, David, Markus, Tobias** and **Lioba**, in particular. All of you helped me a lot in the past years and we had great scientific and not so scientific discussions. Thank you, Bettina, for sharing ups and downs during our time and for being not only a lab partner but also a great friend.

Many thanks for proofreading this thesis and the manuscript go out to: **Julius**, **Sven**, **Bettina** and **David**.

I want to express my greatest appreciation to my **family** and **friends** who always supported and motivated me to pursue this way. I cannot express in words how thankful I am to Julius who always listened to my sorrows and helped me to deal with any hardships coming my way.